Coordination Chemistry Reviews 253 (2009) 1709–1758

Contents lists available at ScienceDirect

Coordination Chemistry Reviews

journal homepage: www.elsevier.com/locate/ccr

Review

Heavy metal organometallic electrophosphors derived from multi-component chromophores

Wai-Yeung Wong*, Cheuk-Lam Ho

Department of Chemistry and Centre for Advanced Luminescence Materials, Hong Kong Baptist University, Waterloo Road, Kowloon Tong, Hong Kong, PR China

Contents

ARTICLE INFO

Article history:
Received 1 October 2008
Accepted 15 January 2009
Available online 23 January 2009

Dedicated to Prof. The Lord Lewis in celebration of his 80th birthday.

Keywords:
Electroluminescence
Metallodendrimers

ABSTRACT

Transition-metal-based phosphorescent materials have recently received considerable academic and industrial attention for fabricating electrophosphorescent organic light-emitting diodes (PHOLEDs), owing to their potential to harness the energies of both the singlet and triplet excitons after charge recombination. Materials suitable for application in PHOLEDs have been actively researched in the past decade and chemical principles have played a crucial role in the evolution of efficient devices for commercialization. More current attention has been paid to the structure–property relationships of phosphorescent small-molecule heavy metal chelate complexes and polymers featuring multiple functional moieties. These organometallic electrophosphors typically possess various hole-transporting, electron-transporting and phosphorescent chromophores with tunable charge-transporting and triplet light-emitting properties. Rational design of multi-component small-molecular metallophosphors,

Abbreviations: acac, acetylacetonate; A, electron acceptor; ADN, 9,10-di(2-naphthyl)anthracene; AFM, atomic force microscopy; Alq_3, tris(8-hydroxyquinolinato)aluminum; BAlq, bis(2-methyl-8-quinolinato)-(1,1′-biphenyl-4-olato)aluminum; BCP, 2,9-dimethyl-4,7-diphenyl-1,10-phenanthroline; BPAPF, 9,9-bis{4-[di(*p*-biphenyl)aminophenyl]fluorene}; CBP, 4,4′-*N*,*N*′-dicarbazolebiphenyl; CCT, correlated color temperature; CIE, Commission Internationale de L'Eclairage; COSY, correlated spectroscopy; CRI, color rendering index; CV, cyclic voltammetry; D, electron donor; DFT, density functional theory; DSA-Ph, *p*-bis(*p*-*N*,*N*-diphenylaminostyryl)benzene; EL, electroluminescence; [FIr(pic)], iridium(III)-bis[(4,6-difluorophenyl)pyridinato-*N*,C^2]picolinate; HOMO, highest occupied molecular orbital; Hpiq, 1-phenylisoquinoline; Hppy, 2-phenylpyridine; ITO, indium-tin oxide; LCDs, liquid-crystal displays; LECs, light-emitting electrochemical cells; LUMO, lowest unoccupied molecular orbital; Me, methyl; ^{3}MLCT, triplet metal-to-ligand charge transfer; 2-MeTHF, 2-methyltetrahydrofuran; NOE, nuclear overhauser effect; NPB, 4,4′-bis[*N*-(1-naphthyl)-*N*-phenylamino]biphenyl; OLEDs, organic light-emitting diodes; OXD-7, 1,3-bis[5-(4-*tert*-butylphenyl)-1,3,4-oxadiazole-2-yl]benzene; PBD, 2-(4-biphenylyl)-5-(4-*tert*-butylphenyl)-1,3,4-oxadiazole; PEDOT:PSS, poly(ethylenedioxythiophene)–poly(styrenesulfonic acid); PF, polyfluorene; PFO-CN, poly(9,9-dihexylfluorene)-*co*-2,5-dicyanophenylene; PFO-ETM, poly(9,9-dihexylfluorene) end-capped with electron-transporting ditolylbiphenylamine; PFO-HTM, poly(9,9-dihexylfluorene) end-capped with hole-transporting ditolylbiphenylamine; Ph, phenyl; phen, 1,10-phenanthroline; PHOLEDs, electrophosphorescent organic light-emitting diodes; PL, photoluminescence; PLEDs, polymer light-emitting diodes; PSBF:TAD, polyspirobifluorene:bis(triphenyl)diamine; PVK, poly(9-vinylcarbazole); TAPC, 1,1-bis[4-(di-*p*-tolylamino)phenyl]cyclohexane; TCCz, *N*-(4-[9,3′:6′,9″]tercarbazol-9′-yl)phenylcarbazole; TD-DFT, time-dependent density functional theory; THF, tetrahydrofuran; TOF, time-of-flight; TEM, transmission electron microscopy; TPBI, 1,3,5-tris[*N*-(phenyl)benzimidazole]benzene; TPD, *N*,*N*′-diphenyl-*N*,*N*′-bis(3-methylphenyl)-[1,1′-biphenyl]-4,4′-diamine; WOLEDs, white organic light-emitting diodes; η_{ext}, external quantum efficiency; η_L, luminance efficiency; η_P, power efficiency; η_t, total power efficiency; η_{OC}, outcoupling efficiency; S_0, singlet ground state; T_1, first triplet excited state; C^N, cyclometalating ligand; λ, wavelength; E_{ox}, oxidation potential; *fac*, facial; fwhm, full-width at half maximum; M_w, weight-average molecular weight; T_d, onset decomposition temperature; T_g, glass-transition temperature; τ_P, phosphorescence lifetime; Φ_P, phosphorescence quantum yield; L_{max}, maximum luminance.

* Corresponding author. Tel.: +852 3411 7074; fax: +852 3411 7348.
E-mail address: rwywong@hkbu.edu.hk (W.-Y. Wong).

0010-8545/$ – see front matter
doi:10.1016/j.ccr.2009.01.013

Metallophosphors
Metallopolymers
Optoelectronics
Phosphorescent OLEDs

metallodendrimers and metallopolymers aiming at color tuning and multiple functions forms the major focus of this review. In this way, different functional groups can perform specific roles such as photoexcitation, charge transportation and phosphorescence so that highly efficient and simple electrophosphorescent device structures can be developed. The electronic, optical, structural, photo- and electroluminescence properties of these multi-component compounds will be surveyed and discussed. This prominent class of organometallic compounds constitutes an attractive new class of electrophosphors that are thermally and morphologically stable, structurally diverse, and potentially important in optoelectronic applications.

1. Introduction

The past two decades have witnessed an explosion in the research of organic-based optoelectronic materials for organic light-emitting diodes (OLEDs), dendrimer light-emitting diodes (DLEDs) and polymer light-emitting diodes (PLEDs) which are promising elements for the huge-market share in the next generation of flat-panel displays [1–6]. Because of their thin-film, light-weight, fast-response, wide-viewing-angle, high-contrast and low-power attributes, OLEDs and alike promise to be one of the major flat-panel-display technologies that can compete with the currently dominant liquid-crystal displays (LCDs) [7]. For most fluorescent-based compounds, only the singlet state is emissive, resulting in a significant limitation in the OLED efficiency [8]. Hole–electron recombination in OLEDs gives rise to the generation of both singlet and triplet excitons within the molecular thin film. Models of spin statistics predict that the electron–hole recombination event should produce three times as many triplets as singlets [9–11], and this has been confirmed experimentally for electroluminescent devices fabricated from small molecules [12]. For polymers, there are reports of the singlet-to-triplet ratio ranging from 1:1 [13] to 1:3 [14,15]. The singlet–triplet ratio is of considerable importance in high-performance OLED work because the radiative decay of triplet excitons to the singlet ground state is formally forbidden by a requirement for spin conservation [16]. Organic electrophosphorescent materials thus provided one of the key breakthroughs in raising the electroluminescence (EL) efficiency, which is usually limited to an external quantum efficiency of around 5% for devices based on singlet-state fluorescent materials. One way to efficiently harvest energy from the triplet states involves the incorporation of third row heavy metals and these metal complexes permit the opening of an additional radiative recombination channel because of the strong metal-induced spin–orbit coupling, resulting in a harvesting of up to nearly 100% of the excited states to photon creation [17–28]. In light of this, research on electrophosphorescence in OLEDs, DLEDs and PLEDs has received much attention in recent years. Heavy metal compounds of third-row iridium(III) [27,28], platinum(II) [8,22], osmium(II) and second-row ruthenium(II) [21,24,25] can be used as emissive traps or dopants in OLEDs, leading to higher quantum efficiencies for these devices. Most of the fundamental concepts related to the development of PHOLEDs are not covered here as they are periodically reviewed elsewhere [17–28]. Interested readers are encouraged to consult the previous literature references [17–28].

The pioneering success of the cyclometalated iridium(III) and platinum(II) complexes with 2-phenylpyridine (Hppy) type ligands in the field of electrophosphorescent OLEDs (PHOLEDs) has triggered substantial research attention in the design, synthesis and EL characterization of this class of luminescent metal complexes [18,27,29]. The high efficiencies of the PHOLEDs derived from these complexes and their derivatives are ascribed to the energy harvesting arising from both the singlet and triplet excitons in the radiative emission process. The ease of emission wavelength tunability over the entire visible spectrum, especially for the iridium(III)-based phosphors, via modifying the cyclometalated ligand structure will render them excellent emitters for efficient, full-color displays. All of these unique features make heavy metal electrophosphors one of the most attractive candidates for current OLED research.

Since the discovery of small-molecule organic green EL devices on a multi-layer configuration of ITO/TPD/Alq_3/Mg:Ag/Ag (ITO = indium–tin oxide, TPD = *N*,*N*′-diphenyl-*N*,*N*′-bis(3-methylphenyl)-[1,1′-biphenyl]-4,4′-diamine, Alq_3 = tris(8-hydroxyquinolinato) aluminum) by Tang and VanSlyke in Kodak in the late eighties [30], this research field has stimulated tremendous impetus to develop OLEDs using organic or metal-organic compounds as emitters. A successful OLED generally requires facile and balanced charge transport as well as a high conversion efficiency of excitons to light [31]. To fulfil these requirements, OLEDs often contain a number of layers that individually perform the roles of charge transport and light emission [32]. PHOLEDs that are constructed with neutral molecular metal complexes typically consist of the phosphor dyes embedded in an organic host matrix (e.g. 4,4′-*N*,*N*′-dicarbazolebiphenyl (CBP)) to prevent self-quenching, sandwiched between multiple layers of charge transport materials (e.g. 4,4′-bis[*N*-(1-naphthyl)-*N*-phenylamino]biphenyl (NPB) as the hole-transporting layer, 2,9-dimethyl-4,7-diphenyl-1,10-phenanthroline (BCP) as the hole-blocking layer and Alq_3 as the electron-transporting layer), followed by capping with a transparent anode (e.g. ITO) and a low work-function cathode (e.g. a bi-layer LiF/Al in which LiF serves as the electron-injection layer). Each layer requires materials with the correct highest occupied molecular orbital (HOMO) and lowest unoccupied molecular orbital (LUMO) energies to either promote or disrupt the flow of charge in the device [26,33]. Over the years, most of the efficient devices are composed of multiple layers serving different functional roles, i.e. hole transport, light emission, charge or exciton blocking, and electron transport. There is a great potential to excel in the exploration of new electrophosphors for simplifying the sophisticated multi-layer EL cell configuration while still maintaining the desired balanced injection and transport of holes and electrons for high-efficiency devices. Since fabrication of multi-layer devices is often tedious, difficult and relatively more expensive than single-layer devices, recent work has proliferated in solution-processed single-layer polymeric or dendritic PHOLEDs as well which rival those from multi-layer devices in performance [28,34–36].

2. Design concepts

Although there were a number of excellent reviews and feature articles dealing with the synthesis and PHOLED properties of mono-functional transition metal complexes exhibiting room-temperature phosphorescence [8,17–28], it was not until recently that the parallel chemistry of well-characterized multi-component congeners becomes a challenging field of endeavor in the research community. In the following sections, we will provide a detailed survey of these multi-functional metallophosphors, metallodendrimers and metallopolymers, with particular emphasis on work published in the last 5 years or so. Here, the key roles of these special chelating chromophores as charge-injection/charge-transporting

units in phosphorescent light-emitting systems will be discussed. This article cannot be considered an exhaustive review of the topic but just a concise presentation of most recent examples, drawn from the work performed in our or others' laboratories, highlighting the special features of the following structural classes of chromophoric cores in molecular, dendritic and polymeric materials.

(1) Carbazole;
(2) Fluorene;
(3) Carbazole–fluorene hybrids;
(4) Arylamine and other related main group 13–16 moieties;
(5) 1,3,4-Oxadiazole;
(6) Arylamine–fluorene and arylamine–oxadiazole hybrids.

In the search for novel phosphorescent materials for PHOLEDs, a good compromise of absorption and emission wavelengths (λ_{abs} and λ_{em}), phosphorescence quantum yields (Φ_P) and lifetimes (τ_P) must be considered. Written from the chemist's point of view, a systematic analysis of absorption and emission characteristics as well as their energetic requirements (i.e. HOMO and LUMO levels) necessary for the design of PHOLEDs is given as far as we can (see Table 1), and their suitability as PHOLED phosphors is evaluated.

3. Structure–property–function relationships of heavy metal organometallic electrophosphors derived from multi-component chromophores

3.1. Carbazole

Research developments based on the use of carbazole ring as the building unit for the design of branched molecules, oligomers, dendrimers or polymers have aroused much attention in recent years, however, most of them are confined to organic systems [37]. Many carbazole derivatives are known to predominantly transport positive charge carriers in organic systems. For example, poly(9-vinylcarbazole) (PVK) is often described as a unipolar hole transporter whereas CBP is recognized to have a more bipolar transport character [38,39]. It is well-known that carbazole group is a good hole-transporting unit and PVK and other related carbazole-containing polymers are especially important charge transport polymers for OLEDs and as photorefractive materials for electro-optic devices [40–43]. Typically, purely organic carbazole-based compounds are high-mobility hole-transport materials with a tunable and high triplet energy level, and they are widely used as the host materials for electrophosphors emitting different colors [44–48]. It is highly desirable that the designed phosphor can show improved charge-balancing features and permit a complete energy transfer between the host and dopant in the device. Interestingly, small-molecule iridium(III) complexes derived from hole-transporting carbazole unit are attracting more recent attention. In order to get multi-component molecules essential for more efficient charge transport in the EL process [3,49,50], the integration of carbazole module and emissive iridium(III) complexes seems to be a wise material choice for vacuum-evaporated or solution-processed PHOLEDs. The following sections will highlight recent advances in the synthesis and phosphorescent properties of heavy metal organometallic chelates of carbazoles. In general, carbazole derivatives with their ready structural functionalization at the 3-, 6-, or 9-position have been extensively used as the hole-transporting components in the construction of numerous photo- and electroluminescent devices.

A range of color-tunable and morphologically-stable 9-alkylcarbazole-based heteroleptic iridium(III) and platinum(II) complexes **1–10** have been prepared and spectroscopically characterized in which the hole-transporting and electrophosphorescent functional groups are hybridized into one molecule [51,52]. The crystal structures of **1**, **3** and **6** were determined by the X-ray diffraction method. A prominent color tuning of phosphorescence emission from blue-green to orange-red is made possible by simply altering the ligation of metal with carbon atom at 2- or 3-position of carbazole unit in these linkage isomers. While the carbon atoms at 2-/7- and 3-/6-position of carbazole have different electronic density, where the 3-/6-position can be activated by the nitrogen atom and hence more electron-rich than the 2-/7-site, the energy level of carbazole-containing complexes can thus be tuned by substitution at the 3-/6- or 2-/7-position. The more electron-donating 3-position on carbon of carbazole pushes up the energy of metal d orbital when it is ligated to the metal ion, resulting in a higher HOMO than that of the less electron-donating 2-position and this is accompanied by significant shifts of ~2700 and 2400 cm^{-1} in emission energy for the iridium(III) and platinum(II) complexes, respectively. This approach is different from those commonly used for other complexes in which the emission wavelength can usually be shifted by changing the electronic nature and/or position of the substituents on the cyclometalated ligands. Complexes **1**, **3**, **5** and **6** have been used as phosphorescent dopants in a configuration of ITO/NPB/dopant:CBP/BCP/Alq_3/LiF/Al which can attain very high efficiencies. A maximum external quantum efficiency (η_{ext}) of 11.0%, luminance efficiency (η_L) of 31.6 cd A^{-1}, power efficiency (η_P) of 19.0 lm W^{-1} can be achieved for the green-emitting **3**-doped device whereas the corresponding values are 13.1%, 35.8 cd A^{-1} and 25.0 lm W^{-1} for the orange-emitting complex **5**. The device made from **5** represents one of the best devices based on platinum(II) cyclometalates reported so far. The remarkable device performance indicates the advantage of the carbazole ligand fragment which has the capability of improving the hole-transporting ability, and thereby facilitating the charge trapping across the bulk for high-performance PHOLEDs. Phosphors **1–4** together with the structurally related compounds **7–10** are also found to be solution-processible emitters and have been used for making PLEDs [53]. The PL spectra of **9** and **10** show vibrational fine structures, suggesting that these complexes emit from a mixed ^{3}MLCT/$^3(\pi-\pi^*)$ state with more $^3(\pi-\pi^*)$ character than those in **2** and **4**, owing to the increase in ligand size. PLEDs based on **1–4** doped in a blend of 2-(4-biphenylyl)-5-(4-*tert*-butylphenyl)-1,3,4-oxadiazole (PBD) and non-conjugated PVK or conjugated silsesquioxane-terminated poly(9,9-dioctylfluorene) host matrix are highly efficient with peak efficiencies of 6.4% and 6.0 cd A^{-1} for **2** and 9.6% and 21.4 cd A^{-1} for **4**. The increased morphological stability of **2** and **4** and the improved compatibility between the polymer host and the complexes imparted by the long *N*-decyl chains of carbazole can give rise to better device performance than that for their shorter chain analogues **1** and **3** under an identical device configuration. In a similar study, Bryce et al. have fabricated solution-processed PLEDs doped with the homoleptic iridium phosphors **7** and **8** which showed EL peaks at 590 and 500 nm, respectively, with poorer η_{ext} values of 1.3 and 0.06% in a simpler device structure of ITO/PEDOT:PSS/PSBF:TAD:**7** or **8**/Ba/Al (PEDOT:PSS = poly(ethylenedioxythiophene)–poly(styrenesulfonic acid), PSBF:TAD = polyspirobifluorene:bis(triphenyl)diamine) [54]. The higher turn-on voltage and lower device conductivity of **7**-doped devices indicate a greater degree of exciton trapping for **7** as compared to **8**, due to the lower triplet state energy of **7**. The marked difference in OLED performance between the devices doped with **7** and **8** is attributed to the relative degree of energy transfer between the host and guest species.

Different from other common iridium(III) complexes, a rarely studied six-membered chelated iridium complex containing aza-aromatic ligands **11** (onset decomposition temperature T_d ~360 °C) is also known which exhibits significant solvent quenching effect in degassed CH_2Cl_2 solution at room temperature [55]. This

Table 1
Photophysical and frontier orbital energies of various multi-component metallophosphors and metallopolymers[a].

	Medium	Absorption (293 K) λ_{abs} [nm]	Emission λ_{em} [nm] 293 K (color)	Φ_P	τ_p [μs]	HOMO[b] [eV]	LUMO[b] [eV]	Ref.
1	CH_2Cl_2	289 344 478 518	594 (orange-red)	0.02		−4.69	−2.30	[51]
2	CH_2Cl_2	289 344 478 518	594 (orange-red)	0.24	3.22 (in PVK)	−4.71	−2.31	[52]
3	CH_2Cl_2	323 420 453	511 (green)	0.22		−4.88	−2.02	[51]
4	CH_2Cl_2	323 420 453	511 (green)	0.31	1.57 (in PVK)	−4.86	−2.04	[52]
5	CH_2Cl_2	274 335 383 452	560 (orange)	0.19		−4.91	−2.49	[51]
6	CH_2Cl_2	299 326 373 400	493 526sh (blue-green)	0.16		−5.03	−2.34	[51]
7	Toluene	335 350 445 468 520 565	590 (orange-red)	0.28	3.2			[54]
8	Toluene	320 330 350 385 425 460 500	505 (orange-red)	0.39	1.9			[54]
9	CH_2Cl_2	300 341 450	548 (yellow)	0.26	3.04 (in PVK)	−5.03	−2.35	[53]
10	CH_2Cl_2	269 332 454	540 (yellow)	0.32	2.87 (in PVK)	−4.86	−2.04	[53]
11	Film	300 360	538 (yellow-green)	0.05				[55]
12	CH_2Cl_2	378	504 (green)	0.38				[56]
13	CH_2Cl_2	322 378 430	520 (yellow-green)	0.52	0.18			[57]
14	CH_2Cl_2	291sh 316 398sh	515 (green)	0.43	0.46	−4.87	−2.24	[58]
15	CH_2Cl_2	281sh 315 400sh	514 (green)	0.33	0.54	−4.93	−2.31	[58]
16	CH_2Cl_2	286 318 399sh	514 (green)	0.43	0.21	−4.93	−1.95	[59]
17	CH_2Cl_2	288 312 402sh	528 (yellow-green)	0.30	0.16	−5.04	−2.08	[59]
18	CH_2Cl_2	293 315 396sh	506 (green)	0.47	0.18	−4.88	−1.84	[59]
19	CH_2Cl_2	250 301 325 358 435	515 (green)	0.41	0.05	−5.03	−1.94	[59]
20	CH_2Cl_2	300 325 356 434sh	514 (green)	0.45	0.16	−5.03	−1.98	[59]
21	CH_2Cl_2	302 323 434sh	515 (green)	0.41	0.27	−5.03	−1.98	[59]

Table 1 (*Continued*)

	Medium	Absorption (293 K) λ_{abs} [nm]	Emission λ_{em} [nm] 293 K (color)	Φ_P	τ_p [μs]	HOMO[b] [eV]	LUMO[b] [eV]	Ref.
22	CH_2Cl_2	308 356 398 440sh	531 (yellow-green)	0.35	0.22	−5.10	−2.15	[59]
23	CH_2Cl_2	297 325 359 424sh	506 (green)	0.41	0.20	−5.01	−1.92	[59]
24	CH_2Cl_2	239 322 375 405sh 475	567 (orange)	0.19	0.58	−5.20	−2.20	[60]
25	CH_2Cl_2	234 268 327 388 450sh	620 (red)	0.19	0.68	−4.96	−2.43	[62]
26	CH_2Cl_2	234 267 328 393 455sh	624 (red)	0.16	0.72	−4.94	−2.43	[62]
27	CH_2Cl_2	232 331 363 399 499sh	628 (red)	0.30	0.79	−5.04	−2.49	[62]
28	CH_2Cl_2	232 265 321 364 405 500sh	628 (red)	0.27	0.82	−5.01	−2.49	[62]
29	CH_2Cl_2	263 296	523 (THF) (green)	0.65 (THF)	0.99 (film)			[67]
30	CH_2Cl_2		510 (THF) (green)	0.48 (THF)	0.78 (film)			[67]
31						−5.06	−1.99	[67]
33	Film		515 (green)					[69]
34	CH_2Cl_2	239 297 313 345 376 412 457 492	520 (green)	0.65				[70]
35	CH_2Cl_2	239 297 313 349 376 414 460 493	522 (green)	0.87				[70]
36	Toluene	242 265 288 297 333 348 433 476 519 561 (CH_2Cl_2)	615 (red)	0.19	τ_1 = 0.015 τ_2 = 0.075 (film)[c]	−5.20	−3.11	[71]
37	Toluene	242 268 286 298 335 350 434	618 (red)	0.20	τ_1 = 0.012 τ_2 = 0.143 (film)[c]	−5.27	−3.19	[71]

Table 1 (*Continued*)

	Medium	Absorption (293 K) λ_{abs} [nm]	Emission λ_{em} [nm] 293 K (color)	Φ_P	τ_p [μs]	HOMO[b] [eV]	LUMO[b] [eV]	Ref.
		519 561 (CH_2Cl_2)						
38	Toluene	242 269 286 298 335 350 433 523 557 (CH_2Cl_2)	622 (red)	0.20	τ_1 = 0.024 τ_2 = 0.155 (film)[c]	−5.39	−3.32	[71]
39	CH_2Cl_2	250 370 440 530	630 (red)	0.45	0.85	−5.20	−3.09	[72]
40	CH_2Cl_2	286 342 379 420	570 (orange)	0.19	0.59			[73]
41a	CH_2Cl_2		484 (blue)	0.20		−5.45	−2.87	[74]
41b	EtOH		434 468 (77 K) (blue)		9.8 (77 K)	−5.54	−2.90	[74]
41c	EtOH		612 broad (red)			−5.58	−2.94	[74]
42a	CH_2Cl_2		521 (green)	0.19		−5.12	−2.76	[74]
42b	EtOH		435 492 (77 K) (blue)			−5.30	−2.98	[74]
42c	EtOH		456 488 (77 K) (blue)			−5.25	−2.97	[74]
43a	CH_2Cl_2		626 (red)	(0.31 in EtOH at 77 K)	17.4 (EtOH at 77 K)	−5.20	−3.09	[74]
43b	CH_2Cl_2		606 (red)	0.01 (0.76 in EtOH at 77 K)	14.4 (EtOH at 77 K)	−5.31	−3.12	[74]
43c	CH_2Cl_2		608 (red)	0.38 (0.52 in EtOH at 77 K)	15.7 (EtOH at 77 K)	−5.47	−3.28	[74]
44a	$CHCl_3$	296 343 379	468 (blue)	0.41	1.30 (THF)			[75]
44b	$CHCl_3$	395 343 382	512 (green)	0.33	1.43 (THF)			[75]
44c	$CHCl_3$	295 342 408	591 (orange-red)	0.10	1.34 (THF)			[75]
44d	$CHCl_3$	297 339 408	600 (orange-red)	0.07	3.71 (THF)			[75]
45a	CH_2Cl_2		549 587sh (yellow-orange)	0.21		−5.04	−2.28	[76]
45b	CH_2Cl_2		550 587sh (yellow)	0.25		−5.02	−2.27	[76]
46	Film		512 (green)					[77]
47a	CH_2Cl_2		553 (orange)	0.02	0.292 (THF)			[78]
47b	CH_2Cl_2		551 (orange)	0.05	0.453 (THF)			[78]
48a	CH_2Cl_2		517 (green)	0.12	0.963 (THF)			[78]
48b	CH_2Cl_2		514 (green)	0.15	1.082 (THF)			[35]
49					1.0 (1,2-dchloroethane)			[35]
50					1.2 (1,2-dichloroethane)			[35]
51					5.4 ($C_2H_4Cl_2$)			[35]
52	CH_2Cl_2	327 348 413sh	545 (yellow)	0.29	1.2			[81]
53	CH_2Cl_2	321 336 405	548 (yellow)	0.49	2.8	−5.02	−2.04	[82]
54	Toluene	330 412 449 470	545 (yellow)	0.59 (λ_{ex} = 330 nm) 0.24 (λ_{ex} = 450 nm)	2.8			[86]

Table 1 (*Continued*)

	Medium	Absorption (293 K) λ_{abs} [nm]	Emission λ_{em} [nm] 293 K (color)	Φ_P	τ_p [μs]	HOMO[b] [eV]	LUMO[b] [eV]	Ref.
55	Toluene	345 401 449 470	550 (orange)	0.61				[86]
56	Toluene	375 441 513	595 (orange-red)	0.63				[86]
57	Toluene	361 (chloroben-zene)	566 (orange)	0.16	7.4			[91]
58	Toluene	377 (chloroben-zene)	566 (orange)	0.14	7.8			[91]
59	CH_2Cl_2	360 376 450 500sh 570sh 620sh	652 (red)	0.19	0.74			[81]
60	CH_2Cl_2	327 341 407 450 477	563 (orange)	0.51	1.51			[57]
61	THF	313 382 456 500 547 600	625 (red)	0.11	1.31 (2-MeTHF)	−5.01	−2.58	[92]
62	CH_2Cl_2	218 239 373 438 498 532	649 (red)	0.103		−4.82	−2.87	[93]
63	CH_2Cl_2	250 370 440 530	633 (red)	0.43	0.23	−5.31	−3.20	[72]
64	THF		530 (yellow-green)	0.76				[74]
65	Film		321			−5.53	−3.39	[95]
67a	Film	380	445 (blue)	0.401	0.0024			[95]
67b	Film	380	624 (red)	0.061	1.51	−5.80	−2.19	[95]
67c	Film	380	625 (red)	0.050	1.20	−5.80	−2.20	[95]
67d	Film	380	628 (red)	0.047	1.10	−5.78	−2.22	[95]
67e	Film	380	629 (red)	0.035	1.01	−5.77	−2.23	[95]
67f	Film	380	631 (red)	0.031	0.52	−5.76	−2.25	[95]
68	Toluene	267 340	594 (orange-red)	0.08	1.34			[96]
69	Toluene	270 328 387	599 (orange-red)	0.11	2.56			[96]
70a	Film	384	443w (blue) 620 (red)	0.12	$\tau_1 = 3.8$ $\tau_2 = 0.9$[c]			[97]
70b	Film	384	443w (blue) 620 (red)	0.19	$\tau_1 = 3.7$ $\tau_2 = 0.9$[c]			[97]
70c	Film	384	443w (blue) 620 (red)	0.22	$\tau_1 = 4.3$ $\tau_2 = 1.5$[c]			[97]
70d	Film	391	443w (blue) 620 (red)	0.40	$\tau_1 = 4.0$ $\tau_2 = 0.9$[c]			[97]
71a	Film	380	440 (blue) 590 (orange)					[98]
71b	Film	380	440 (blue) 590 (orange)					[98]
71c	Film	380	440 (blue) 590 (orange)					[98]
72a	Film	380	450 (blue) 565 (orange) 591sh					[98]

Table 1 (*Continued*)

	Medium	Absorption (293 K) λ_{abs} [nm]	Emission λ_{em} [nm] 293 K (color)	Φ_P	τ_p [μs]	HOMO[b] [eV]	LUMO[b] [eV]	Ref.
72b	Film	380	450 (blue) 565 (orange) 591sh					[98]
72c	Film	380	450 (blue) 565 (orange) 591sh					[98]
73	$CHCl_3$	343 386 450sh 515sh	607 (red)					[99]
74	Toluene	293 375	425 (blue) 440sh 517 (green)					[100]
75a	Toluene	293 375	426 (blue) 439sh 611 (red)					[100]
75b	Toluene	289 375	425 (blue) 439sh 613 (red)					[100]
76	CH_2Cl_2	294 342 398 463	552 (orange) 593sh	0.20	0.09	−5.04	−2.65	[101]
77	CH_2Cl_2	293 347 466	562 (orange) 605sh	0.12	0.09	−4.96	−2.54	[101]
78	CH_2Cl_2	294 347 466	560 (orange) 604sh	0.10	0.12	−5.09	−2.72	[101]
79	CH_2Cl_2	295 366 466	566 (orange) 608sh	0.09	0.13	−5.06	−2.67	[101]
80a	CH_2Cl_2	294 347 471	621 (red)	0.027 (film)		−5.35	−2.99	[103]
80b	CH_2Cl_2	294 346 466	622 (red)	0.027 (film)		−5.35	−2.99	[103]
81	CH_2Cl_2		553 581sh (orange)	0.10		−5.34	−2.12	[76]
82	Toluene	350 360 400 418 465 490 550	560 (orange)	0.30	4.8			[54]
83	Toluene	362 382 415 425 465 490 550	565 (orange)	0.39	7.4			[54]
84	Toluene	348 360 395 420 460 490 550	560 (orange)	0.32	4.4			[54]
85	Toluene	360 370 420 460 490 550	565 (orange)	0.31	6.6			[54]
86	CH_2Cl_2	320	524 (green)	0.75				[104]
87	CH_2Cl_2	320	510 (green)	0.68				[104]
88	CH_2Cl_2	320	512 (green)	0.66		−5.05	−2.14	[104]

Table 1 (*Continued*)

	Medium	Absorption (293 K) λ_{abs} [nm]	Emission λ_{em} [nm] 293 K (color)	Φ_P	τ_p [μs]	HOMO[b] [eV]	LUMO[b] [eV]	Ref.
89	Toluene	263 294 332 345 355sh	594 (orange-red)	0.08	1.39			[96]
90	Toluene	263 294 330 345 385	599 (orange-red)	0.11	2.76			[96]
91 (0.5 mol% Ir in feed)	CH_2Cl_2	350	415 (blue) 595w (orange-red)	0.29		−5.46	−2.24	[105]
92 (0.5 mol% Ir in feed)	CH_2Cl_2	350	420w (blue) 610 (red)	0.56		−5.49	−2.26	[105]
93 (0.5 mol% Ir in feed)	CH_2Cl_2	350	420w (blue) 580 (orange)	0.65		−5.53	−2.20	[105]
94 (0.5 mol% Ir in feed)	CH_2Cl_2	385	435 (blue) 610 (red)	0.60		−5.74	−2.21	[105]
95 (0.2 mol% Ir in feed	CH_2Cl_2	350	580 (orange)	0.62		−5.75	−2.20	[105]
96a	Film	390	440 (blue) 580w (orange-red)					[106]
96b	Film	390	440 (blue) 580w (orange-red)					[106]
96c	Film	390	440 (blue) 580w (orange-red)					[106]
96d	Film	390	440 (blue) 580w (orange-red)					[106]
97a	Film	390	440 (blue) 520w (green)					[106]
97b	Film	390	440 (blue) 520w (green)					[106]
97c	Film	390	440 (blue) 520w (green)					[106]
97d	Film	390	440 (blue) 520 (green)					[106]
97e	Film	390						[106]
98 (0.5 mol% Ir in feed)	CH_2Cl_2	346	588 (orange)	0.203 ($CHCl_3$)		−5.47	−2.41	[107]
99 (0.5 mol% Ir in feed)	CH_2Cl_2	349	619 (red)	0.238 ($CHCl_3$)		−5.49	−2.41	[107]
100a	Film		420 (blue) 520 (green) 660 (red)					[108]
100b	Film		420 (blue) 520 (green) 660 (red)					[108]
100c	Film		420 (blue) 520 (green) 660 (red)					[108]
100d	Film		420 (blue) 520 (green) 660 (red)					[108]
100e	Film		420 (blue) 520 (green) 660 (red)					[108]
101 (0.5 mol% Ir in feed)	Film	350	620 (red)	0.238 ($CHCl_3$)		−5.49	−2.41	[109]
102 (1.0 mol% Ir in feed)	Film	350	410 (blue) 575 (orange)	0.25		−5.56	−2.50	[110]
103 (1.0 mol% Ir in feed)	Film	350	410 (blue) 575 (orange)	0.31		−5.50	−2.45	[110]
104a (3.0 mol% Ir in feed)	Film	270 320 420	532 (green) 574sh	0.20				[111]
104b (3.0 mol% Ir in feed)	Film	260 310 430	531 (green) 567sh	0.34				[111]

Table 1 (*Continued*)

	Medium	Absorption (293 K) λ_{abs} [nm]	Emission λ_{em} [nm] 293 K (color)	Φ_P	τ_p [μs]	HOMO[b] [eV]	LUMO[b] [eV]	Ref.
104c (3.0 mol% Ir in feed)	Film	260 330 420	531 (green) 569sh	0.27				[111]
105 (5.0 mol% Ir in feed)	Film	350 450	560 (orange) 601sh	0.09				[111]
106a	Film	385	632 (red)	0.138	1.43	−5.36	−1.78	[112]
106b	Film	385	632 (red)	0.057	1.44	−5.35	−1.77	[112]
106c	Film	385	631 (red)	0.047	1.01	−5.34	−1.77	[112]
106d	Film	385	635 (red)	0.042	0.99	−5.34	−1.78	[112]
107	Film		625 (red)					[112]
108	Film	345	638 (red)	0.075	0.98	−5.13	−1.52	[112]
109c	Film	383	422 444sh (blue) 622 (red)					[113]
110	CH_2Cl_2	262 269 320 367 399 450	528 (yellow-green)	0.13	0.10	−4.95	−1.81	[115]
111	CH_2Cl_2	247 287 384 471 503	525 (yellow-green)	0.70	0.18	−5.25	−2.24	[115]
112	CH_2Cl_2	297 336 407 506	591 (orange-red)	0.25	0.12	−5.29	−2.29	[d]
113	CH_2Cl_2	255 293 388 465 502	530 (yellow-green)	0.48	0.11	−5.03	−1.92	[115]
114	CH_2Cl_2	253 291 388 465 502	525 (green)	0.53	0.11	−5.04	−1.92	[115]
115	CH_2Cl_2	243 290 364 400 476	497 (blue-green)	0.57	0.10	−5.15	−1.97	[115]
116	CH_2Cl_2	251 289 322 376 423 499	520 (green)	0.42	0.15	−5.15	−2.12	[115]
117	CH_2Cl_2	247 285 388 473 506	527 (yellow-green)	0.91	0.25	−5.45	−2.48	[115]
118	Toluene	257 301 379 393 450	533 (yellow-green)	0.14	5.00	−5.11	−1.98	[122]
119	Toluene	261 274 280 353 393 420 476 510	541 (yellow)	0.19	2.56	−5.38	−2.40	[116]

Table 1 (*Continued*)

	Medium	Absorption (293 K) λ_{abs} [nm]	Emission λ_{em} [nm] 293 K (color)	Φ_P	τ_p [μs]	HOMO[b] [eV]	LUMO[b] [eV]	Ref.
120	Toluene	289 334 419 513 576sh	605 (red)	0.18	2.67	−5.16	−2.39	[116]
121	Toluene	264 272 281 349 414 473 508	535 (yellow-green)	0.39	2.44	−5.18	−2.11	[116]
122	Toluene	263 279 347 412 467 505	530 (yellow-green)	0.40	2.17	−5.22	−2.08	[116]
123	Toluene	282 403 430 481	505 (green)	0.40	1.66	−5.22	−2.00	[116]
124	Toluene	255 291 322 414 445 502	527 (yellow-green)	0.52	2.53	−5.21	−2.08	[116]
125	Toluene	263 280 356 395 422 478 513	550 (orange)	0.86	2.69	−5.46	−2.54	[116]
126	CH_2Cl_2	375sh	509 (green)	0.17				[56]
127	CH_2Cl_2	275 360 469	518 (green)					[122]
128	CH_2Cl_2	303 400 495	585 (orange)					[122]
129	CH_2Cl_2	300 503	611 (red)					[122]
130	CH_2Cl_2	312 439 580	671 (red)					[122]
131	CH_2Cl_2	300 420 470	555 (orange)					[122]
132	CH_2Cl_2	300 422 448 520	636 (red)	0.13	1.21	−4.99	−2.34	[125]
133	CH_2Cl_2	312 376 436 461 530	641 (red)	0.12	1.40	−4.96	−2.38	[125]
134	CH_2Cl_2	293 327 409 471	620 (red)	0.023	0.91			[57]
137	CH_2Cl_2	246 291 361 418 456	520 548sh (green)	0.283		−5.04	−2.55	[138]
138	CH_2Cl_2	251 296 367 422 454	518 545sh (green)	0.326		−5.05	−2.54	[138]

Table 1 (*Continued*)

	Medium	Absorption (293 K) λ_{abs} [nm]	Emission λ_{em} [nm] 293 K (color)	Φ_P	τ_p [μs]	HOMO[b] [eV]	LUMO[b] [eV]	Ref.
139	CH_2Cl_2	248 296 365 410 443	501 536sh (blue-green)	0.132		−5.25	−2.52	[138]
140	CH_2Cl_2	250 300 373 412 445	507 538sh (green)	0.195		−5.22	−2.53	[138]
141	CH_2Cl_2	246 298 355 424 465	500 529sh (blue-green)	0.35		−5.30	−2.45	[139]
142	CH_2Cl_2	230 312 369 432 468	479 510sh (blue)	0.44		−5.47	−2.40	[139]
143	CH_2Cl_2	238 323 402 436 472	470 501sh (blue)	0.32		−5.52	−2.39	[139]
144	CH_2Cl_2	241 313 397 434 469	466 498sh (blue)	0.10		−5.57	−2.38	[139]
145	THF	267 289 415	524 (yellow)	0.41				[140]
146	THF	269 300 407	512 (green)	0.10				[140]
147	THF	290 397	508 (green)	0.33				[140]
148	THF	290 415	519 (yellow)	0.19				[140]
149	THF	266 293 410	516 (green)	0.12				[140]
150	THF	261 315 477	569 (orange)	0.28				[140]
151	THF	290 344 445	536 (yellow-green)	0.65				[140]
152	CH_2Cl_2	388	497 (blue-green)	0.001		−5.79	−3.36	[141]
153	CH_2Cl_2	409	474 (blue)	0.003		−5.38	−3.45	[141]
154	CH_2Cl_2	309 375 415 478sh	555 595sh (orange)	0.12	0.08	−4.95	−2.93	[142]
155	CH_2Cl_2	297 387 408sh 478sh	564 607sh (orange)	0.13	0.11	−5.06	−3.13	[142]
156	CH_2Cl_2	303 364 382 415 435	498 569 628sh (yellow-green)	0.039	58.3	−5.12	−2.36	[144]
157	CH_2Cl_2	305 368 387 423 440	516 570sh 632sh (yellow-green)	0.086	54.6	−5.06	−2.38	[153]
158	CH_2Cl_2	311 326 363sh 405 422	538 582sh 624sh (yellow)	0.17	25.0	−5.29	−2.34	[153]

Table 1 (*Continued*)

	Medium	Absorption (293 K) λ_{abs} [nm]	Emission λ_{em} [nm] 293 K (color)	Φ_P	τ_p [μs]	HOMO[b] [eV]	LUMO[b] [eV]	Ref.
159	CH_2Cl_2	264 297 402 443	568 603sh (orange)	0.11	0.02	−5.22	−2.89	[150]
160	CH_2Cl_2	270 298 403 441	570 605sh (orange)	0.05	0.01	−5.20	−2.92	[150]
161	CH_2Cl_2	309 390 475	544 583sh (yellow-orange)	0.26	1.3	−5.15	−2.20	[151]
162	CH_2Cl_2	309 395 483	551 589sh (orange)	0.21	1.1	−5.14	−2.30	[151]
163	CH_2Cl_2	309 375 455 559	649 (red)	0.21	1.0	−5.09	−2.48	[151]
164	CH_2Cl_2	309 364 406 422	540 580sh (yellow-orange)	0.18	8.2	−5.15	−2.38	[151]
165	Film	342 440	675 (red)			−5.55	−3.55	[152]
166	Film	364 478	670 (red)			−5.65	−3.45	[152]
170	CH_2Cl_2	293 370	429sh 533 573sh (yellow-green)	0.03	3.1	−5.50	−2.77	[156]
171	CH_2Cl_2	294 372	471sh 533 570sh (yellow-green)	0.02	7.0	−5.42	−2.72	[156]
172	CH_2Cl_2	295 381	496sh 534 571sh (yellow-green)	0.02	5.4	−5.29	−2.64	[156]
173	CH_2Cl_2	294 385	468sh 534 572sh (yellow-green)	0.7	3.1	−5.05	−2.48	[156]
174	CH_2Cl_2	322 341 421sh	422sh 533 573sh (yellow-green)	0.5	4.9	−5.69	−2.74	[156]
175	CH_2Cl_2	307 337 421	479 535 (yellow-green)	0.5	4.1	−5.09	−2.45	[156]

[a] sh = shoulder peak.
[b] The HOMO and LUMO energies were estimated by cyclic voltammetry.
[c] τ_1,τ_2: lifetimes were obtained by an exponential fit of emission decay curves. [d]Unpublished data.

phenomenon can be attributed to the bipolar structure derived from the electron-rich nitrogen atom and the electron-deficient metal framework, so that rapid energy-transfer quenching, probably incorporating internal conversion and solvent collision deactivation, occurs. Interesting emission color tuning from yellow at 570 nm for the doped OLED device (10 wt.% **11**) to the red at 652 nm for the non-doped device is observed, which is presumably due to the solid-state solvation effect. Complex **12** was also synthesized in which the 9-carbazole ring serves as a potential hole-trapping moiety for *fac*-[Ir(ppy)$_3$] [56]. The Φ_P of **12** is comparable to that of *fac*-[Ir(ppy)$_3$] but its PL peak is slightly blue-shifted by about 370 cm^{-1}. The oxidation state of **12** becomes more unstable due to the addition of carbazole unit (E_{ox} = 0.48 and 0.32 for **12** and *fac*-[Ir(ppy)$_3$], respectively). PHOLEDs doped with **12** (12 wt.%) gave a peak η_{ext} of 9.1% at 4.8 V and a luminance of 14,600 cd m^{-2} at 13.6 V using 1,1-bis[4-(di-*p*-tolylamino)phenyl]cyclohexane (TAPC) as the hole-transport layer. In another report, Lin and co-workers have described the use of **13** containing benzoimidazole-carbazole mixed ligands in PHOLED applications [57]. Phosphor **13** possesses high Φ_P of 52% in toluene at 293 K and its EL spectrum shows a green-yellow signal at ~530 nm with narrow full width at half maximum (fwhm) of 80 nm. The device using 9,9-bis{4-[di(*p*-biphenyl)aminophenyl]fluorene (BPAPF) as the hole-transporting layer gave impressive efficiencies of 12.1% and 44 cd A^{-1} at 20 mA cm^{-2}.

Recently, some electrophosphorescent multi-component iridium(III) guest complexes **14–28** based on the rigid 2-[3-(*N*-arylcarbazolyl)]pyridine possessing dual functions (i.e. light emission and hole transportation) are available in the literature, and they show improved charge-transporting properties and morphological stability [58–62]. The synthetic yields for these phosphors are moderate to good. The X-ray crystal structures of **14**, **18**, **24**, **25** and **27** were successfully established. All of them were oxidized at less positive potentials than the parent iridium(III) ppy and 1-phenylisoquinolinato (piq) complexes without the electron-rich and electron-donating carbazole ring, indicating a greater propensity for these complexes to lose an electron and to have a lower ionization potential. This would lead to their better hole-transporting abilities to favor the transport of holes and thus these complexes can serve as promising dual functional triplet emitters.

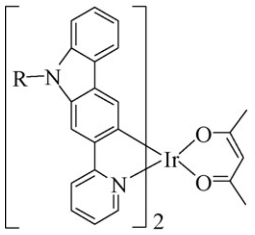

R = C_2H_5 **1**, $C_{10}H_{21}$ **2**

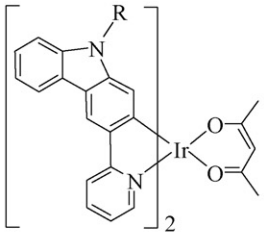

R = C_2H_5 **3**, $C_{10}H_{21}$ **4**

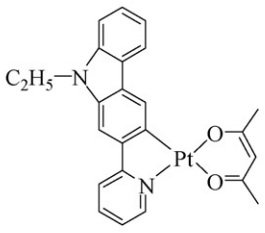

5

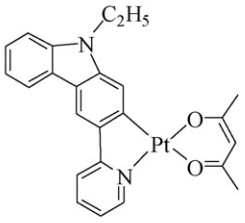

6

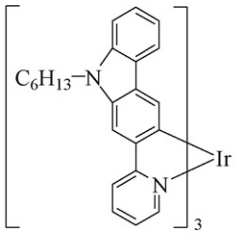

7

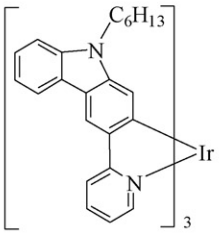

8

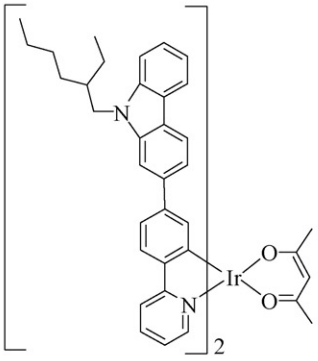

9

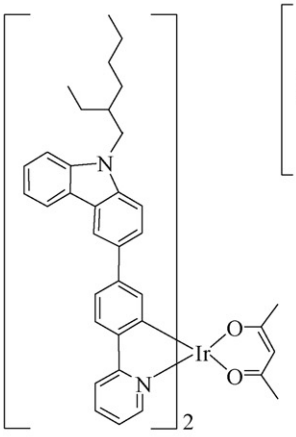

10

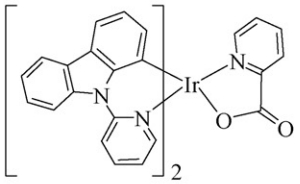

11

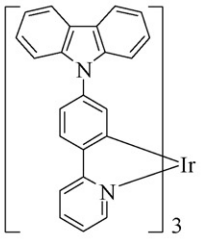

12

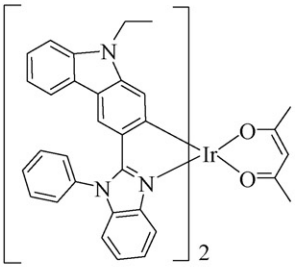

13

As far as the emission properties of **14–28** are concerned, green-emitting metal chelates **14** and **15** emit strong phosphorescence (λ_{em} ~514 nm) at room temperature in both solution and solid states [58]. The first triplet energy levels (T_1 ~2.41 eV) of both complexes are close to each other and that of *fac*-[Ir(ppy)$_3$] (2.43 eV). The Φ_P values of **14** and **15** in CH_2Cl_2 are ca. 0.33–0.43, relative to *fac*-[Ir(ppy)$_3$]. Each of the phosphors **14** and **15** shows a sharp EL peak at 508 (fwhm = 56 nm) and outstanding EL performance, presumably thanks to the short τ_P and good hole-transporting properties of carbazole, which may help diminish the quenching of the triplet exciton. The performance parameters of the device can reach a maximum η_{ext} of 11.6%, η_L of 38.0 cd A^{-1} and η_P of 23.9 lm W^{-1}, which outweigh those of *fac*-[Ir(ppy)$_3$]-based device by as much as 55% in η_{ext} under a similar device structure [18]. Presumably, the carbazolyl structural moiety brings about a more balanced electron and hole recombination in the host matrix of CBP, and/or that the rigid carbazole spacers play a crucial role in alleviating the self-quenching of the luminophores, and consequently increase the EL efficiency. Given the ease of synthesis and performance advantage inherent to these carbazole-based phosphors, extension of the system to other emission colors is particularly challenging. There are thus many merits of this prominent class of carbazole-based Ir phosphors in high-efficiency PHOLED applications.

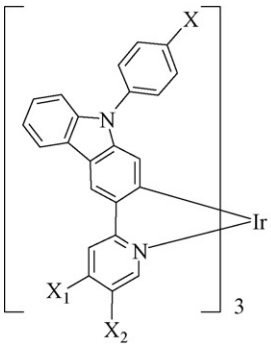

$X = X_1 = X_2 = H$ **14**
$X = F, X_1 = X_2 = H$ **15**
$X = Me, X_1 = X_2 = H$ **16**
$X = X_1 = H, X_2 = F$ **17**
$X = X_2 = H, X_1 = Me$ **18**

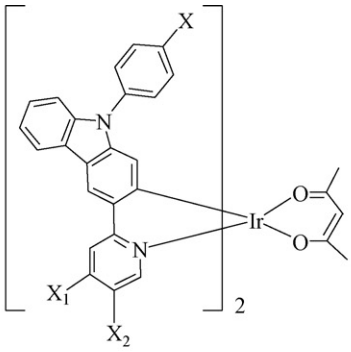

$X = X_1 = X_2 = H$ **19**
$X = F, X_1 = X_2 = H$ **20**
$X = Me, X_1 = X_2 = H$ **21**
$X = X_1 = H, X_2 = F$ **22**
$X = X_2 = H, X_1 = Me$ **23**
$X = X_1 = H, X_2 = CF_3$ **24**

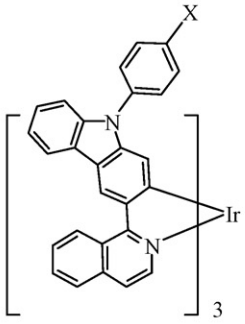

X = H **25**
X = OMe **26**

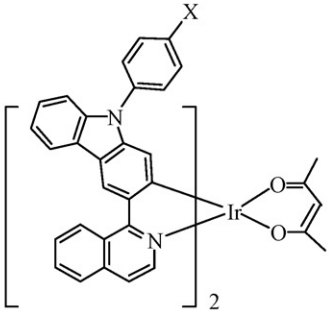

X = H **27**
X = OMe **28**

Another series of homoleptic and heteroleptic cyclometalated iridium(III) complexes containing fluoro- or methyl-substituted 2-[3-(*N*-phenylcarbazolyl)]pyridine molecular framework (**15–18** and **20–23**) has also been described in order to study the substituent effect of carbazole ring on the emission characteristics of the resulting metallophosphors [59]. The optical, electrochemical, photo- and electrophosphorescence traits of these iridium phosphors have been elucidated as a function of the electronic nature and coordinating site of the aryl or pyridyl ring substituents. The emission properties of these phosphors were correlated with the results of density functional theory (DFT) calculations. We also paid special attention to the effect of isomerism in governing the functional properties of these phosphors and the resulting device performance. Changing the substituents on the phenyl ring of 9-phenylcarbazole, no matter whether they are fluoro or methyl groups, does not show much influence on the emission spectral features for **15–16** (or **20–21**). These results indicate that the 9-phenyl ring substituent on the carbazole unit plays a minor role in governing the energy of the lower-lying transitions, plausibly due to the blocking of electronic conjugation from the carbazolyl nitrogen atom. For their corresponding geometrical isomers **17–18** (or **22–23**), we note, however, that a greater substituent effect on the emission position is achieved by attaching F or Me group to the pyridine ring. While the pyridine ring contributes mostly to the LUMO level, the electron-withdrawing fluoro group tends to lower the LUMO energy and thereby decreases the energy gap of the emitting excited state (**15** versus **17**, $\Delta\lambda \sim 520\,cm^{-1}$; **20** versus **22**, $\Delta\lambda \sim 620\,cm^{-1}$). The electron-donating 4-methyl-substituted complexes **18** and **23** show the highest energy gap, resulting in a slight spectral blue shift in wavelength from that of **16** and **21**, respectively ($\Delta\lambda \sim 310\,cm^{-1}$ for both series: **16** versus **18** and **21** versus **23**). This can be attributed to the notion that an electron-donating group on pyridine would increase the LUMO energy and the HOMO–LUMO gap [33]. The steric effect of the Me group also forces the carbazole-pyridine aromatic rings out of coplanarity and twists the ligand, thus reducing delocalization and π-acceptor ability of the molecule. This makes charge transfer event more difficult that is accompanied by a spectral blue shift. PHOLEDs with outstanding device performance can be fabricated based on these 9-arylcarbazole-based materials, which show a maximum η_L of ~43.4 cd A^{-1}, corresponding to η_{ext} of ~12.9% and η_P of ~33.4 lm W^{-1} for the best device.

By incorporating a bulky, inductively electron-withdrawing CF_3 group into the pyridyl ring, an interesting orange electrophosphor can be produced for **24** [60,61]. These orange-emitting PHOLEDs can give a maximum η_L of ~40.2 cd A^{-1}, corresponding to η_{ext} of ~12.4% and η_P of ~24.0 lm W^{-1}. Saliently, it was also demonstrated that compound **24** can be used to afford high-performance simple and color-stable two-element white organic light-emitting diodes (WOLEDs) which are devoid of voltage dependence by color mixing with a complementary blue fluorescent emitter in the device configuration of ITO/MoO_3/NPB/2% **24**:CBP/NPB/0.75% DSA-Ph:ADN/BAlq/LiF/Al (DSA-Ph = *p*-bis(*p*-*N*,*N*-diphenyl-aminostyryl)benzene, ADN = 9,10-di(2-naphthyl)anthracene, BAlq = bis(2-methyl-8-quinolinato)-(1,1′-biphenyl-4-olato)aluminum). The white light devices exploit exciton-managed blue electrofluorescence/orange electrophosphorescence (Fig. 1) and require less dyes and simpler fabrication process. By using this new device design where the host singlet is resonant with the blue fluorophore singlet state and the host triplet is resonant with the orange phosphor triplet level [63], the white light-emitting structure can achieve peak EL efficiencies of 26.6 cd A^{-1} and 13.5 lm W^{-1}. These are generally superior to other two-element all-fluorophore or all-phosphor OLED counterparts in terms of both color stability ($\Delta(x, y) < \pm(0.01, 0.01)$) and emission efficiency [64,65]. As a small device approximation, the maximum total power efficiency (η_t) of the best WOLED can reach 23.0 lm W^{-1} (versus η_t = 12–17 lm W^{-1} for a typical incandescent light bulb). If a sky blue styrylamine-type fluorescent material, BUBD-1 [64] uniformly doped in MADN is used instead with the configuration of ITO/2-TNATA/NPB/x% **24**:CBP/TPBI/3% BUBD-1:MADN/TPBI/LiF/Al (2-TNATA = tris[2-naphthyl(phenyl)amino]triphenylamine, TPBI = 1,3,5-tris[*N*-(phenyl)benzimidazole]benzene, MADN = 2-

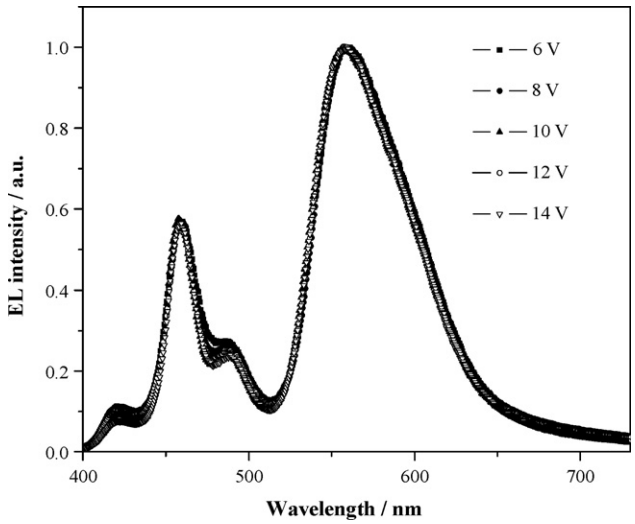

Fig. 1. EL spectra of the **24**-doped WOLED at different voltages in a configuration of ITO/MoO_3 (5 nm)/NPB (100 nm)/2% **24**:CBP (30 nm)/NPB (3 nm)/0.75% DSA-Ph:ADN (40 nm)/BAlq (10 nm)/LiF:Al (1:100 nm) (see Ref. [60]).

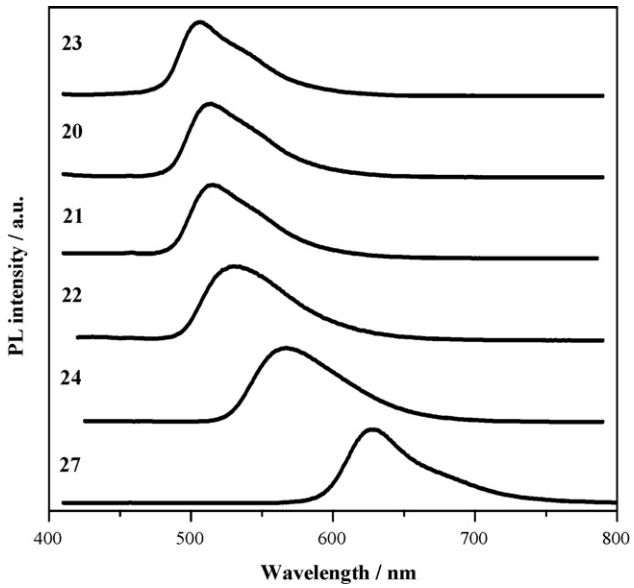

Fig. 2. Color tuning of the phosphorescence spectra of carbazole-based heteroleptic iridium(III) phosphors in CH_2Cl_2 at 293 K (see Ref. [59]).

methyl-9,10-di(2-naphthyl)anthracene), the best device reaches peak efficiencies of 7.0%, 19.3 cd A^{-1} and 11.1 lm W^{-1}. Accordingly, the peak η_t of the best devices is 18.8 lm W^{-1} [61]. Such a stratagem provides an improved color stability as the aging rate is determined by only two emitters. In these fluorescent/phosphorescent-based devices, the blue fluorescent dopant harnesses a majority of singlet excitons, with the remainder of lower energy triplets diffusing through the conductive host to directly excite the orange phosphor. Diffusion of singlet excitons to the phosphor dopant is negligible due to their intrinsically short diffusion lengths [63]. This architecture allows for increased η_P by resonant energy transfer from the host into both the singlet and triplet energy levels, thus minimizing the exchange energy losses caused by intersystem crossing from the host singlet into a blue phosphor triplet state which is commonly the case in all-phosphor-doped devices. This certainly reveals a better efficiency/color purity trade-off necessary for the future design of practical WOLEDs.

In accordance with the energy-gap law, the design and synthesis of efficient red emitters is intrinsically more difficult. Generally, a dilemma facing dopant-based red OLEDs has been realized in which efficient and bright dopants are not red enough, and red-enough dopants are not efficient and bright [66]. Highly efficient OLEDs exhibiting saturated red EL with Commission Internationale de L'Eclairage (CIE) chromaticity coordinates at $x = 0.67$, $y = 0.33$ have attracted increasing attention for their applications in full-color flat-panel displays. Very recently, highly efficient pure red PHOLEDs based on multi-component iridium(III) electrophosphors functionalized with hole-transporting carbazole modules have appeared in a seminal paper [62]. These bifunctional complexes give a peak efficiency of 11.8% with excellent CIE color coordinates of (0.68, 0.32) and offer an attractive avenue to developing metal phosphors with optimized efficiency/color purity trade-offs for the pure red-emitting devices. They were made into PHOLEDs either via vacuum thermal deposition or solution processing techniques.

To date, we have gained a comprehensive understanding of using rigid 2-[3-(*N*-arylcarbazolyl)]pyridine derivative as the building unit in the phosphorescence color tuning of iridium(III) complexes and reported highly efficient PHOLEDs spanning the color range from bluish-green to pure red based on metallophosphors **14–28** (Fig. 2). Remarkably, the excited-state properties can be manipulated through ligand and substituent effects which allow the tuning of phosphorescence energies. The present work provides a new avenue for the rational design of multi-functional iridium–carbazolyl electrophosphors by synthetically tailoring the carbazolylpyridine ring that can reveal a superior device performance coupled with good color-tuning versatility suitable for multi-color display technology.

A convergent synthetic strategy was developed by Samuel et al. for the preparation of solution-processible green phosphorescent iridium(III) dendrimers **29** (first generation, T_d ~412 °C) and **30** (second generation, T_d ~309 °C) with carbazole dendrons and 2-ethylhexyloxy surface groups [67,68]. The glass-transition temperature (T_g) of **29** is significantly higher than that found for the first-generation phenylene-based counterpart (193 versus 132 °C), which is attributed to the higher molecular mass and the rigidity imparted by the carbazole groups in the former case. No T_g was noted for the higher-generation **30** within the limits of the experiment, reflecting the increased molecular weight and number of carbazole rings in **30**. The photoluminescence (PL) properties of these carbazole-containing dendrimers have been studied relative to the model complex **31** and other dendritic systems with phenyl moieties at the branching points of the dendrons. The neat film PL quantum yields of **29** and **30** are significantly higher than those for the corresponding phenylene-derived dendrimers and such an improvement can be attributed to the increased steric demand of the carbazole ring relative to the phenyl core, which reduces more effectively the intermolecular interactions, causing the core to be less emissive. Thin film hole mobilities of **29** also appear to be higher than those of the phenylene-based counterpart. The same research team also examined the triplet–triplet annihilation in neat films of **29** using the time-resolved PL method. The triplet–triplet annihilation constant and exciton diffusion length of **29** in the film were estimated to be 30×10^{-14} cm^3 s^{-1} and 6 nm, respectively. The current density for the effect to halve the device efficiency is 2.6 A cm^{-2} and the hopping rate is 9×10^6 s^{-1}. The nearest-neighbor hopping rate decreases exponentially with intermolecular spacing, signaling that energy migration is dominated by the exchange mechanism [68].

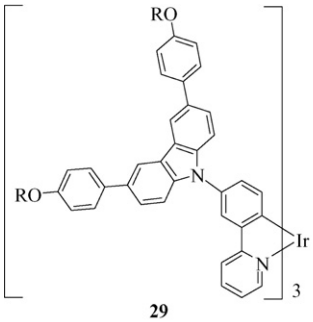

29

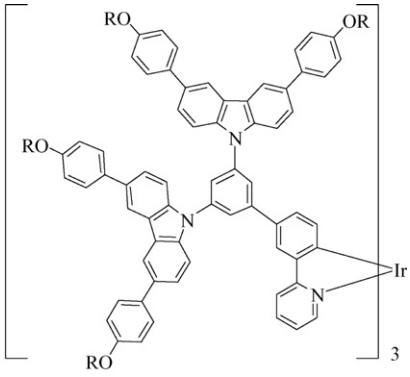

30

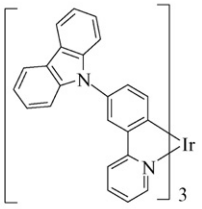

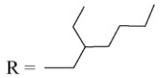

31

Two green to yellow-green multi-functional phosphorescent dendrimers **32** and **33** bearing the hole-transporting phenylcarbazole-based dendrons were also reported [69] which were superior to those with phenylene-based dendrons by allowing charge transport (or improving the hole drift mobility) via the carbazole units while retaining the phosphorescence of *fac*-[Ir(ppy)$_3$] core. Using the non-conjugated CH_2 linkage to bridge the carbazole moieties, this will render the materials more soluble and prevent the triplet energy of the dendron from decreasing. The PHOLEDs using a blend film of the first generation molecule **32** and an electron-transporting 1,3-bis[5-(4-*tert*-butylphenyl)-1,3,4-oxadiazole-2-yl]benzene (OXD-7) showed high η_{ext} at 7.6%, which is better than the peak value of 5.2% for the device from **33**. Since holes transported through the carbazole units are trapped on the *fac*-[Ir(ppy)$_3$] cores and recombine with electrons there, OXD-7 molecules capable of transporting electrons must be positioned close to the *fac*-[Ir(ppy)$_3$] cores for optimizing the efficiency. In this way, **32** will favor the recombination because its dendron size is smaller and OXD-7 molecules can be in close proximity to the iridium centers. Another pair of green-emitting dendrimers **34** and **35** has been examined by Wang et al. and a comparison was made to that for the model complex in the absence of carbazole dendrons [70]. The T_1 energy states are very similar at 2.43–2.44 eV for **34–35** and the model compound but the quantum yields increase steadily from 0.18 to 0.45 by increasing the dendron size. Both phosphors **34** and **35** can be used for the fabrication of high-performance solution-processible DLEDs. At the same luminance, the performance of **34**- and **35**-doped devices is much higher than that of the non-carbazole-containing complex. The authors attributed such an improvement to the higher Φ_P of **34** and **35** and the ability of carbazole dendritic wedges to reduce the intermolecular interactions. With neat layers of **34** and **35**, η_L values of 17.3 and 29.6 cd A^{-1} were realized, respectively, at a brightness of 100 cd m^{-2}. On doping **35** into a *N*-(4-[9,3′:6′,9″]tercarbazol-9′-yl)phenylcarbazole (TCCz) host, the peak η_L can be further increased up to 57.9 cd A^{-1}. The same research team very recently described some solution-processible red iridium(III) dendrimers **36–38** up to the third generation based on oligocarbazole host dendrons for both non-doped and doped red DLEDs and the results are compared with their zeroth-generation prototype [71]. Complexes **37** and **38** contain up to 6 and 14 carbazole rings in their structures. All of them emit bright red light in toluene and thin films, and the T_1 energy levels do not seem to vary with the dendrimer generation. A decreased red shift in λ_{em} from **36** to **38** suggests reduced aggregation between emissive metal cores upon increasing the size of the dendrons. The oligocarbazole host as the functional dendrons can take part in the redox process and charge transport of the molecules as well as controlling intermolecular interactions. Moreover, the improved performance may be attributed to the high triplet energies (>2.9 eV) of the oligocarbazole units, which prevent the back energy transfer from iridium units to the peripheral dendrons, and the unique bonding mode between the metal cores and the dendrons via *N*-position linkage so that the optoelectronic properties of the iridium groups are not significantly influenced by the dendritic structures. The best non-doped device was obtained using **38** which gave peak efficiencies of 6.3%, 4.1 cd A^{-1} and 2.4 lm W^{-1} at 5.5 V with CIE coordinates of (0.67, 0.33), and the device performance is well comparable to the best ever reported for non-doped vacuum-deposited small molecular phosphors (~6.0%). From the results of doped devices, their η_{ext} increases gradually from the zeroth-generation to the third-generation and the problem of carrier-mobility reduction with increasing dendritic size, typical of the phenylene dendrimers, may be largely relieved. The highest efficiencies at 11.8%, 13.0 cd A^{-1} and 7.2 lm W^{-1} were observed for **38** at the 5 wt.%.

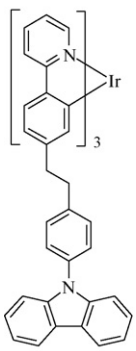

32

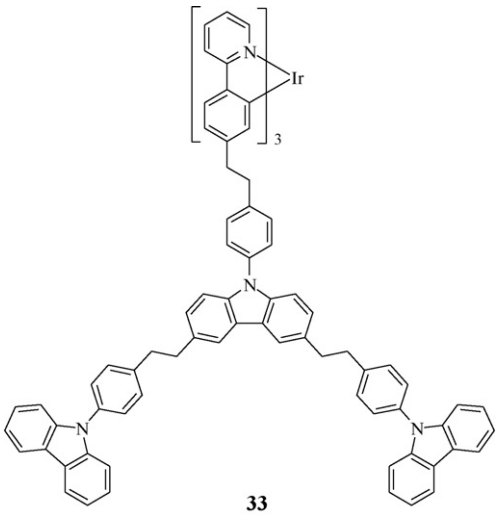

33

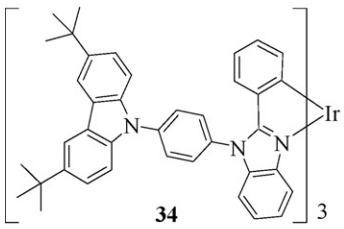

34

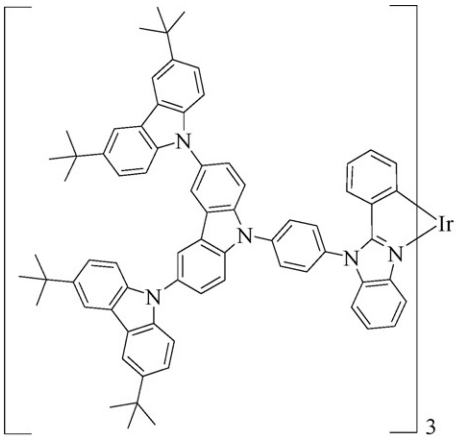

35

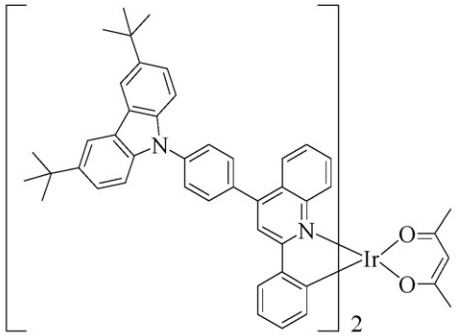

36

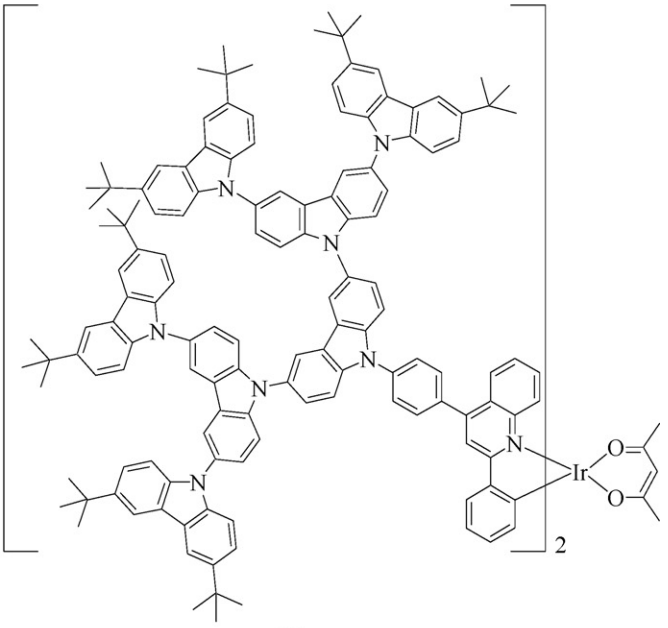

38

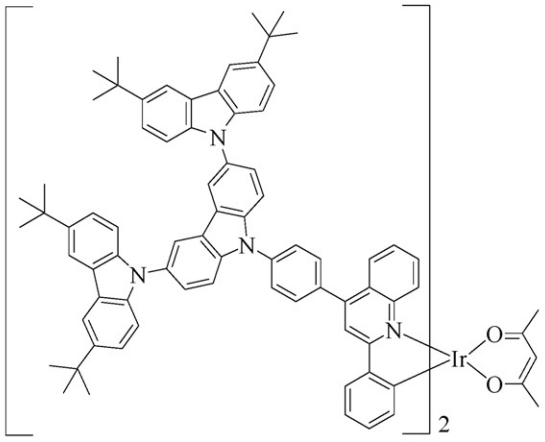

37

Apart from the above cases in which the carbazole groups are present in the cyclometalating ligands, complexes **39–43** are recent examples of heteroleptic phosphors with the carbazole modules incorporated into the third auxiliary ligand in the six-coordinate iridium(III) skeleton [72–74]. An orange-red phosphor **39**, whose structure was characterized by X-ray crystallography, was developed as a non-doped triplet emitter which can be used to build up efficient neat emissive layer PHOLEDs with peak efficiencies of 6.2% and 3.5 lm W^{-1}. This is one of the best reported power efficiency value for red emission in non-doped PHOLED devices. There is also a good sign of slow efficiency roll-off at higher current densities for such devices. To understand the role of carbazole addition, a reference complex of **39** in which the carbazole ring is replaced by a hydrogen atom to give an acetylacetonate (acac) anion was tested under the same device geometry. The lower efficiency of the reference phosphor (1.10% and 0.26 lm W^{-1}) corroborates with the notion that **39** with a bulky carbazole-functionalized β-diketonate has a better hole-transporting property and a larger exciton recombination area than the acac-congener, leading to the decrease of intermolecular interactions between emissive centers and reduction of the triplet–triplet annihilation effect. A cationic species **40** containing imidazo[4,5-f]-[1,10]phenanthroline-carbazole derivative was prepared and the effects of pH and anions on the

photophysics and electrochemistry of this complex were studied [73]. The emission wavelength of **40** was red-shifted significantly upon addition of CF_3COOH whereas the emission was quenched completely in the presence of F^-, CH_3COO^- and $H_2PO_4^-$ (with binding constants of 3.86×10^4, 3.11×10^4 and $5.78 \times 10^3\ M^{-1}$, respectively). But other anions such as halide and nitrate ions did not induce any quenching effect. The mechanisms for the chemosensing and quenching phenomenon were briefly discussed by the authors. Although **40** has not been employed for light-emitting devices, it sets out a new case in the exploration of new applications of phosphorescent chemosensors for anions. The synthesis and photophysical characterization of a series of iridium(III) complexes **41–43** with various carbazole-coordinated β-diketonates were described. This study provides an opportunity for tracing the effect of triplet energy level of diketonate ligands on the photophysical and redox behavior [74]. It was found that superposition of the state density map of the triplet energy levels between the β-diketonate and the cyclometalating ligand (C^N) is the key factor in optimizing the emission features of the complexes for the consequential OLED applications. The lowest excited state is mainly determined by C^N but not the β-diketonate unit when the energy difference between the triplet energy levels of the two parts is large. When such difference is very small, the lowest excited state is governed by both components.

A family of solution-processible norbornene-derived copolymers **44** of controllable molecular weights featuring both the phosphorescent iridium groups and a bis(carbazole)-based host material were reported [75]. This design endows good solution processibility and prevents phase separation of the metallopolymers. The fundamental phosphorescent properties of the copolymers are typical of the parent small-molecule iridium cores, and the polymer chains do not interfere with these properties. Green and red PLEDs based on all of these polymeric materials were fabricated in which the highest efficiency of 1.9% at 100 cd m^{-2} was obtained for **44c**. These demonstrate the potential of these copolymers as emissive materials for display and lighting applications.

Lu and Ding also prepared two interesting yellow-emitting dendrimers **45** in which the presence of hyperbranched oligocarbazole structure can maintain high triplet energy of the ligands so that phosphorescence quenching in **45a** and **45b** can be avoided [76]. Both amorphous dendrimers show high T_g of 182 and 223 °C, respectively. There is no sign of blue carbazole emission in the solution PL spectra of **45a** and **45b**, signaling an efficient Förster energy transfer from the oligocarbazole substituted ligands to the iridium(III) part. The EL performance of **45** was evaluated in the ITO/PEDOT:PSS/**45**:TPBI/TPBI/LiF/Al cell and the best device was obtained for **45b** showing a maximum η_L of 4.3 cd A^{-1}.

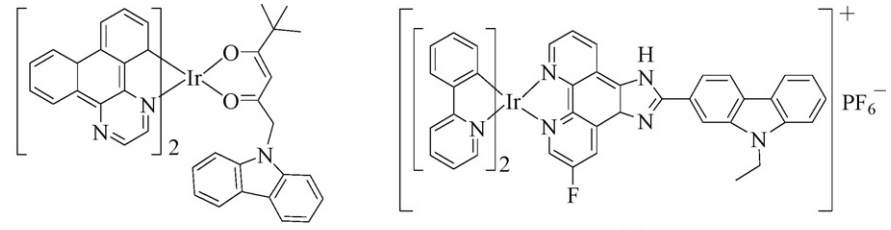

39 **40**

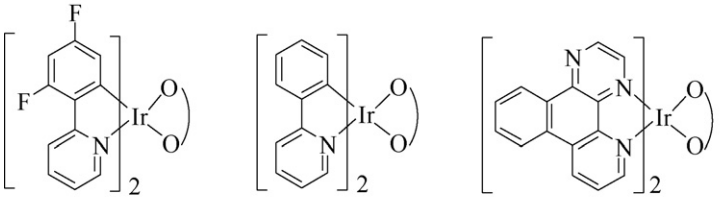

41 **42** **43**

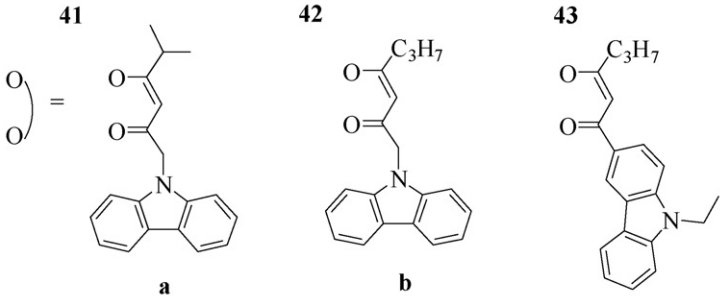

a **b** **c**

Kim et al. then prepared a vinyl-type terpolymer **46** functionalized with both carbazole and iridium(III) complexes as side groups which can be processed to make electrophosphorescent PLEDs with peak η_{ext} of 4.4% and η_P of 5.0 lm W^{-1} [77]. Comparison of the PL and EL data in solution and film provides an experimental support that the energy transfer from carbazole to iridium core occurs primarily via the intermolecular energy transfer mechanism with no sign of intramolecular energy transfer and this behaves like *fac*-[Ir(ppy)$_3$]-doped PVK. A weaker host emission in EL rather than in PL shows that not only energy transfer but charge trapping and direct formation of exciton in *fac*-[Ir(ppy)$_3$] takes place in the PLED. This work demonstrates that the idea of incorporating both triplet-emitting metal complex in a polymer backbone and fluorescent chromophore will invoke new concepts in active materials for the technological advancement of PLEDs. This would also pave the way to solve the phase separation problem commonly observed in the polymeric device. An efficient route to the synthesis of solvent-processible *fac*-[Ir(ppy)$_3$]-functionalized poly(9-vinylcarbazole)-*co*-poly(styrene)s (**47–48**) and their parent non-carbazole poly(styrene)s was developed which has potential to excel in the future PLED applications [78]. The emission wavelength of these polymers could be tuned from 550 to 515 nm by chemical reduction of the Schiff base C=N linkage of **47** to an amine group in **48**. The reduced form of the metallopolymers **48** retained the phosphorescent features of the corresponding *fac*-[Ir(ppy)$_3$] unit, although they have different localization of the excited state as revealed from the transient absorption spectroscopic studies. The copolymers containing carbazole have luminescence lifetimes that are comparable to their analogues without the carbazole, suggesting that there is no strong evidence for quenching of the ^{3}MLCT state in the iridium complex by the carbazole group. The Φ_P values of **48** (15% for **48a** and 12% for **48b**) are much larger than those for **47** (2% for **47a** and 5% for **47b**). Likewise, a set of three random copolymers **49–51** with a charge transport carbazole monomer unit and a phosphorescent iridium monomer unit in the blue (**49**), green (**50**) and red (**51**) regions were tested for their PLED performance in which the emissive layer consists of a blend of iridium-containing polymer and a suitable electron-transporting material [35]. Optimized devices for **49–51** led to η_{ext} of 3.5%, 9.0% and 5.5% for the blue, green and red colors, respectively. The authors also achieved white light emission by color mixing of **49** and **51** (in ratios of 1:0.2, 1:0.1 and 1:0.01). By controlling the energy transfer and light generation in the blue/red emissive layer, the best efficiency for white PLEDs was 4.5%.

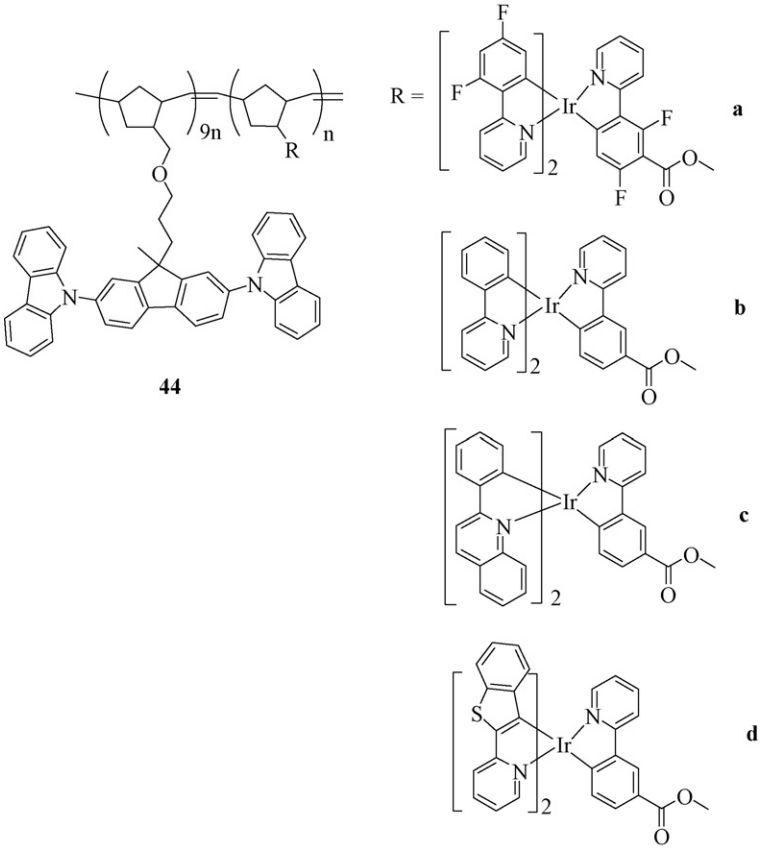

44

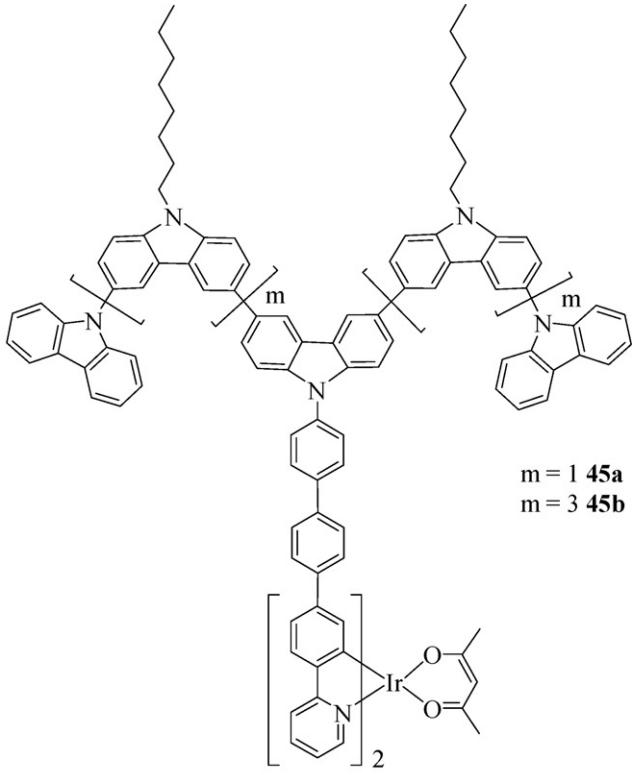

m = 1 **45a**
m = 3 **45b**

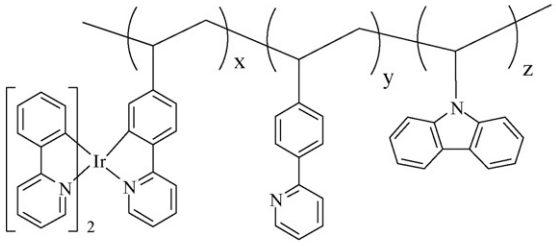

4

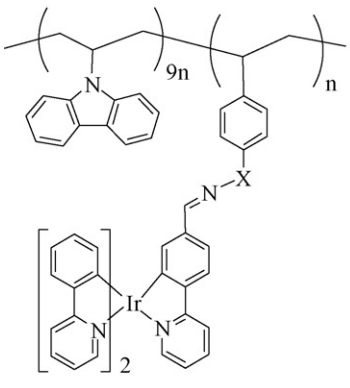

47

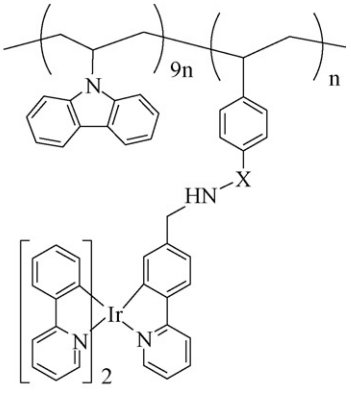

48

X = –CH_2– **a**
– $CH_2NH(CH_2)_4$– **b**

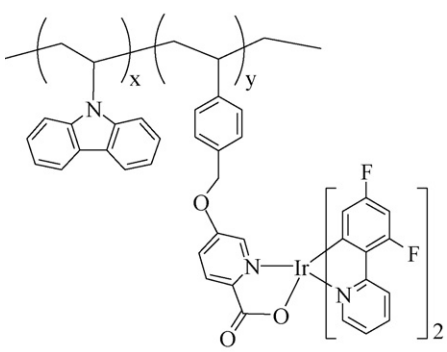

49

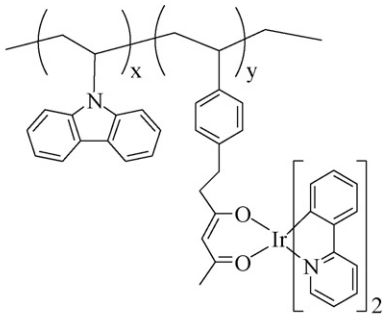

50

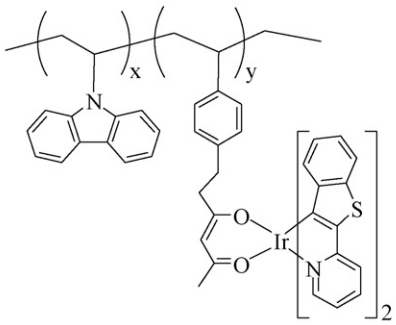

51

3.2. Fluorene

Fluorene and its derivatives offer an important contribution to the field of electronic materials [79,80]. They have attracted extensive attention for their distinguished electronic and optoelectronic activities. The ease of modification and knowledge of the structure–property relationships of polyfluorene (PF) homopolymers and copolymers continue to make the fluorene-functionalized compounds very promising candidates in the development of new functional materials. The fluorene structural moiety furnishes a rigidly planar biphenyl unit within the molecular backbone. Substituent derivatization at the C-9 position of the monomeric fluorenes provides the prospect of controlling polymer properties such as solubility, emission wavelength, processibility and mediating potential interchain interactions in thin films. They are also synthetically easily accessible and possess high thermal and chemical stability as well as high PL quantum yields. Recent research endeavor along this line has involved the use of fluorene-based chromophores which hold great promise as highly stable and efficient emissive cores in the synthesis of useful cyclometalated iridium(III) complexes.

A group of 9,9-dialkylfluorenylpyridine ligands have been employed in producing three structurally similar iridium(III) complexes **52–54** [81–83]. They all emit at 545–548 nm in the solution state and the emission wavelength is relatively independent of the alkyl chain length. A marked bathochromic shift in the emission wavelength for **52–54** relative to *fac*-[Ir(ppy)$_3$] is attributed to a larger π-conjugation system of the fluorenyl ligand. The yellow phosphor **53** was recently exploited in the fabrication of both yellow and white PHOLEDs with excellent performance [82]. The yellow-emitting device with **53** at the 2 wt.% doping concentration shows the highest η_{ext} of 10.3%, which corresponds to a peak η_L of 36.7 cd A^{-1} and η_P of 17.7 lm W^{-1}. The WOLED device consists of a four-emissive-layer architecture (made of blue, green, yellow and red colors) sandwiched by some charge-injection and charge-blocking layers without the necessity for the more sophisticated stacked design [84]. The excitons are effectively confined by the properly interposed hole-blocking material, which helps the formation of the hole limitation region. With a proper position of the hole barrier layer and the construction of a four-emission-layer structure involving the use of **53**, the resulting WOLED shows sound device performance as well as very stable color even under operation at high luminances. These WOLEDs have demonstrated superior white light color stability/efficiency trade-off optimization. The CIE coordinate differences Δx and Δy are confined to ±0.015 as the luminance increases from 13 to 14,806 cd m^{-2}. The color rendering index (CRI) of the device is also very good, which varies only very little (from 86 to 87) by changing from the normal direction to 80° off-normal at 12 V. The WOLED performance can be improved by enhancing the outcoupling efficiency (η_{OC}) in which the luminaire was optically coupled to the OLED glass substrate. Luminaire increases the amount of outcoupled light by reducing wave guiding in the glass substrate, hence enhancing η_{OC} [85]. After optimization of the WOLED device structure for the electrical and optical performance, the highest efficiencies can reach 13.0%, 23.4 cd A^{-1} and 12.4 lm W^{-1}, giving a maximum η_t of ~21 lm W^{-1}.

Two iridophosphors with fluorene-modified phenylpyridine ligands **55** and **56** were prepared [86–90]. They, together with **54**, are isolated as amorphous solids (T_g = 98, 110 and 83 °C for **54–56**, respectively) and are, therefore, resistant to crystallization [89]. Each of them shows weaker transitions red-shifted from the $^1(\pi-\pi^*)$ band, corresponding to excitation to ^{1}MLCT, ^{3}MLCT and $^3(\pi-\pi^*)$ states. Observation of the ^{3}MLCT and $^3(\pi-\pi^*)$ bands indicates strong spin-orbit coupling. Complexes **54–56** can be used in the fabrication of single-layer PHOLEDs. Modest efficiencies of 0.10, 0.04 and 0.07 cd A^{-1} were observed for **54–56**, respectively, for devices with a general architecture of ITO/PEDOT:PSS/neat Ir complex/Ca/Ag. In all cases, the quantum efficiencies are ca. 0.1%. High-efficiency yellow-green polymer-based PHOLEDs can be fabricated by doping **54** into a host polymer matrix of PVK blended with the electron-transporting PBD [89]. The highest η_{ext} was 10% at a concentration of 0.3 wt.% **54** in PVK-PBD (40 wt.%). The highest η_L of 36 cd A^{-1} (η_P of 2.5 lm W^{-1}) was observed

at 45 V. Brightness in excess of 8000 cd m^{-2} was achieved at 75 mA cm^{-2}. Emission from the dopant molecules in such devices involves localization of the injected electrons and holes on the organometallic center. No evidence of phase separation in the films of the devices was revealed by transmission electron microscopy (TEM). The same research team also reported electrophosphorescence from a polymer guest–host system with **55** as the guest and a blend of PVK and PBD as the host [86]. The PLEDs turned on at ~10 V and emitted green light at 550 nm. An η_{ext} of 8% and a η_L of 29 cd A^{-1} were achieved at 1 wt.% concentration of **55**. The devices exhibited no emission from PVK or PBD, even at 0.1 wt.% doping level of **55**. The results reveal that Förster energy transfer plays a minor role in achieving high efficiencies in these devices. Direct charge trapping appears to be the main operating mechanism. Along the same line, these authors also demonstrated red electrophosphorescent PLEDs with high brightness and promising operational stability fabricated by blending **56** with a number of copolymer hosts including poly(9,9-dihexylfluorene)-*co*-2,5-dicyanophenylene (PFO-CN), poly(9,9-dihexylfluorene) end-capped with hole-transporting ditolylbiphenylamine (PFO-HTM) and electron-transporting 5-biphenyl-1,3,4-oxadiazole (PFO-ETM) [87,88]. High-performance devices with 1 wt.% **56** in PFO-CN exhibited efficiencies of 3.0 cd A^{-1} and 1.5% at 142 cd m^{-2} [87] whereas those in PFO-HTM and PFO-ETM at the same doping level gave values at 1.4 and 1.8 cd A^{-1}, respectively, at 4.5 mA cm^{-2} [88]. These data suggest that end-capping PFO with hole-transporting and electron-transporting groups offers a good strategy for tuning the charge injection/transport without altering the electronic properties of the semiconducting polymer. The work was then extended to the small-molecule host, 6,6-dicarbazoyl-2,2′-dihexyloxy-1,1′-binaphthol, in which a bi-layered PLED containing an additional film of Alq_3 yielded a luminance of 1,830 cd m^{-2} at 30 V and a η_L of 2.5 cd A^{-1} at 18 mA cm^{-2} [90].

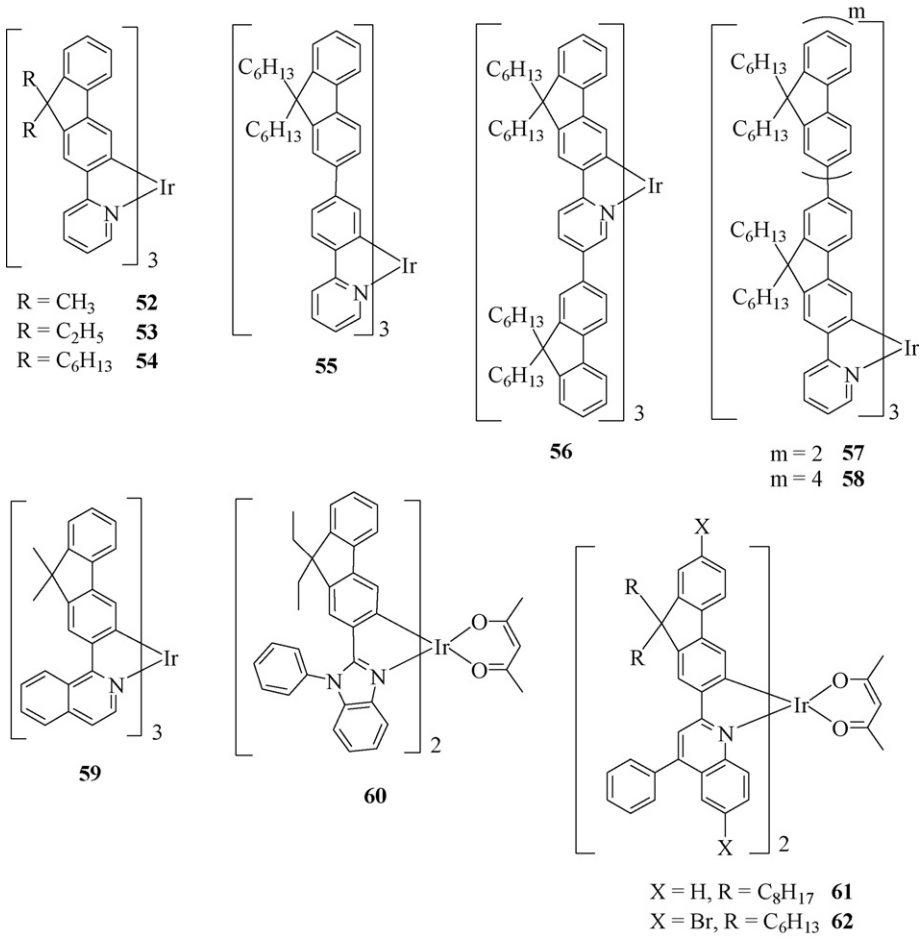

An in-depth investigation of the synthesis and photophysics of **57** and **58** with extended oligo(fluorenyl)pyridine ligands was made and the data were compared to those for the analogue **54** of smaller ligand size [91]. Their phosphorescence peaks originate from the ligand-centered $^3(\pi-\pi^*)$ states rather than ^{3}MLCT states. As the ligand length is increased from **54** to **57** and **58**, the strength of spin-orbit perturbation on intersystem crossing and hence heavy-atom effect rapidly diminish, leading to lower quantum yields. Simple PLEDs with the configuration of ITO/PEDOT:PSS/Ir complex:poly(9,9′-spirobifluorene)/Ca/Al were constructed for **54**, **57** and **58** and the best results were obtained for **58** with η_{ext} of 2.8% and η_P of 4.3 lm W^{-1} at 30 mA cm^{-2}. The peak η_{ext} values increase with the ligand length and shift to higher current densities from **54** to **57** and **58**. With longer complexes, there is less chance of energy transfer back to the host but there is more transfer with the shorter complex because the triplet energy of the phosphor is greater than that for the host. Remarkably, exploitation of **57** in the fabrication of stable and bias-independent WOLEDs has been demonstrated in which a single active blend layer of **57** with a blue-emitting fluorene-based polymer host was used. The compatibility between the iridium guest and host ensures good homogeneous mixing and the fluorene-like ligands prevent phase segregation and enhance energy transfer from the host to the guest. The maximum efficiencies obtained were 2.8% and 4.6 cd A^{-1}.

A red-emitting phosphor **59** based on fluorenylisoquinoline was reported to emit at 652 nm with Φ_P of 0.19 in toluene [81]. The rigidochromic shift of **59** is found to be large, indicating that the ^{3}MLCT excited state has a more polar structure than the ligand-centered

$^3(\pi-\pi^*)$ excited state. The introduction of an electron-rich fluorene ring into the electron-deficient isoquinoline moiety is expected to increase the donor-acceptor character of the whole ligand, which gives rise to red-shifts of both absorption and emission spectra of **59** with respect to the tris(1-phenylisoquinolinato)iridium(III) *fac*-[Ir(piq)$_3$] counterpart. Another yellow-orange phosphorescent material **60** derived from fluorenylbenzoimidazole ligands is also known with its crystal structure established by X-ray diffraction [57]. Akin to the devices made from the carbazole-based analogue **13**, PHOLEDs made from **60** furnished an EL peak at 570 nm (fwhm = 70 nm) with attractive efficiencies of 8.2%, 24.0 cd A^{-1} and 6.8 lm W^{-1} at the benchmark current density of 20 mA cm^{-2}. The good performance has been attributed to the high solution quantum efficiency of **60**. Two saturated red phosphors **61** and **62** based on heteroleptic iridium(III) complexes containing 2-fluorenylquinoline units were prepared and their utility in PHOLEDs was studied [92,93]. The emission stems primarily from the ^{3}MLCT state due to the broad, featureless PL peak observed and the phosphorescence shifts to the red upon adding a large conjugating and electron-accepting heterocyclic portion of the ligands. Complex **61** with T_g of 92 °C afforded PLEDs in a PVK/PBD host with a pure red emission at 627 nm (CIE at x = 0.68, y = 0.32), showing maximum efficiencies of 10.3% and 11.0 cd A^{-1} at 2.7 wt.% doping level. The authors attributed such good performance to the short τ_P of **61** (1.3 μs), which tends to suppress the triplet–triplet and polaron–triplet annihilations and diminish the quenching of the triplet exciton. Also, its highly amorphous nature due to the presence of long alkyl chains on the fluorene ring leads to a more uniform distribution of the dopant in the polymer host. Surprisingly, deep red PHOLEDs emanating from **62** appears less efficient when the dye is being doped in the CBP host.

A fluorene-functionalized diketonate group is present in complex **63** which gave EL efficiencies of 1.21% and 0.37 lm W^{-1} in a non-doped device structure [72]. The performance is inferior to that from **39** but is still better than the purely acac-based phosphor. Burn and Samuel's groups have discussed the role of fluorene surface groups in the efficiency enhancement of dendrimer **64** in solution-processed DLEDs relative to the model compound without the fluorene rings [94]. The presence of sterically bulky fluorene side rings can improve the solubility as well as the solution processibility and can thus enhance the PL quantum yield by relieving the intermolecular interactions of the emissive chromophores. A peak η_{ext} of ~13% (η_L of 49.8 cd A^{-1}) for the bi-layer DLEDs with **64**:CPB blend and TPBI as the electron-transport layer is obtained which outperforms that for the non-fluorene dendrimer (~10%, 38.0 cd A^{-1}).

A series of charged iridium(III)-based small molecules **65–66** and their π-conjugated chelating iridium-tethered copolymers **67** were reported by Huang and co-workers [95]. Compound **65** serves as the model for the copolymers **67** which are prepared from the dibromo precursor **66** via the Suzuki polycondensation reaction. The ionic metallopolymers (weight-average molecular weight M_w ~9.6–23.2 × 10^3), which consist of the fluorene and bipyridine units as the polymeric backbones, are thermally very stable (T_d ~324–414 °C) and can cast good-quality thin films for optoelectronic characterization. They all displayed good redox reversibility in both *p*- and *n*-doping processes. Interesting energy transfer events were observed for these compounds and **67** showed more efficient energy transfer than for the corresponding blended system. An almost complete energy transfer from the host fluorene groups to the guest iridium cores was attained in the solid state when the feed ratio was 2 mol% (i.e. for **67c**). However, the energy transfer was not complete even when the content of iridium complexes was as high as 16 mol% in the blended mixture. While intra- and inter-chain energy transfer mechanisms co-existed in the energy migration process of this host–guest system, the former process occurred more efficiently. These charged phosphorescent copolymers (with triplet emission peaks at 624–631 nm for **67b–e**) are potentially appealing to the advance of optoelectronic devices such as OLEDs and light-emitting electrochemical cells (LECs). Afterwards, Bryce and co-workers developed some cationic bis(cyclometalated) iridium(III) complexes bearing extended π-conjugated fluorenyl-anchored 1,10-phenanthroline (phen) ligands **68** and **69** [96]. The geometries and electronic structures for the singlet ground state (S_0) and first triplet excited state (T_1) of **68** and **69** were elucidated in detail using computational DFT calculations. Analysis of orbital localizations for the T_1 state has been carried out and correlated to the experimental optical data. Both of them are soluble in non-polar solvents and characterized by a broad PL band at ~595 nm due to a combination of ^{3}MLCT and $^3(\pi-\pi^*)$ states. This is consistent with the DFT data in which the HOMOs are spread between the iridium center and the phenyl rings of the ppy ligands whereas the LUMOs are mainly located on the pyridyl rings of the phen ligand. The increased ligand conjugation length in **69** causes an increase in its τ_P relative to that for **68**. The good film-forming properties and DFT results of these molecules render them potential candidates for the future design of spin-coated LECs. Orange-emitting LECs based on **69** were successfully made by the authors.

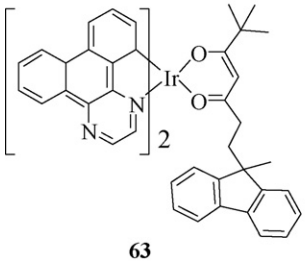

63

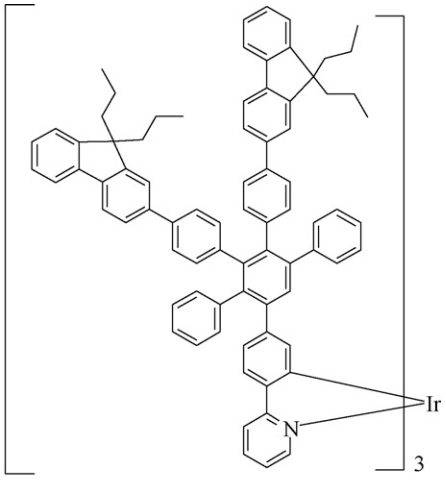

64

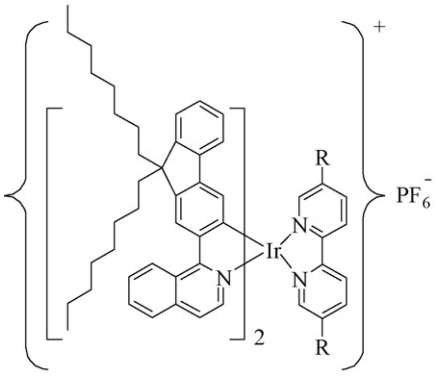

R = H **65**
R = Br **66**

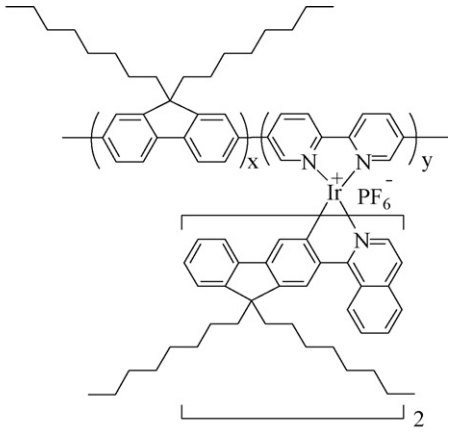

x = 100 **67a**
x = 99.5, y = 0.5 **67b**
x = 98, y = 2 **67c**
x = 92, y = 8 **67d**
x = 84, y = 16 **67e**

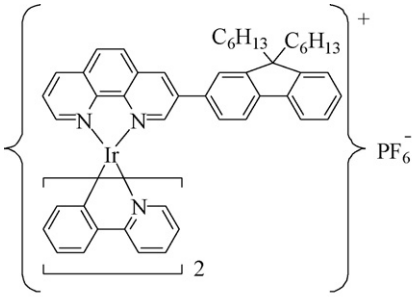

68

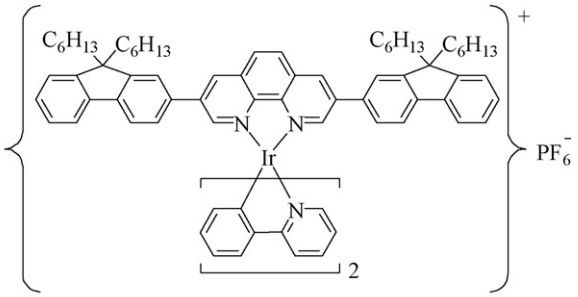

69

A significant step in the development of highly efficient OLEDs was the addition of phosphorescent dopants to the emissive layers in order to harvest both the singlet and triplet excitons as light. Important issues such as triplet energy confinement and phase separation must be considered. Holmes et al. have studied the triplet energy back transfer in some solution-processible conjugated polyfluorene polymers **70** carrying pendant red phosphorescent iridium(III) groups via spacerless and octamethylene-tethered units [97]. The T_g values of the polymers range 60–74 °C for **70**. The emission yields for **70a–d** are 12, 19, 22 and 40% (for PL) and 1.1, 1.7, 2.0 and 1.9% (for EL), respectively. The lower PL and EL efficiencies of **70a–b** than **70c–d** suggest greater Dexter triplet energy transfer in the former spacerless systems and more back transfer of triplet excitons from the iridium phosphor to the PF backbone in reducing the triplet population at the iridium complexes. However, triplet energy back transfer is suppressed in **70c–d** by the distance imposed through the C_8 alkyl-tether. The authors concluded that the introduction of a long non-conjugated spacer between polymer host and phosphorescent guest represents a viable design strategy toward achieving higher efficiencies in PHOLEDs for which the triplet energy levels of the host and guest are similar.

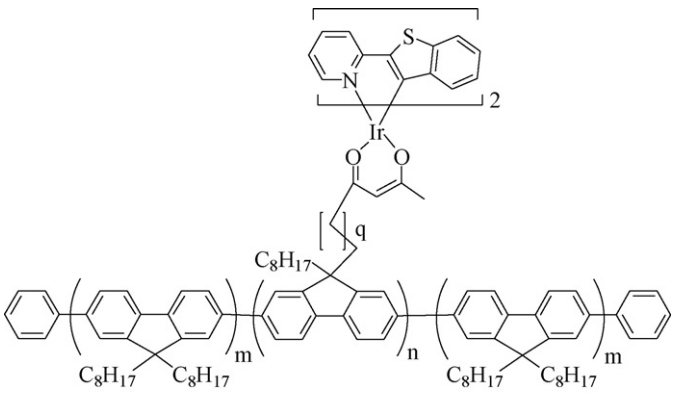

q = 0, m = 9.6, n = 0.06 **70a**
q = 0, m = 8.5, n = 0.18 **70b**
q = 8, m = 9.6, n = 0.08 **70c**
q = 8, m = 9.3, n = 0.30 **70d**

By covalently grafting orange iridium phosphor units to blue fluorescent PF, two series of high molecular-weight white-emitting copolymers **71–72** were prepared (T_g ~69–77 °C) in which the purity of white light can be controlled by variation of the x value and the nature of quinoline ligand. Both the PL and EL spectra of the polymer films show two main components corresponding to the blue-emitting PF and orange-emitting iridium-containing chromophore. With increasing the iridium complex content, the orange emission intensity increases in both series. However, the orange phosphorescence in **71** is stronger than that in **72** at the same doping concentration. The iridium core contributes more to the light emission in EL than that in PL, due to the charge-trapping effect of the metal unit. In one instance, a white light PLED fabricated from **71a** was achieved with maximum η_L of 4.49 cd A^{-1} and η_P of 2.35 lm W^{-1} showing CIE color coordinates of (0.46, 0.33) at 6 V. For **72a**, the device exhibited a much better color purity at CIE of (0.34, 0.33) but the efficiencies are significantly lower (0.81 cd A^{-1}, 0.42 lm W^{-1}) [98]. Another fluorene-based conjugated polymer chelated with an iridium complex **73** was isolated which possesses a bandgap of 2.2 eV [99]. The ionization potential and electron affinity of **73** are 5.4 and 3.2 eV, respectively, which compare well with typical hole-transporting and electron-transporting materials. Polymer **73** has a very high thermal stability (T_d ~400 °C) which arises from the rigidity of fluorene groups and the relatively large iridium organometallic portions attached to the main chain. It is able to emit red PL and EL at 610 nm. Due to the bulky iridium core, there is no observable excimeric emission in the polymer film. Red PLEDs using CBP and PBD blended into polymer **73** showed peak efficiencies of 3.19%, 4.71 cd A^{-1} and 1.56 lm W^{-1}.

A series of PF copolymers **74** and **75** substituted with both iridium(III) complexes and carbazole or 1,3,4-oxadiazole peripherally functionalized dendrons on the side chain as well as their derivatives were recently synthesized in an efficient manner using "click chemistry" through the CuI-catalyzed Huisgen azide-alkyne 1,3-dipolar cycloaddition [100]. The methodology is simple and modular, with potential to be expanded to other iridium and dendritic systems. These high-molecular-weight polymers displayed good solubility and thermal stability (>300 °C), which make thin film preparation as well as the subsequent optoelectronic characterization amenable. In all cases, an incomplete energy transfer from the PF chain to the phosphorescent centre was noted. Dual emission peaks (blue from PFs and green (for **74**) or red (for **75**) from the iridium core) were detected but the intensities of the triplet emission in films were significantly higher than those in dilute solutions. This was partially attributed to the close packing of polymer backbone which enhanced the energy transfer.

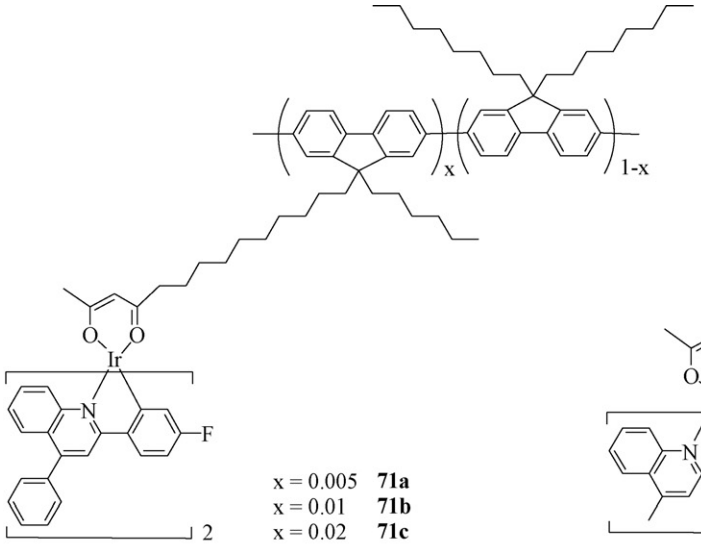

x = 0.005 **71a**
x = 0.01 **71b**
x = 0.02 **71c**

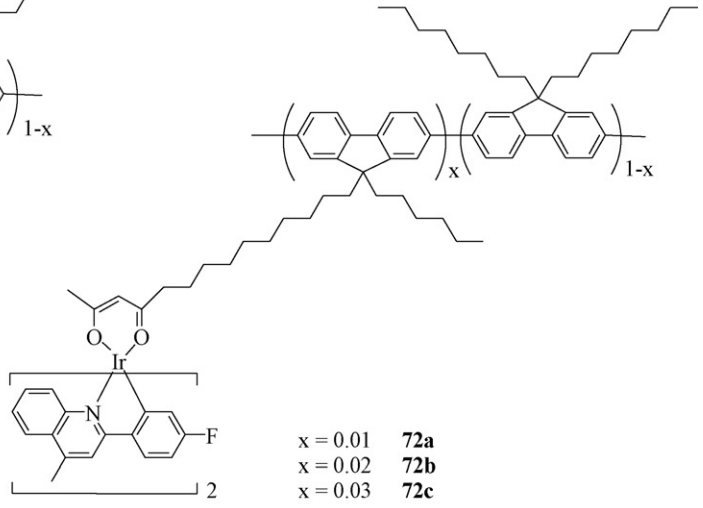

x = 0.01 **72a**
x = 0.02 **72b**
x = 0.03 **72c**

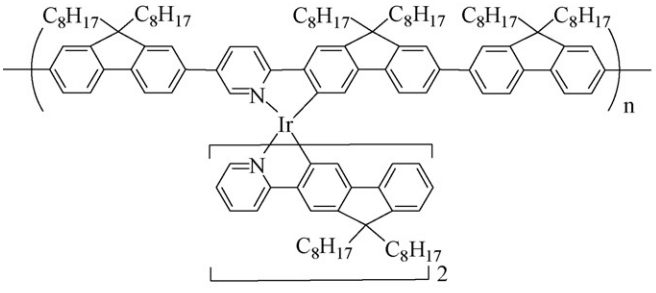

73

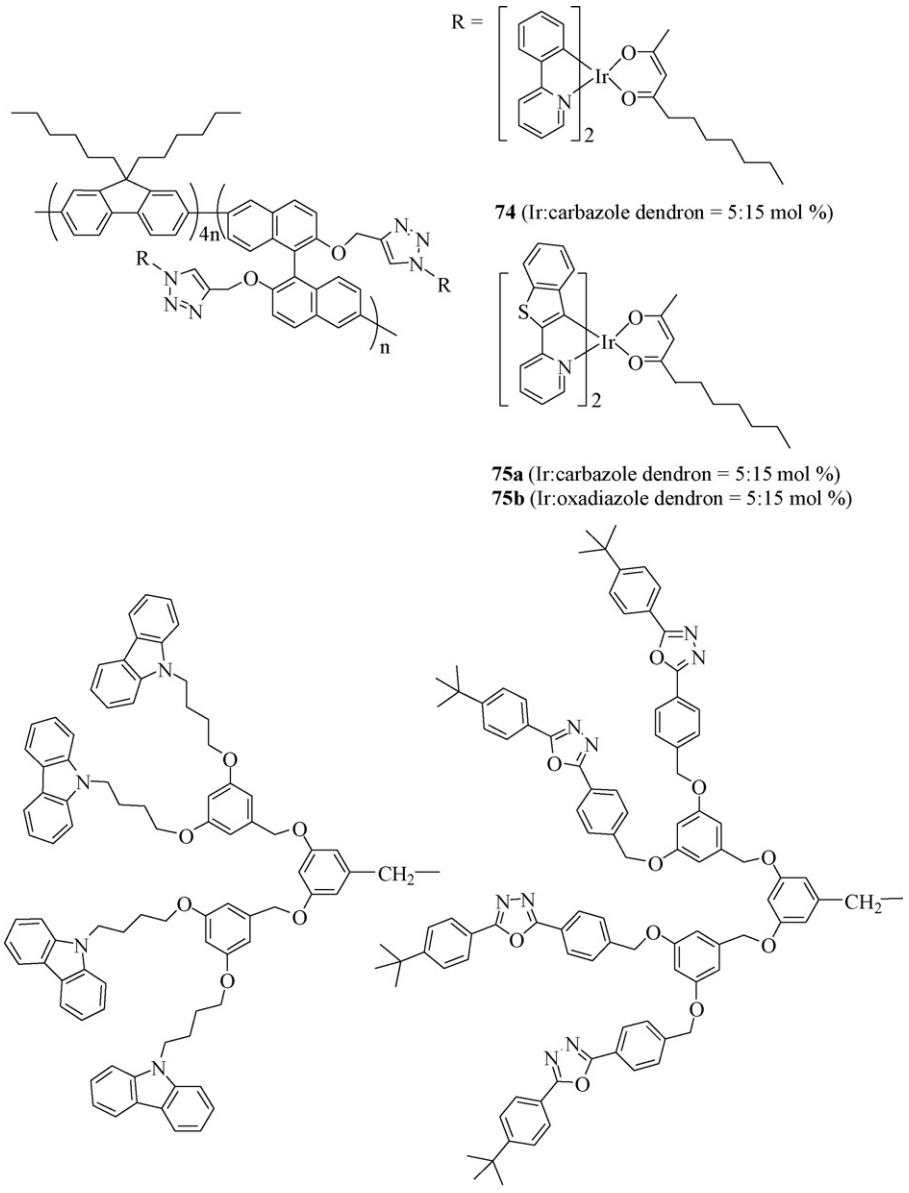

74 (Ir:carbazole dendron = 5:15 mol %)

75a (Ir:carbazole dendron = 5:15 mol %)
75b (Ir:oxadiazole dendron = 5:15 mol %)

3.3. Carbazole–fluorene hybrids

There are also many reports on the use of a combination of both carbazole and fluorene groups in the design of novel phosphorescent complexes and polymers for light-emitting devices. We have recently presented the synthesis and photophysical studies of several multi-functional phosphorescent iridium(III) cyclometalated complexes **76–79** by coupling the hole-transporting carbazole units to the fluorene-based ppy moieties [101]. The influence of the coupling site on carbazole to the central fluorene ring in governing the EL behavior of the resulting complexes has been discussed. Presumably because of their high molecular weights, they do not sublime readily under vacuum and should preferably not be used for evaporated PHOLED devices. As compared to the non-carbazole capped parent complex **53** (λ_{abs} = 321, 336, 405 nm, λ_{em} = 548 nm in CH_2Cl_2), phosphors **76** (λ_{abs} = 294, 342, 398, 463 nm, λ_{em} = 552 nm) and **77** (λ_{abs} = 293, 347, 466 nm, λ_{em} = 562 nm) in the same solvent show an obvious red shift in the absorption and emission features in the presence of the electron-pushing carbazole moiety which can destabilize the ground state by electron donation for the complex. This is also the case for the complexes **12** and **76**. The attachment of carbazole derivatives extends the electronic π-conjugation framework of the ligands which can decrease the LUMO energy levels. Extension of the π-conjugation through incorporation of electron-pushing carbazole units to the fluorene fragment leads to bathochromic shifts in the emission profile, increases the HOMO levels and improves the charge carrier balance of the resulting complexes because of the propensity of the carbazole unit to facilitate hole transport. The HOMO levels of **76–79** are relatively close to the Fermi level of PEDOT (−5.0 eV), resulting in a good hole-injection contact and an improvement in the hole carrier balance in the OLEDs. PHOLEDs using these multi-component complexes **76–79** as the solution-processed emissive layers have been fabricated which show very high efficiencies even without the need for the typical hole-transporting layer. In the literature, only a rather limited number of orange electrophosphors for OLEDs are reported where almost all of them were fabricated by the vacuum deposition approach [102]. Orange-emitting active layers obtained by spin-coating are very scarce to date for PHOLEDs. These orange-emitting devices doped with **76–79** can produce a maximum η_L of ∼30.0 cd A^{-1} corresponding to η_{ext} of ∼9.6% and η_P of ∼13.4 lm W^{-1}. The present work clearly confers a good platform

for affording robust triplet emitters in the fabrication of solution-processed efficient orange-emitting PHOLEDs through the design of some multi-functional chelating ligands. Next, the orange color from the **77**-doped device can be coupled with the blue light for color mixing to achieve multi-layer WOLEDs. The electrophosphorescent WOLED device structure studied is ITO/PEDOT:PSS/0.1% **77**:CBP/15% [FIr(pic)]:CBP/BCP/Alq_3/LiF/Al ([FIr(pic)] = iridium(III)-bis[(4,6-difluorophenyl)pyridinato-*N*,C^2]picolinate). The peak EL efficiencies are η_{ext} = 1.9%, η_L = 5.2 cd A^{-1} and η_p = 2.0 lm W^{-1} and the efficiencies can be maintained at 1.8%, 4.8 cd A^{-1} and 1.9 lm W^{-1} at the reference luminance of 100 cd m^{-2}. The CIE coordinates at 0.1 wt.% **77** are located at (0.36, 0.42), close to those found in incandescent bulbs and tungsten halogen lamp (0.45, 0.41). It should be highlighted that the fluorene-based chromophore in the emitting layer prevents phase segregation and enhances energy transfer from the host to the guest due to efficient overlap of excitonic wave function (Dexter process) and host singlet emission and guest absorption bands (Förster process) which reduces the loading level (~0.05–0.30%) necessary for white light generation.

Zhu and co-workers have elegantly attached 9-carbazole ring to the red-emitting iridium-fluorene heteroleptic chromophore to give **80a** and **80b** with 2-(2-pyridyl)benzimidazolate as the co-ligand by using the post-Suzuki coupling synthetic route [103]. Here, the fluorene spacers are key to improving the solubility and solution processibility and the hole-transporting carbazolyl end groups are critical in driving the phosphorescence into the red region at λ_{em} = 622 nm and in increasing the amorphous morphological stability (T_g ~123 °C for **80a**, 127 °C for **80b**). All of these features render these hole-transport-enhanced iridium(III) complexes great potential for use in solution-processible high-efficiency doped PHOLEDs to address the fatal phase segregations in the doped emissive layer. Another amorphous dendritic molecule **81** (T_g = 144 °C) was also studied in which the oligofluorene dendrons tend to lead to undesired phosphorescence quenching as compared to the purely oligocarbazole counterpart **45** (Φ_P = 0.10 versus 0.21–0.25 for **45**). The HOMO of **81** is lowered with respect to **45**, reflecting its higher ionization potential [76].

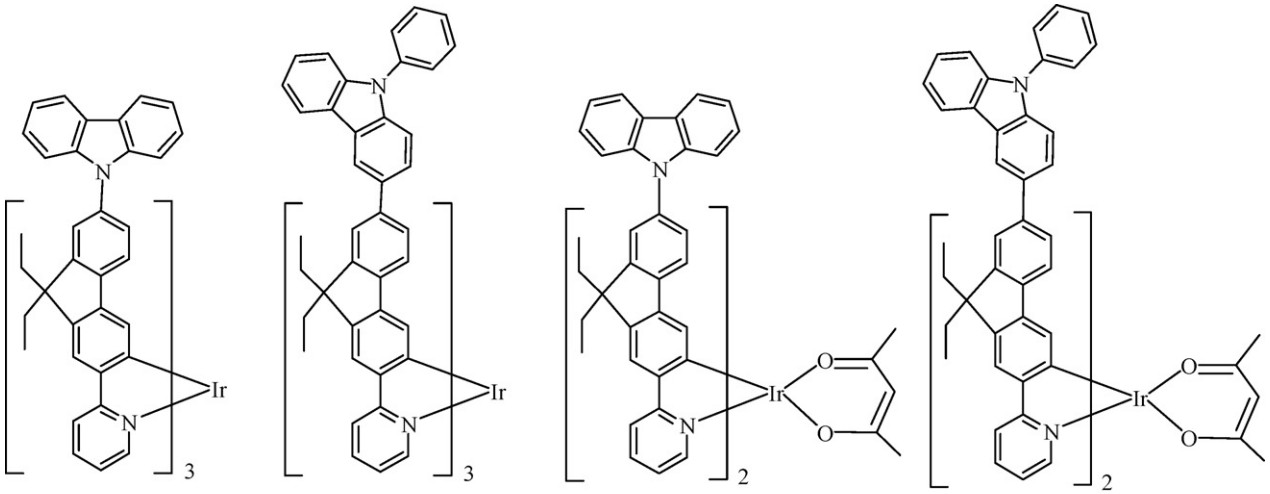

76 **77** **78** **79**

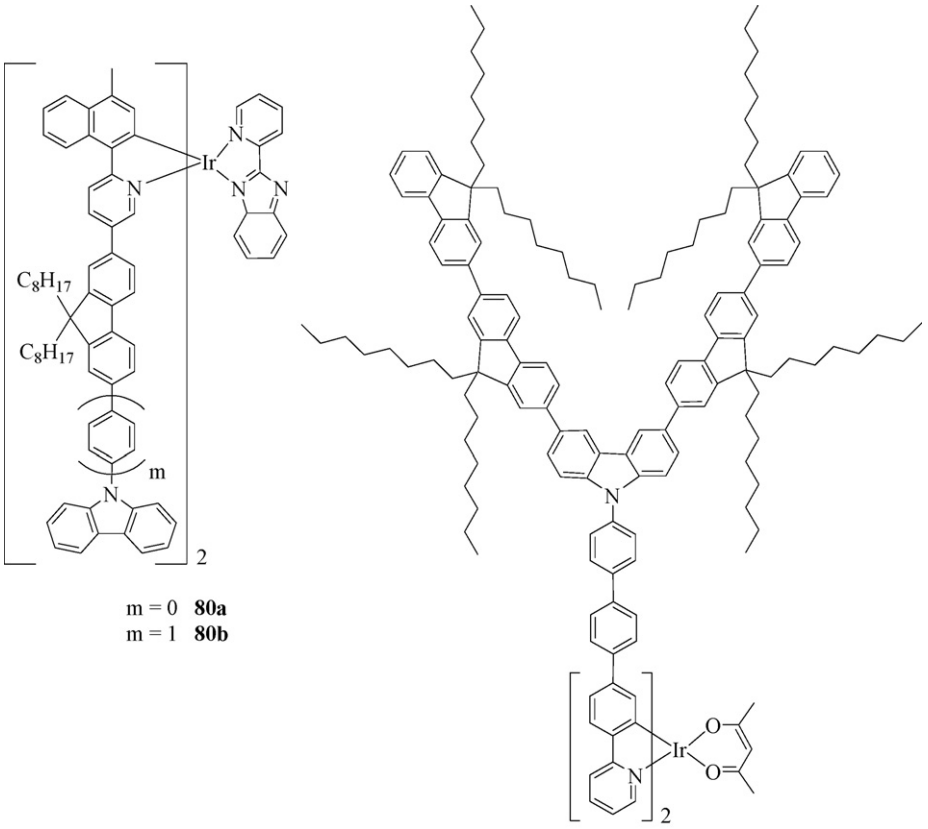

m = 0 **80a**
m = 1 **80b**

81

Two isomeric series of phosphorescent homoleptic iridium(III) complexes with mixed carbazole(fluorenyl)pyridine ligands **82–85**, in which the carbazole moieties are bonded at the C-2 and C-3 positions to the fluorene ring, have been synthesized and their redox and photophysical properties well studied [54]. They possess very good solution processibility and are highly light emissive (Φ_P ~0.30–0.39 in degassed toluene) at λ_{em} = 560–565 nm. Increasing the conjugation length from one fluorene unit in **82** to two in **83** (or from **84** to **85**) can red-shift both the $^1(\pi-\pi^*)$ transitions and to a lesser extent the MLCT bands to lower energies. The τ_P values increase with the ligand size in the complexes from **7** to **82** and **83** (3.2–4.8 and 7.4 μs, respectively), suggestive of a weakening of the spin-orbit coupling and an increasing amount of $^3(\pi-\pi^*)$ character in the lowest energy excited state. Although marked changes are seen in the emission features on changing the carbazole substitution from C-2 to C-3 for **7** and **8**, the effect is greatly diminished for **82–85** as the carbazole ring is not directly attached to iridium. A convenient and fast synthetic route to the phosphorescent iridium(III) dendrimers in three different generations containing carbazole dendron units **86–88** was developed using the convergent approach [104]. They consist of three, nine and twenty-one carbazole rings in the dendritic structures, respectively. The 9,9-dibutylfluorenyl surface groups were found to confer improved solubility to these materials. All of them are essentially green triplet emitters and their emission colors are relatively independent of the dendron size. Ground-state molecular orbital calculations indicated that while the LUMO was concentrated on the metal core, the HOMO was delocalized over both the iridium group and the carbazolyl units in the dendrons. Accordingly, the delocalized HOMO has the effect of increasing the hole-transporting properties of **86–88**, which is manifested by the electrochemical properties in which the increased carbazolyl character of the HOMO gave the first oxidation potential being moved to the more positive values.

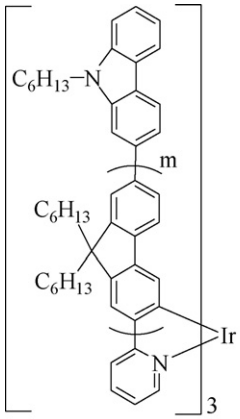

m = 1 **82**
m = 2 **83**

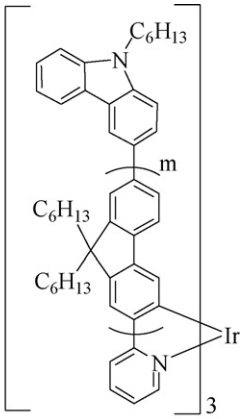

m = 1 **84**
m = 2 **85**

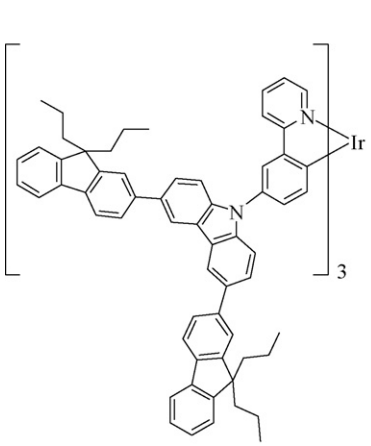

86

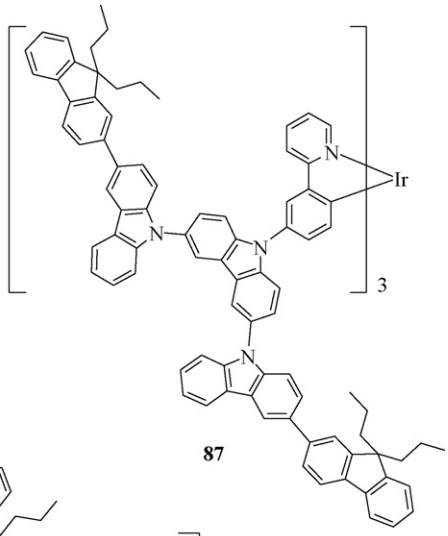

87

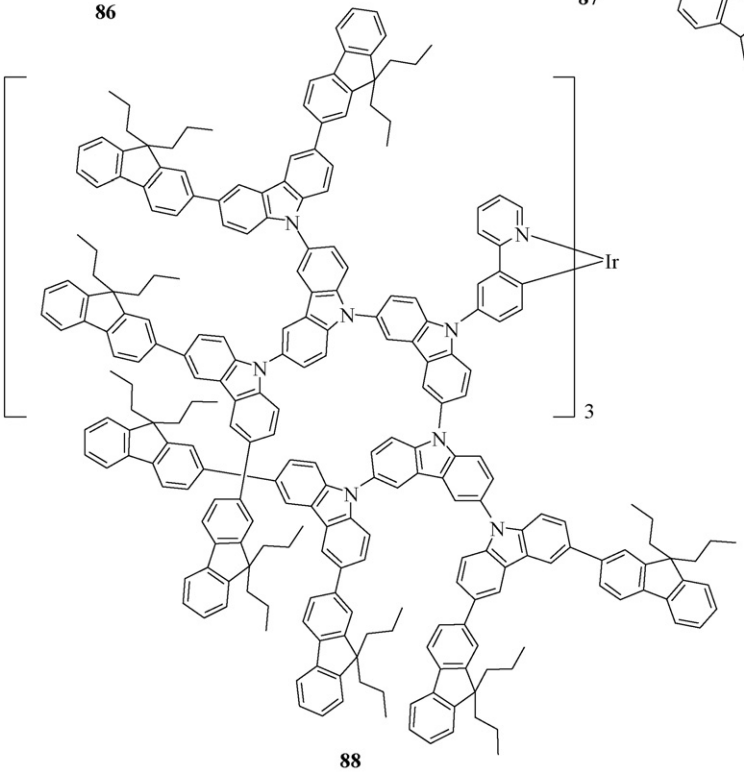

88

Functionalizing the alkyl chains at the termini of **68** and **69** by carbazole units resulted in two soluble and processible ionic iridium(III) complexes **89** and **90** [95]. Significant red shifts in λ_{em} were observed relative to the parent complex $[Ir(ppy)_2(phen)]^+$ ($\Delta\lambda$ ~440 cm^{-1} for **68**, 580 cm^{-1} for **69**), which are consistent with the extended conjugation involving the π systems of phen and fluorene units. Spin-coated LECs based on **90** in the structure of ITO/PEDOT:PSS/**90**/Al have been fabricated and tested. A peak efficiency of ~9 cd A^{-1} has been obtained at 9 V using a bi-layer Ba/Al cathode. The devices operated in air with no reduction in efficiency after storage for 1 week in air. An atomic force microscopy (AFM) study suggested that with <1 nm deviation, the average surface roughness is very low for a spin-coated thin film of **90** using toluene solvent and microcrystallites of **90** can be observed as regular needles (~15 nm in length), positioned perpendicular to the film surface. The LEC performance of **90** does not differ much from that fabricated using **69**.

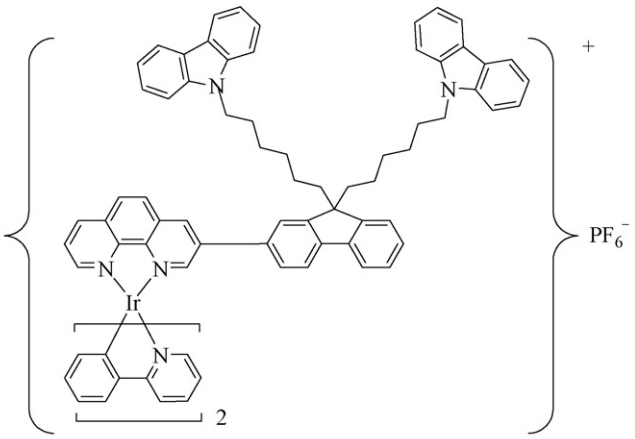

89

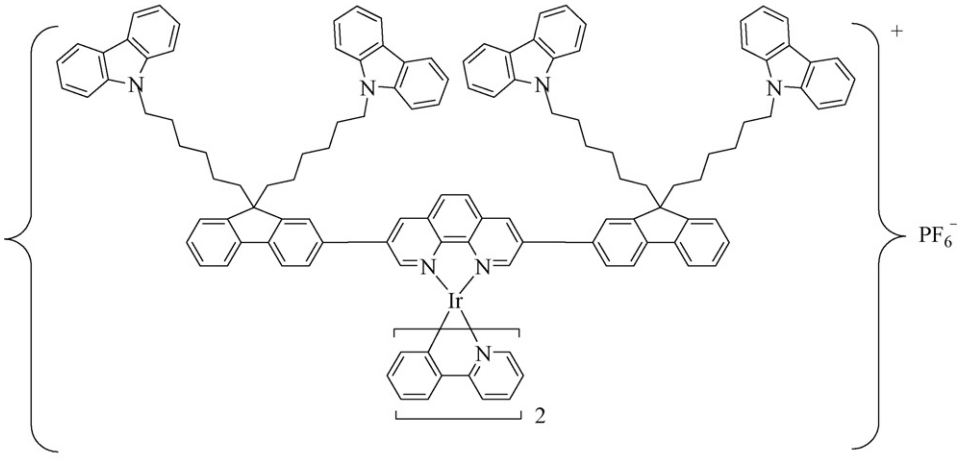

90

Cao and co-workers have investigated extensively the electrophosphorescence of a series of highly efficient carbazole–fluorene-based copolymers with cyclometalated iridium(III) chromophores either as the side group or in the main chain. Conjugated fluorene-*alt*-carbazole copolymers **91–95** of various comonomer feed ratios were prepared in which the different phosphorescent iridium cores were incorporated to the pendants of a diketonate alkyl chain on *N*-carbazole ring [105]. The M_w values lie within ca. 51,000–188,000 with a narrow distribution (polydispersity index = 1.7–2.2). The PL efficiencies of **92–95** range from 56 to 75% whereas those for **91** are lower at 20–29%. The intense absorption peaks below 350 nm are attributed to the spin-allowed $^1(\pi-\pi^*)$ transitions of cyclometalated ligands, and the weak absorption bands around 420 nm are due to the spin-allowed ^{1}MLCT transition. The strong visible absorption peaks are assigned to the ^{3}MLCT event, corresponding to the individual iridium complex in each case. Based on the fact that the PL spectrum of the host polymer and the absorption spectra of the iridium guests can show good spectral overlap, it was observed that there is an efficient Förster energy transfer from the main chain of the copolymer to the metal complex and complete quenching of the EL emission from the organic backbone occurs even at 0.5 mol% metal content in the polymers. Electrophosphorescent PLED characterization results suggest that devices from carbazole-based copolymers **91–93** outperform those from the fluorene-based congeners (**94–95**) which indicates that carbazole unit in the polyfluorene main chain at the 3,6-linkage renders the hole-transport easier due to the elevated HOMO level of the copolymer as revealed from cyclic voltammetry (CV) results. Also, the higher triplet level of the copolymer host than the iridium guest prevents triplet energy transfer from the guest to the host, thus improving the device performance. In all cases of **91–93**, the best efficiencies were obtained for copolymers with an initial iridium chelate content of 0.5 mol% in the feed ratio and devices blended with PBD by supplying a large number of electrons via electron injection to inhibit the buildup of the space-charge due to trapping of holes on the heavy metal complex. The device of **92** blended with PBD exhibited the red EL maximum at 610 nm with peak η_{ext} of 4.9% and η_L of 4.0 cd A^{-1} at 7.7 V.

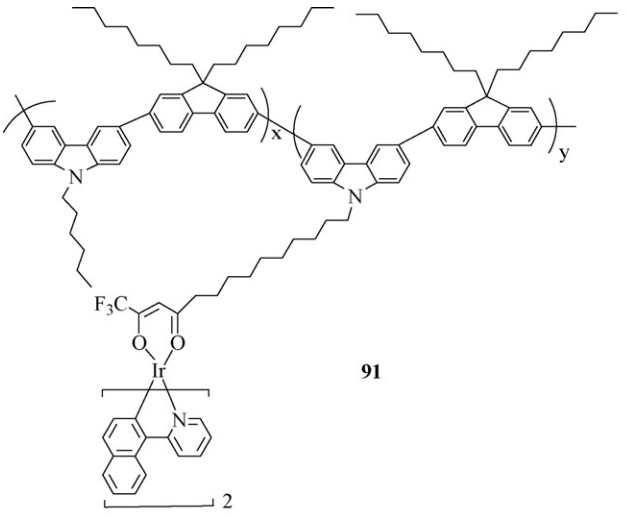

91

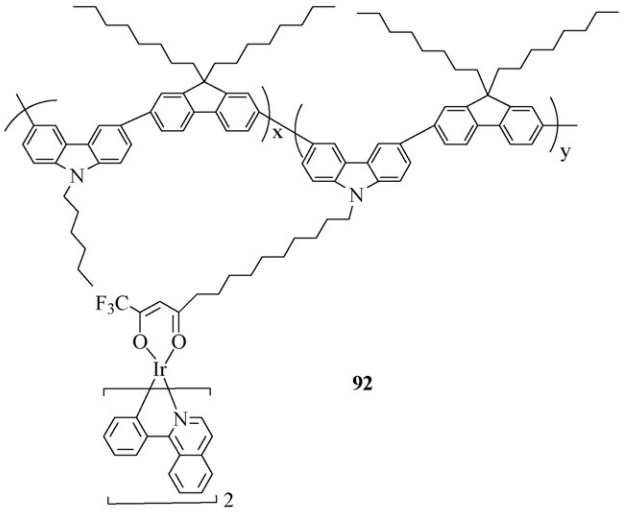

92

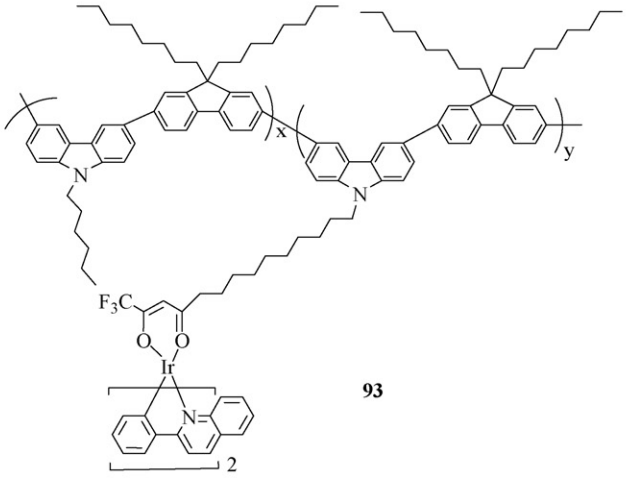

93

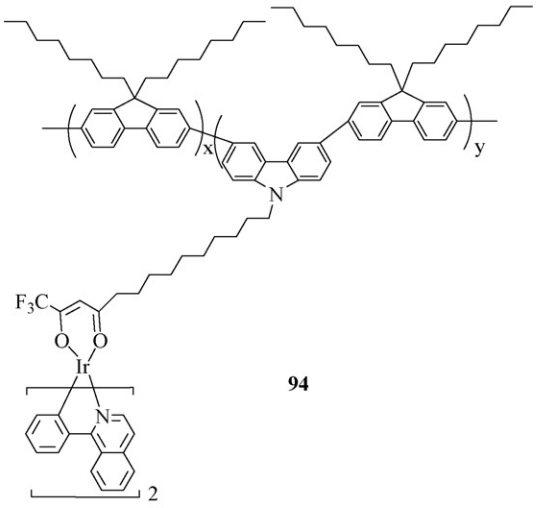

94

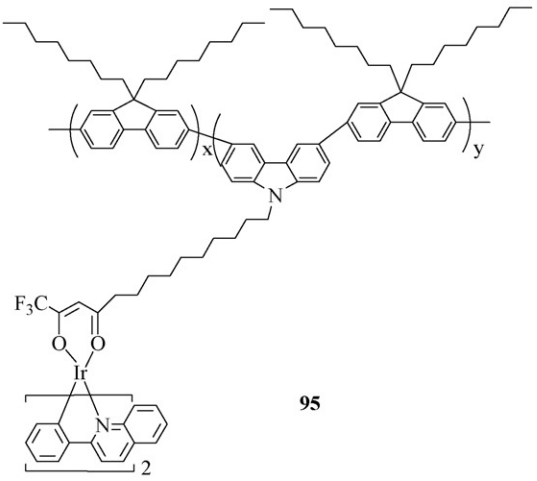

95

Binary fluorene-based copolymers **96** and ternary copolymers **97** were also promising candidates for white light PLEDs by mixing singlet and triplet emission within the polymer [106]. The efficiency and color purity of the devices made from **97** were improved by adding fluorescent green benzothiadiazole unit into PF backbone relative to those from **96**. This can be attributed to the exciton confinement of the benzothiadiazole moiety, which permitted efficient singlet energy transfer from fluorene group to benzothiadiazole and avoided the triplet quenching due to the higher triplet energy levels of green phosphors than that of PF. This provides a good step forward in the molecular design of white PLEDs. In essence, polymer **97e** afforded pure white-light emission showing excellent color purity at (0.31, 0.34) and peak η_L of 4.6 cd A^{-1}.

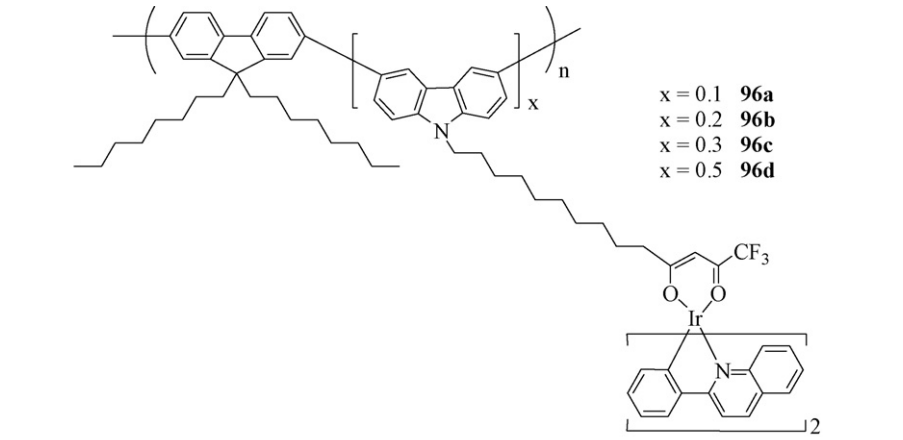

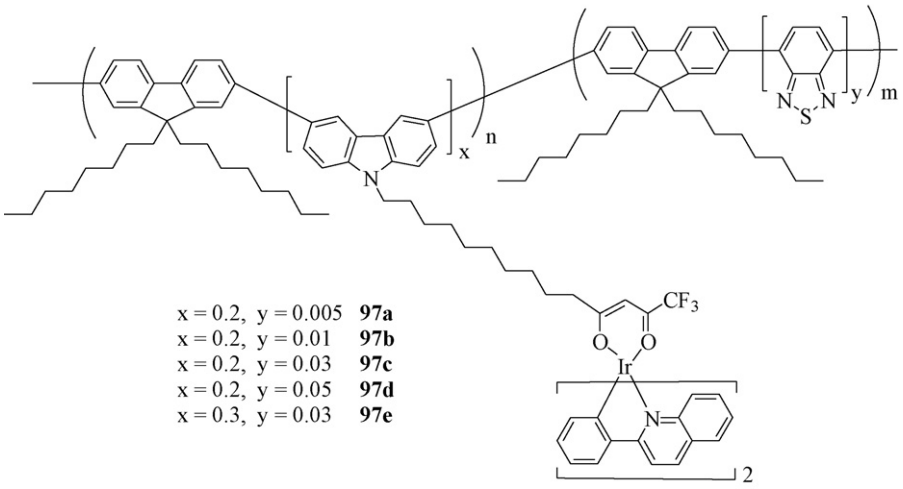

In another report, the first examples of some novel copolymers **98** and **99** with iridium phosphor linked to the polymer main chains via auxiliary β-diketonate units are known and opened the door for more efficient device structures [107]. Both copolymers are amorphous with high T_g of 152–175 °C. The synthetic strategy avoided the preparation of dibrominated bis(cyclometalated) iridium(III) complexes. All of them show almost the same PL spectra as their monomeric iridium units, allowing the versatile color tunability by simply changing the metalated groups. These polymeric materials are highly desirable as emissive layers in PLEDs and all of the fabricated devices show negligible efficiency roll-off even at high current density, due to the covalent linkage of phosphorophore into the copolymer chain. The best saturated-red PLEDs with **99**:PBD blend gave the highest efficiencies of 0.60% and 0.34 cd A^{-1} at 39 mA cm^{-2}, which may either result from a poor solid PL efficiency of the polymer or a lack of additional charge/exciton confinement.

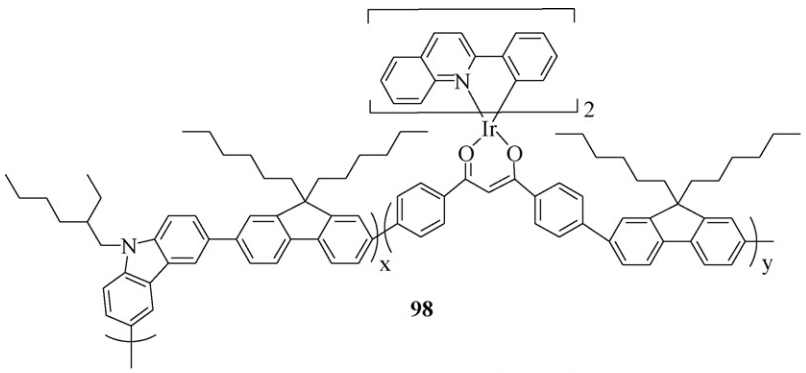

98

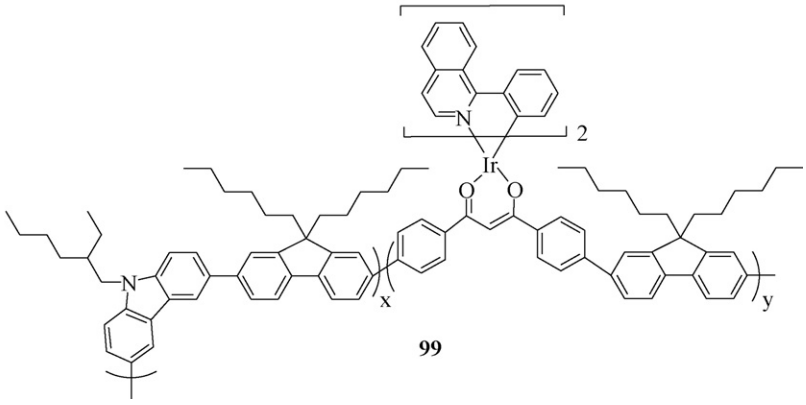

99

An interesting series of metallopolymers **100** consisting of three separate emission centers emitting the primary colors in the blue, green and red regions were prepared which can be used to generate efficient white light emission [108]. Fluorene, benzothiadiazole and iridium complex serve as the blue, green and red emitters, respectively in **100**. By mixing fluorescence with phosphorescence emission arising from a single polymer, the PLED device with the configuration of ITO/PEDOT:PSS/PVK/**100b**/CsF/Al displayed maximum efficiencies of 3.7% and 3.9 cd A^{-1} at 1.6 mA cm^{-2} with excellent white CIE coordinates of (0.33, 0.34). The EL spectra comprise of main peaks at 420, 520 and 660 nm. While the PL and EL processes arise from different mechanisms, white EL emission can be attributed to the individual emission from blue-, green- and red-emitters with the partial energy transfer from the wide bandgap species to the narrow bandgap species and charge trapping on the narrow bandgap emitters. This novel approach provides a useful avenue toward white PLEDs from a single polymer associated with the singlet and triplet chromophores in the main chain.

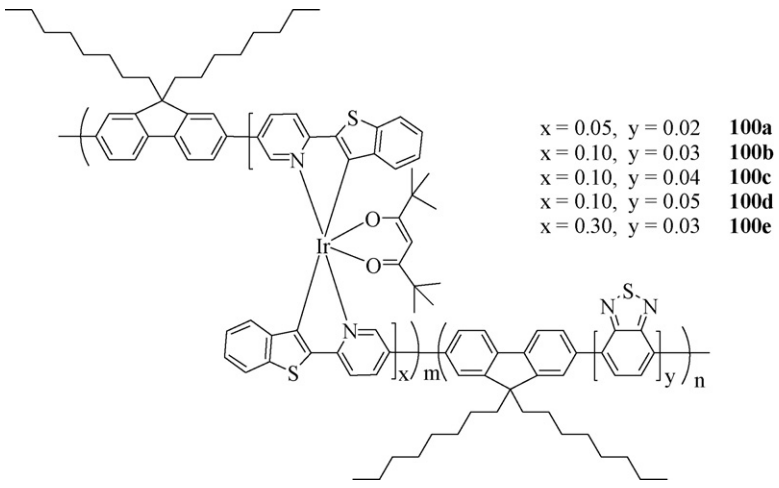

x = 0.05, y = 0.02 **100a**
x = 0.10, y = 0.03 **100b**
x = 0.10, y = 0.04 **100c**
x = 0.10, y = 0.05 **100d**
x = 0.30, y = 0.03 **100e**

Another group of fluorene-*alt*-carbazole-containing copolymers functionalized with Ir(C^N)$_2$(diketonate) units in the main chain **101** was reported in which the PL spectra are characterized by saturated-red phosphorescence from the parent iridium complex at 620 nm [109]. Peak efficiencies of 0.60% and 0.34 cd A^{-1} were achieved for the red PLED based on **101**:PBD blend. In addition, the efficient synthesis and characterization of electrophosphorescent chelating polymers **102–103** were studied in detail in which the iridium moiety appears in the conjugated backbone [110]. Efficiencies of the devices made with polymer **103** reach 4.1% and 5.4 cd A^{-1} at 32.3 mA cm^{-2}. It is remarkable that the incorporation of carbazole and iridium groups in **101–103** can reduce the barrier for both hole- and electron-transport compared with the parent PF. The more efficient energy transfer observed in **101–103** versus the

corresponding blended systems of the same composition signifies that intramolecular energy transfer is a more efficient process than interchain interaction. Most importantly, the devices made from **101** to **103** show no notable efficiency decay with increasing driving current density due to the suppression of concentration quenching and triplet–triplet annihilation, which are the primary quenching mechanisms for blended systems at high current density. Direct introduction of the iridophosphor unit into the conjugated polymer main chain helps simultaneously in realizing high efficiency and simple processing of electrophosphorescent PLEDs. In addition, phosphorescent main-chain iridium-chelating copolymers bearing carbazole (**104**) and fluorene-*alt*-carbazole (**105**) spacers were reported [111]. Three different photoactive difluoro-substituted [Ir(ppy)$_2$] cores with various auxiliary ligands were incorporated into the poly(3,6-carbazole) backbone. Copolymers **104** are strong green emitters with solid-state emission quantum yields up to 62% for **104b** at the 5 mol% of iridium in the feed ratio whereas the yellow-emitting **105** has a much lower yield of 9%. This work indicated that the 3,6-carbazolyl ring plays a vital role in serving as the host for the green electrophosphorescent polymer guest. The PLED device behavior blended with PBD is superior to that with PVK, which is a good manifestation of the poor electron-transporting capability of the iridium-chelating copolymers and thus PBD needs to be used for effective charge balance. The best device from **104b** (5 mol% Ir monomer feed content) in a structure of ITO/PEDOT:PSS/**104b**:PBD (30%)/Ba/Al furnished maximal efficiencies of 2.2% and 4.4 cd A^{-1} at 10.3 mA cm^{-2}.

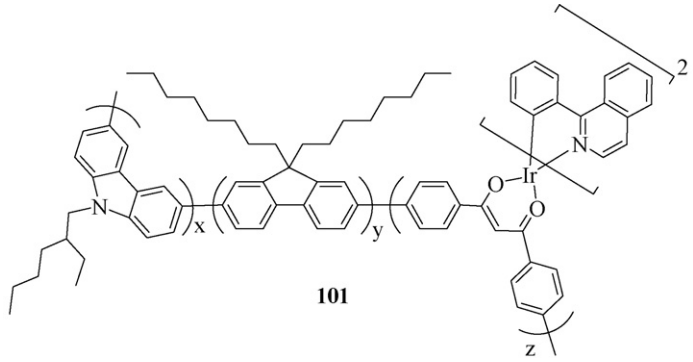

101

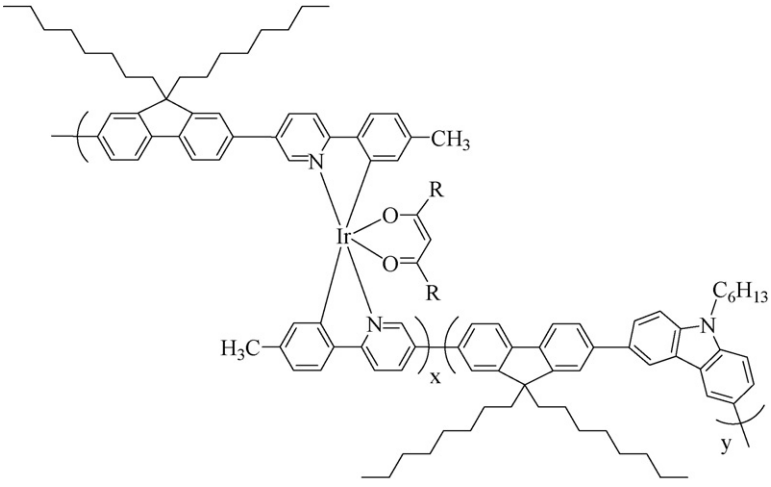

R = CH_3 **102**
R = $C(CH_3)_3$ **103**

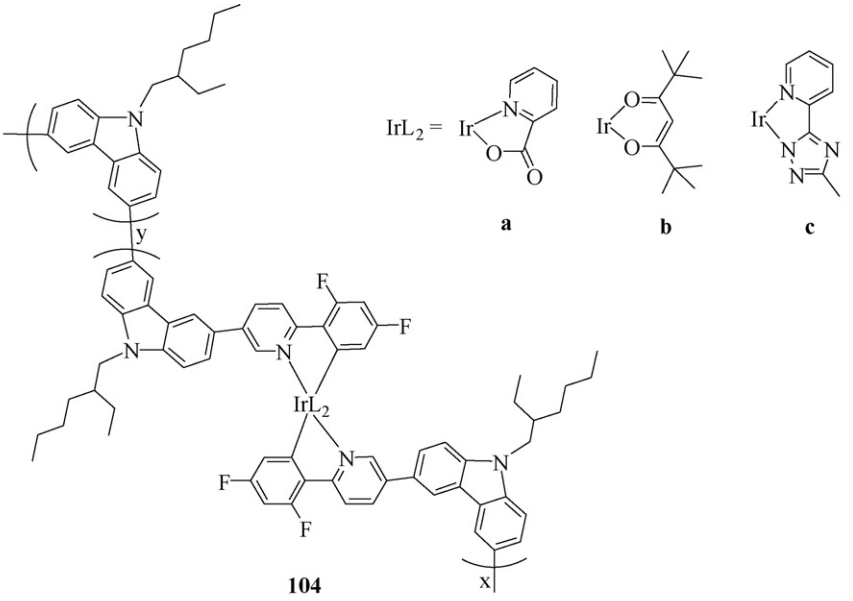

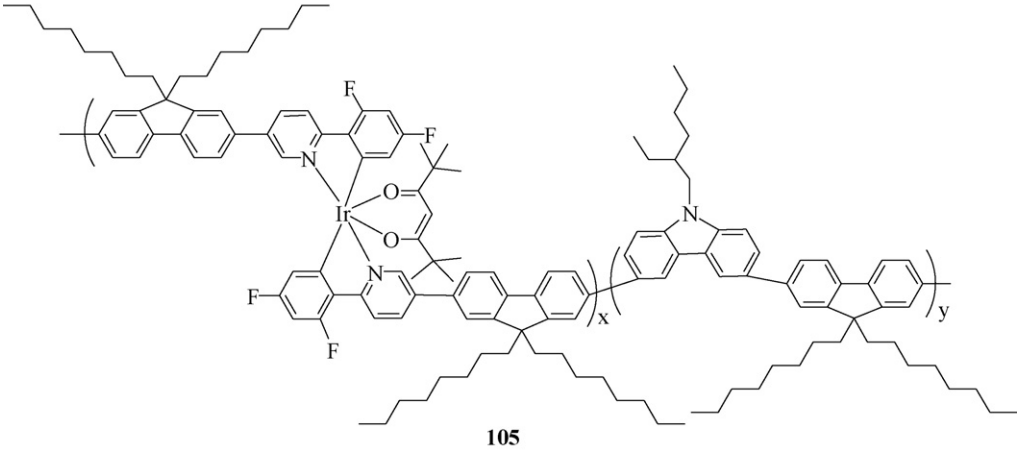

The teams of Fan and Wang have looked into the first literature study on saturated-red light-emitting properties of several π-conjugated chelating polymers **106–108** with charged $Ir(C^{\wedge}N)_2$ units based on phen in the main chain through classical Suzuki polycondensation method [112]. Polymer **108** differs from **106** in the introduction of an additional carbazole functional moiety. The energy-transfer, thermal stability, photophysical and redox properties of **106–108** were examined. They are all thermally very stable (T_d ~390–415 °C) and highly amorphous (T_g ~110–113 °C versus ~103 °C for poly(9,9-dialkylfluorene)). Evidently, the charged iridium moiety could function as both hole and electron traps, and the carbazole incorporation causes a rise in the HOMO level in **108** relative to those without carbazole groups. While these guest–host systems are not yet optimized in terms of device performance, the addition of carbazole units into the iridium-based chelating polymers does not seem to change the EL spectra (EL peak at ~634 nm), however, it gave better luminance and current density at a given drive voltage. Conjugated PF-based materials grafted with cyclometalated iridium complexes and hole-transporting carbazole moieties **109** were reported by Chen et al. [113]. The HOMO and LUMO energy levels of the red iridium core lie between those of the main chain, permitting both hole and electron trapping during the electrical excitation. Energy transfer from the PF chain as well as a green electroplex due to the PF and side-chain carbazole units to the red-emitting iridium complex can markedly enhance the device performance. An efficient single-layer red-emitting PLED device, with efficiencies of 1.6% and 2.8 cd A^{-1} and a brightness of 65 cd m^{-2} at 7 V was obtained for **109f**. The presence of carbazole can significantly increase the EL efficiency and lower the turn-on voltage.

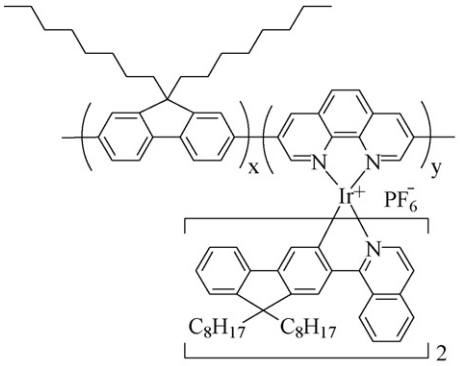

x = 99.5, y = 0.5 **106a**
x = 99.9, y = 0.1 **106b**
x = 98, y = 2 **106c**
x = 96, y = 4 **106d**

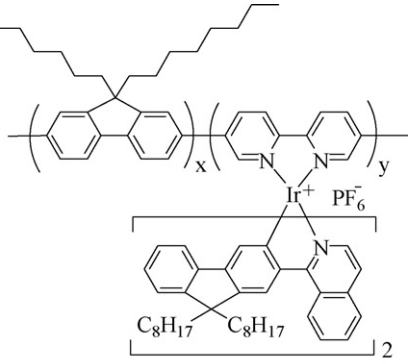

x = 98, y = 2 **107**

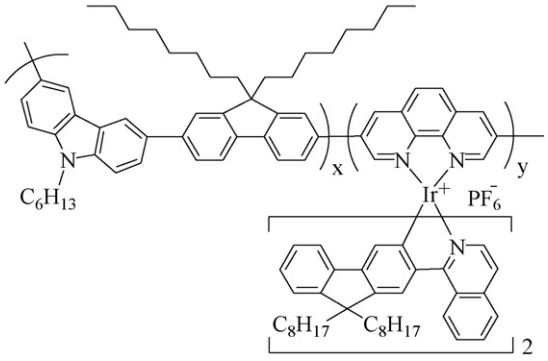

x = 98, y = 2 **108**

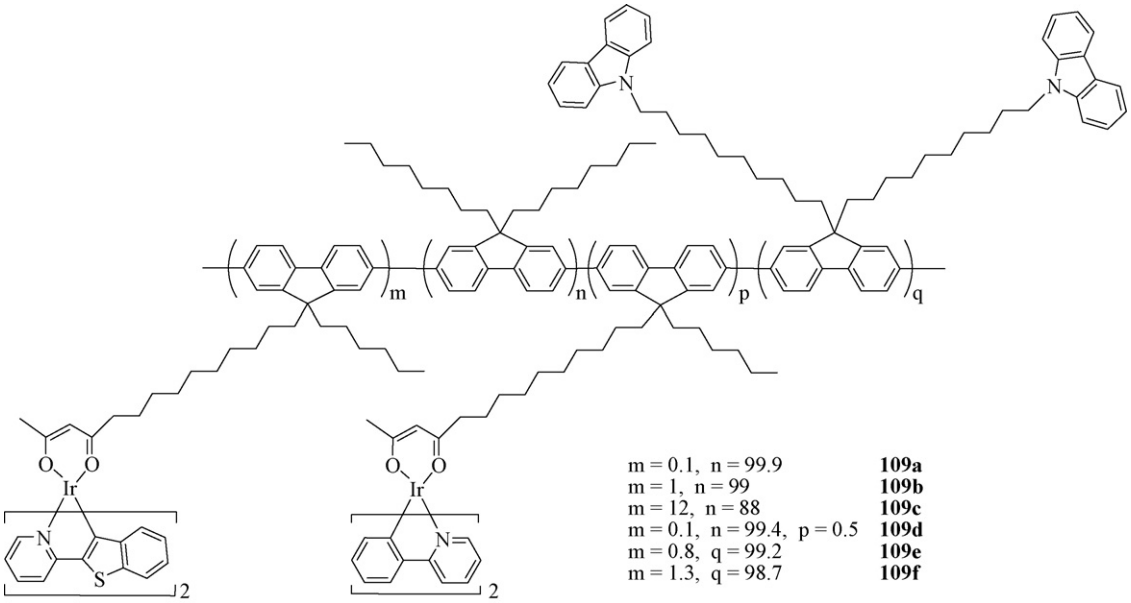

m = 0.1, n = 99.9 **109a**
m = 1, n = 99 **109b**
m = 12, n = 88 **109c**
m = 0.1, n = 99.4, p = 0.5 **109d**
m = 0.8, q = 99.2 **109e**
m = 1.3, q = 98.7 **109f**

3.4. Arylamine and other related main group 13–16 moieties

Generally, a large hole-injection barrier for organic materials often limits the device efficiency. Since most of the hole-transporting materials reported are derived from aromatic amines, the incorporation of arylamine units into the metallophosphor skeleton should be beneficial to the hole-injection/hole-transporting properties of the resulting materials and hence the EL efficiency. A homoleptic phosphor **110** was first used in this regard in both doped and polymer-based devices [56,114]. The EL maximum from **110** (~530 nm) was red-shifted as compared to that from *fac*-[Ir(ppy)$_3$] (514 nm), due to the electron-donating effect of the arylamine group, which destabilizes the HOMO level by the mesomeric effect and raises the HOMO level of the former relative to that of *fac*-[Ir(ppy)$_3$]. The diphenylamine units act as effective hole-trapping moieties and confer a better hole-transporting capacity, therefore, **110**-doped devices showed lower operational voltage and higher EL efficiency than *fac*-[Ir(ppy)$_3$]-based devices under identical device structures. Using TAPC as the hole-transport layer, devices doped with 10 wt.% **110** gave the peak η_{ext} of 12.2% at 6.6 V and a high luminance of 51,900 cd m^{-2} at 13 V. High-efficiency electrophosphorescent PLED devices based on **110** was also demonstrated by Ma et al. in which a **110**:PVK blend consisting of both NPB and TPBI showed η_L as high as 25.2 cd A^{-1} at 0.85 mA cm^{-2} [114]. The introduction of NPB and TPBI in PVK layer improves the balance of the charge carrier injection and transport, and largely inhibits the buildup of space charge caused by direct trapping of charge carriers on dopant **110**. We also fabricated highly efficient PHOLEDs (doped with 8 wt.% **110**) which showed a very attractive performance (η_{ext} of 13.9%, η_L of 60.8 cd A^{-1}, η_P of 49.1 lm W^{-1}, L_{max} of 48,576 cd m^{-2} at 12.3 V).

It is anticipated that non-metallic functional main-group elements show distinct electronic features according to their intrinsic nature. In view of this, a series of bluish-green to red-orange (ca. 498–582 nm) phosphorescent tris-cyclometalated homoleptic iridium(III) complexes *fac*-[Ir(ppy-*X*)$_3$] (*X* = NPh$_2$, POPh$_2$, B(Mes)$_2$, SiPh$_3$, GePh$_3$, OPh, SPh, SO$_2$Ph, **110–117**) was developed by Wong and co-workers [115]. The crystal structures of **110** and **117** have been determined. Each of them showed very high T_g in excess of 157 °C and their highly amorphous nature in the solid state can be attributed to the branched and twisted configuration of the substituted main-group moieties as the pendant antennas although the ligand size of the complexes is relatively small. By chemically manipulating the lowest triplet state character of *fac*-[Ir(ppy)$_3$] with some functional main-group 13–16 moieties on the phenyl ring of ppy, a new family of metallophosphors with high Φ_P, short τ_P and good hole-injection/hole-transporting or electron-injection/electron-transporting properties can be obtained. They exhibit appealing characteristics such as highly emissive ^{3}MLCT excited states at room temperature and facilely tunable emission color in the visible spectrum. Remarkably, all of these iridium(III) complexes show outstanding electrophosphorescent performance in multi-layer doped devices which surpass that of *fac*-[Ir(ppy)$_3$]. Other than **110** as described above, highly efficient PHOLEDs have been fabricated which can reach the maximum η_{ext} of 12.3%, η_L of 50.8 cd A^{-1}, η_P of 36.9 lm W^{-1} for **113**, and 10.1%, 37.6 cd A^{-1}, 26.1 lm W^{-1} for **117**. These results provide a completely new and effective strategy for carrier injection into the electrophosphor to afford high-performance doped PHOLEDs suitable for various display applications.

The work was also extended to another series of heteroleptic iridium counterparts **118–125**, whose solid-state structures were all ascertained by X-ray crystallography in our recent seminal paper [116]. Because of the more weakly π-bonding ability of the oxygen atoms in the acac ligand compared to ppy, such color-tuning venture would be expected to be even more effective for the heteroleptic series **118–125** (Fig. 3) [116] than that for **110–117**. The color tuning can be achieved by shifting the charge-transfer character from the pyridyl groups in some traditional iridium ppy-type complexes to the electron-withdrawing main-group units, which is conceptually different from the classical color tuning protocols reported in the literature [117]. These iridium(III) complexes show PL spectra with the emission maxima ranging from ca. 505 nm to 605 nm. Interestingly, the complexes with electron-withdrawing groups (i.e. **119**, **120** and **125**) show bathochromic shifts in their MLCT absorptions compared with other complexes in the series and the parent complex [Ir(ppy)$_2$(acac)] (520 nm). Generally, the emission spectra of iridium(III) complexes show hypsochromic shifts when an inductively electron-withdrawing group (such as F) is introduced to the phenyl moiety of ppy [118–121]. On the contrary, complexes **119**, **120** and **125**, with an electron-withdrawing group on the phenyl moiety of ppy, show red shifts in their PL spectra compared with other complexes in the relevant series. The spectroscopic data are also consistent with electrochemical results and time-dependent DFT (TD-DFT) calculations. The present work furnished PHOLED colors spanning from bluish-green to red (505–609 nm) with high EL efficiencies which have great potential for application in multi-color displays. The maximum efficiencies of 9.4%, 10.3 cd A^{-1} and 5.0 lm W^{-1} for the red OLED doped with **120**, 11.1%, 35.0 cd A^{-1} and 26.8 lm W^{-1} for the bluish-green device doped with **123**, 10.3%, 36.9 cd A^{-1} and 28.6 lm W^{-1} for the bright green device based on **118** as well as 10.7%, 35.1 cd A^{-1} and 23.1 lm W^{-1} for the yellow-emitting device doped with **125** can be obtained. In the devices for **118** reported by Yamashita et al., the device performance (11.8%, 23.7 lm W^{-1}) also surpassed those for [Ir(ppy)$_2$(acac)] (11.4%, 22.4 lm W^{-1}), echoing with the good merits of introducing NPh$_2$ substituent to the phenyl ring [122].

On the other hand, the effect of fused ring and ring substitution on some NPh$_2$-ppy-based iridium complexes was studied in two independent reports. Complexes **12** and **126** were prepared as structural analogues of **110** to seek for an effective method for carrier injection into the electrophosphor of iridium(III) [56]. The effects of hole-trapping carbazole, diphenylamine and phenoxazine moieties in **12**, **110** and **126**, respectively, on the luminescence properties of the iridium complexes were examined. Heteroleptic compounds **127–131** [122] were also designed and studied in comparison to the unsubstituted congener **118**. These substituent effects are considered to be closely related to the HOMO and

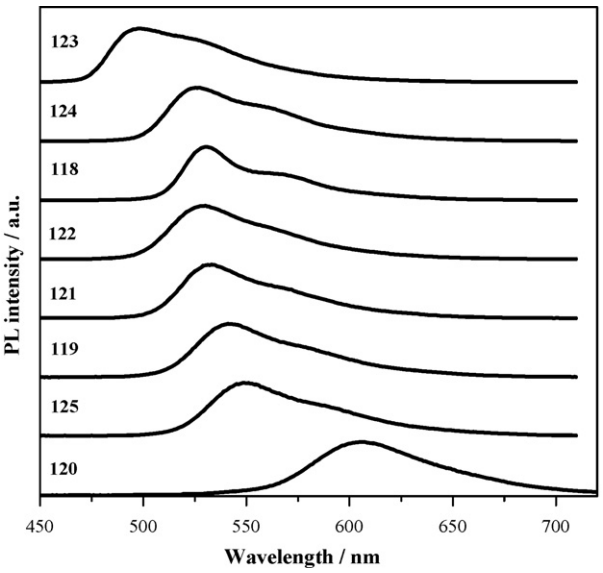

Fig. 3. Phosphorescence color tuning of **118–125** triggered by tailoring the phenyl ring of ppy with various main-group moieties (see Ref. [116]).

LUMO levels of the complexes. The order of emission wavelengths is **127** < **118** < **131** < **128** < **129** < **130**, in line with an increase of the π-conjugation length along the series and the effect of an electron-withdrawing CF_3 group on the pyridyl ring in lowering the LUMO level.

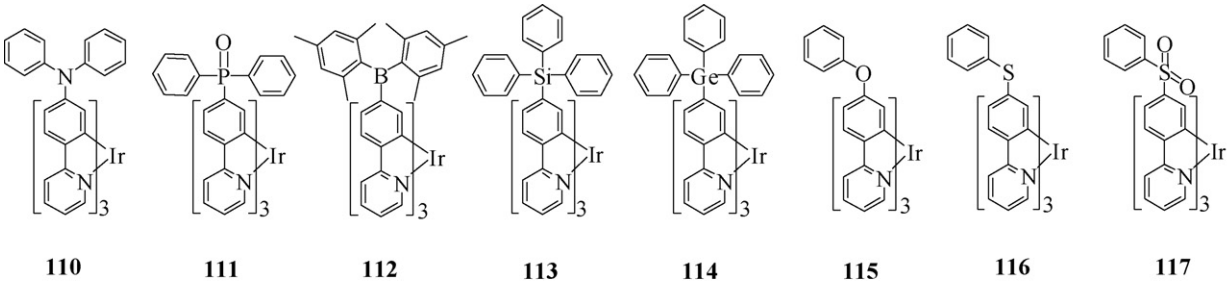

110 **111** **112** **113** **114** **115** **116** **117**

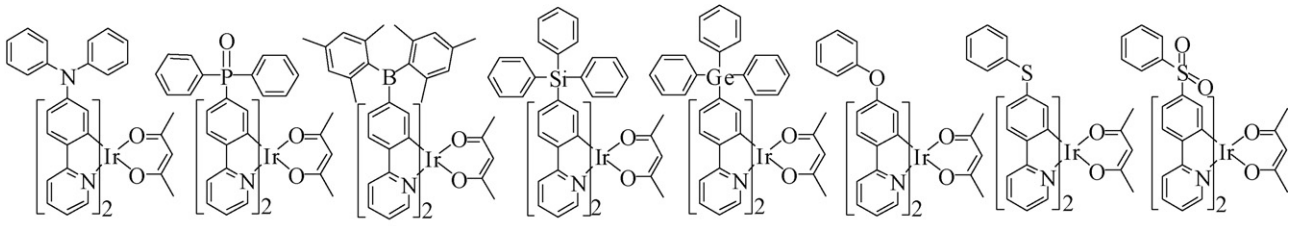

118 **119** **120** **121** **122** **123** **124** **125**

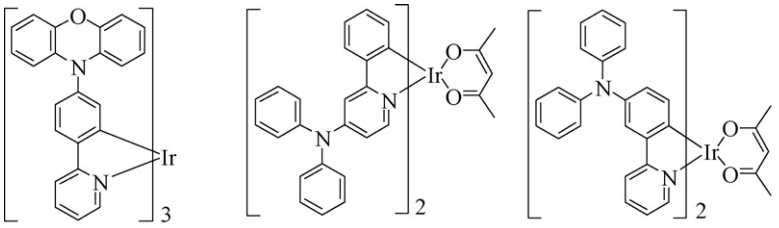

126 **127** **128**

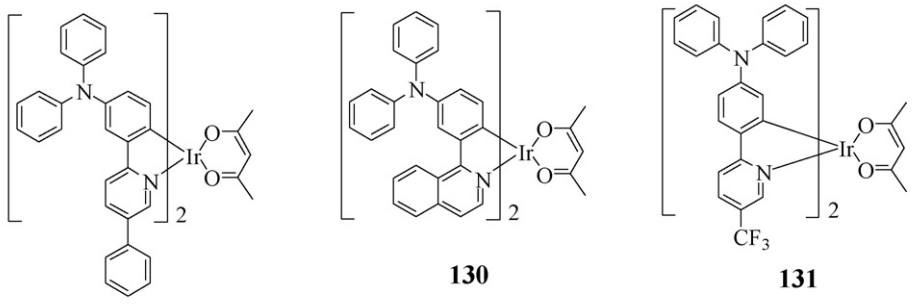

129 **130** **131**

Recent research endeavors were paid to PHOLED devices using solution-processible phosphorescent dendrimers and polymers by virtue of their advantages as low-cost, large-area displays and lighting sources [28,35,91,123]. In this regard, only a limited number of examples of red phosphorescent dendrimers were developed and their solution-processed DLEDs showed a maximum η_{ext} of 5.7% for the red light [124]. With this spirit, pure red-emitting bifunctional iridium(III) complexes with triphenylamine dendrons **132–133** were synthesized and compared with the zeroth generation species *fac*-[Ir(piq)$_3$] [125]. The new dendrimers and *fac*-[Ir(piq)$_3$] are isolated as highly amorphous (T_g ~145–220 °C) and thermally stable (T_d > 417 °C) solids. The T_g value increases gradually with the dendron size for *fac*-[Ir(piq)$_3$], **132** and **133**. They show deep red PL in CH_2Cl_2 at 620 nm for *fac*-[Ir(piq)$_3$], 636 nm for **132** and 641 nm for **133**, respectively and τ_P as short as 0.81–1.40 μs in degassed toluene. From the PL spectra of the neat film of the dendritic complexes, a substantial increase of PL intensity with increasing dendritic generation can be seen, which indicates that the dendritic structures will block the self-quenching of the triplet emission core effectively. The HOMO energy levels determined from the redox data for **132** (−4.99 eV) and **133** (−4.96 eV) are notably higher than that of *fac*-[Ir(piq)$_3$] (−5.11 eV), showing that incorporation of the aromatic amine dendrons into iridium core in **132** and **133** has a great impact on tackling the self-quenching problem for the phosphor and can improve their hole-injection/hole-transporting properties. DLEDs fabricated using **132** and **133** in the configuration ITO/PEDOT:PSS/*x*% Ir:CBP/BCP/Alq_3/LiF/Al emit pure red light with an EL maximum at ca. 640 nm and excellent CIE color coordinates of (0.70, 0.30) in each case. The best device achieved a turn-on voltage of 4.4 V, a maximum brightness of 7,450 cd m^{-2} at 17 V and EL efficiencies of 11.7%, 5.8 cd A^{-1} and 3.7 lm W^{-1} at 5 V. The triphenylamine dendritic ligands might help in overcoming

the classical problem of carrier mobility reduction with increasing dendron generation. Furthermore, the detrimental intermolecular interactions among the emission cores was improved with increasing dendron generation. The efficiencies of these red devices with CIE of (0.70, 0.30) (η_{ext} = 11.7% for **132** and 7.4% for **133**) represent one of the highest ever reported for pure red spin-coated devices and are even superior or comparable to the vacuum-deposited devices with similar CIE color [126–128]. It also compares well to the ~12% efficiency reported by Cao et al. for phosphorescent PLEDs with saturated red emission [129], but is remarkably better than those for reported first-generation red-emitting iridium(III) dendrimers based on *meta*-bonded phenylene in terms of EL efficiency (5.7 and 4.3%) and color purity ((0.64, 0.36) and (0.67, 0.30)) [124]. The device fabricated with 8 wt.% **132** also outperforms the best vacuum-evaporated device with the dopant *fac*-[Ir(piq)$_3$] in CBP, which showed η_{ext} ~10.3% and CIE (0.68, 0.32) [81]. We attribute the excellent performance to the hole-trapping triphenylamine dendritic structure of the complexes showing more favorable hole-injection/hole-transporting properties. More importantly, these materials offer an attractive avenue to developing metallophosphors with optimized efficiency/color purity trade-offs for the pure red-emitting devices. An orange powder of **134** containing diphenylthienylamine-benzoimidazole ligands with strong intramolecular charge-transfer character was also isolated which emits at 620 nm in toluene with a low quantum yield [57]. No device data are, however, available.

In a related context, Sauvage's team has prepared a metal-containing triad **135** based on iridium(III) terpyridine-type core with an aromatic amine electron donor and a bisimide electron acceptor on opposite sides (abbreviated as D–Ir–A) [130]. The spectroscopic, redox and photophysical properties of **135** were compared to those for the component models and the simpler constituent dyad. The photoinduced processes in the triad, which is >4 nm long, have been studied by steady-state and time-resolved optical spectroscopy and the results were correlated to their models. Electron transfer occurs upon excitation of the amine donor and iridium units, giving rise to the charge-separated state D^+–Ir^-–A in quantitative yield and subsequently to D^+–Ir–A^- in ~10% charge-separation yield. Excitation of the A units does not show intramolecular reactivity, however, the final triplet-excited state localized on A, i.e. D–Ir–^{3}A, exhibits intermolecular reactivity. Recently, the same group overcame the unsatisfactory charge-separation yield of **135** by designing dyad molecules **136** (m = 1, 2) which contain a triphenylamine donor and a bis(terpyridine)iridium(III) acceptor core linked via one or two benzamide moieties, respectively [131]. The photoinduced processes involved in **136** were studied in detail. While the charge-separation steps remain very efficient in the longer dyad **136b** (≥99%), charge recombination is slowed down by a factor 3 relative to the shorter dyad **136a**. These results favor the future use of such dyad systems in the assembly of D–Ir–A bridged by two benzamide units.

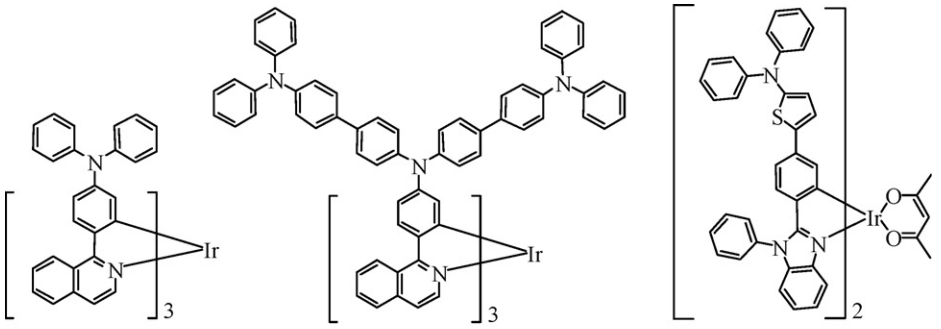

132 **133** **134**

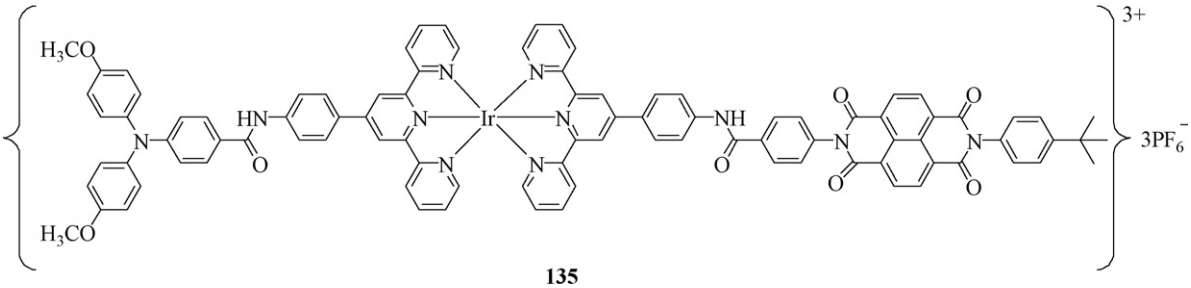

135

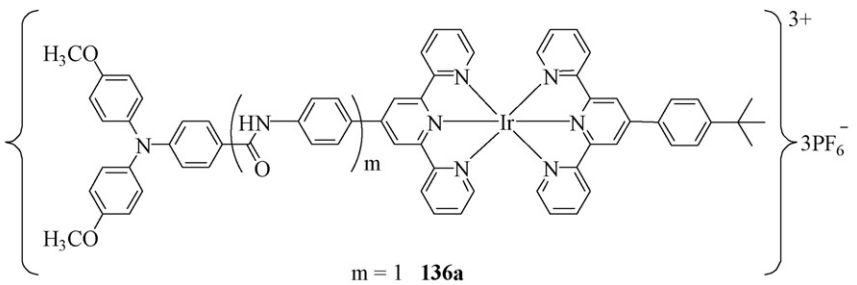

m = 1 **136a**
m = 2 **136b**

3.5. 1,3,4-Oxadiazole

1,3,4-Oxadiazole derivatives are one of the most widely studied classes of electron-injection/hole-blocking materials due to their electron deficiency, high PL quantum yield, and good thermal and chemical stability [31,132–134]. Among these, small-molecule PBD is widely used as an electron-transporting material in multilayer OLEDs [135–137]. However, reported examples of heavy metal phosphors bearing this functionality are relatively rare. In one study, a family of bis(cyclometalated) iridium(III) complexes of 2,5-ditolyl-1,3,4-oxadiazole derivatives **137–140** were reported for the first time in which they differ by the third auxiliary ligand among themselves [138]. The single-crystal structures of **138–140** were established and the solution structures of **139** and **140** were studied using 2D H–H and C–H COSY and NOE spectra (COSY = correlated spectroscopy, NOE = nuclear overhauser effect). The LUMO levels of the complexes are quite insensitive to the variation of the auxiliary group whereas the HOMO levels can be easily tuned. Complexes **139** and **140** have higher oxidation potentials and lower HOMO levels than **138** since the dithiolate auxiliary ligand has a stronger ligand field than acac. This is consistent with the notion that the PL emissions of **139** and **140** appear at 501 and 507 nm, respectively, which are blue-shifted from that for **137** (520 nm) and **138** (518 nm). The PHOLEDs based on **138** show better device performance than those for **139** and **140**. A high-efficiency green EL emission with peak efficiency of 5.28 cd A^{-1} at 1.37 mA cm^{-2} has been achieved for **138**. Another series of related compounds **141–144** have also been synthesized and fully characterized in which novel blue-emitting phosphorescent iridium(III) complexes with fluorinated 1,3,4-oxadiazole derivatives as the cyclometalated ligands and stronger ligand-field dithiocarbamate and dithiophosphate as ancillary ligands **143–144** are particularly attractive [139]. Oxadiazoles, by virtue of their electron-transporting ability, facilitate charge trapping across the bulk for high-performance PHOLEDs. The LUMO levels of **142–144** are almost invariant among them but their HOMO levels decrease from **142** to **144** (−5.47, −5.52 and −5.57 eV, respectively) due to the different auxiliary ligands involved. The PL spectra of **141–144** reveal ligand-based $^3(\pi-\pi)^*$ transition for the lowest triplet excited states. Color tuning becomes possible by using electron-withdrawing fluoro substituents and dithiolate ligands relative to [Ir(ppy)$_2$(acac)] and **141** and the emission wavelength order is [Ir(ppy)$_2$(acac)] (516 nm) > **141** (500 nm) > **142** (479 nm) > **143** (470 nm) > **144** (466 nm). Highly efficient PHOLEDs in the light-blue to blue-emitting region have been achieved using **142**–**144**. Remarkably, PHOLED based on 3 wt.% **143** gave a very promising blue-emitting device (CIE of $x = 0.16$, $y = 0.27$) with a maximum luminance of 22,250 cd m^{-2} at 22.5 V and peak efficiencies of 9.88 cd A^{-1} and 2.38 lm W^{-1} at 3.05 mA cm^{-2}. A device made from 5% **144** afforded blue PHOLED with 5.41 cd A^{-1} and 1.01 lm W^{-1} at 2.49 mA cm^{-2} and CIE coordinates of $x = 0.14$, $y = 0.25$. These devices are comparable in performance to, if not better than, those for the state-of-the-art blue phosphors [FIr(pic)] and iridium(III)-bis(4,6-difluorophenylpyridinato)-5-(pyridine-2-yl)-1H-tetrazolate.

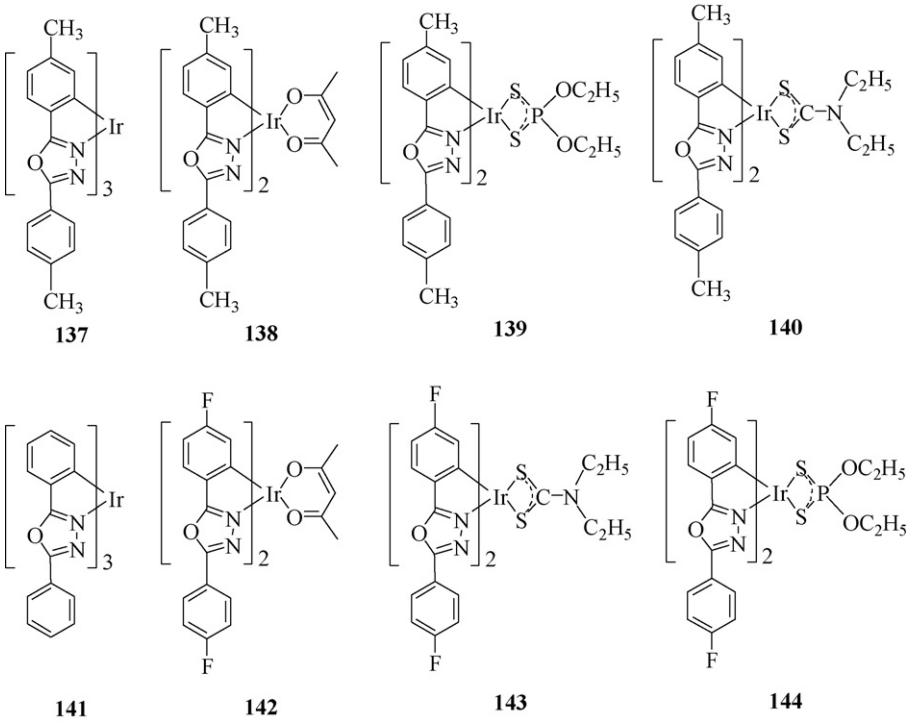

More recently, Tian and co-workers have synthesized a group of interesting green to yellow heteroleptic iridium(III) phosphors containing various 2,5-diaryl-1,3,4-oxadiazole ligands **145–151** [140]. The single-crystal structural analysis was carried out for **149**. Their photophysical, redox and EL properties were studied in terms of the nature of ligand substituents. The emission colors of these complexes depend on the electronic nature of the aryl ring substituent and the PL maximum can scan a range of 508–569 nm in THF. For **145–148**, the authors found that both electron-donating and electron-withdrawing groups on the phenyl ring can lower the HOMO levels to give shorter-wavelength emissions. The presence of naphthyl ring in **150** red-shifts the emission maximum by 1500 cm^{-1} with respect to **145**. Complex **151** with two *N*-carbazole rings also experiences a bathochromic shift of 430 cm^{-1} from **145** due to the electron donation effect and an increase of ligand π-system. PHOLEDs derived from **145**, **146** and **149** have been fabricated in this study.

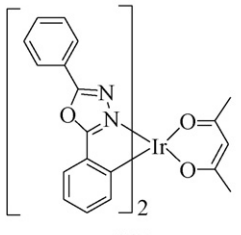

145

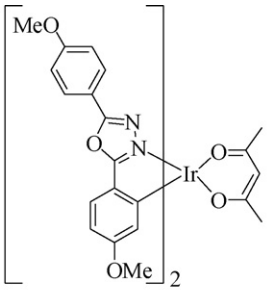

146

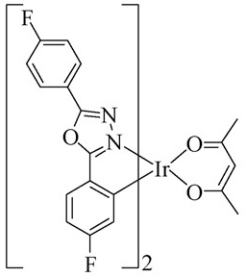

147

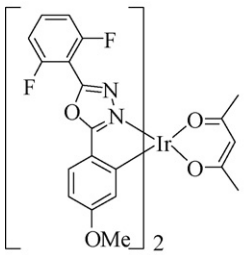

148

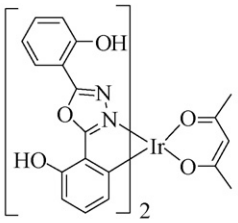

149

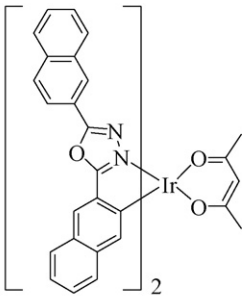

150

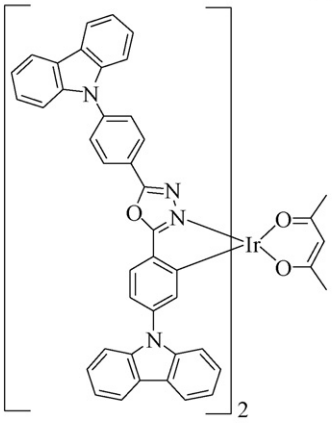

151

Gordon et al. have reported some decent results on the use of an oxadiazole-containing rhenium(I) carbonyl complex **152** in the generation of a novel multi-functional complex **153** [141]. Complex **153** is essentially trifunctional in nature in which it contains a highly emissive rhenium(I) polypyridyl chromophore, an electron-transporting 1,3,4-oxadiazole unit and a hole-transporting terthiophene ring. Complex **153** emits at 474 nm with a PL emission yield of 0.3%. It has a bandgap of 1.93 eV based on CV data which would favor transport of both holes and electrons. Although actual OLED devices have not been made, the properties of **153** are anticipated to meet the energy requirements among different layers for a device using PVK as the host.

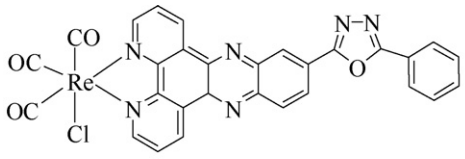

152

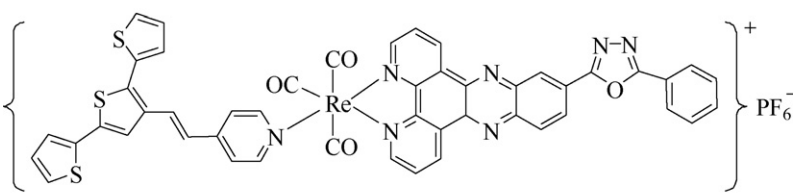

153

3.6. Arylamine–fluorene and arylamine–oxadiazole hybrids

To design new ligand systems for iridium complexes with good amorphous properties and improved functional properties, Wong et al. have reported the synthesis, redox, photophysical and electroluminescent properties of two bifunctional robust bis- and tris-cyclometalated iridium(III) complexes containing diphenylaminofluorene unit **154** and **155** in which the hole-transporting and light-emitting functional groups are integrated into one molecular unit essential for more efficient charge transport in the EL process [142]. We demonstrated that the diphenylamino moiety end-capped onto highly luminescent fluorene backbone can offer a good channel to lower the ionization potential, induce morphologically stable amorphous thin-film formation, and enhance the thermal stability of the complexes. Both of them showed orange electrophosphorescence with very high EL efficiencies. Complex **154** showed an elevated HOMO energy level as compared to the unsubstituted complex **53**, indicating that compound **154** is more electropositive than the non-NPh_2 capped analogue, and a better hole-transporting ability in **154** can be expected. For optimized devices at 5 wt.% doping level of **154**, it was found that a luminance of 4800 cd m^{-2} can be achieved at 8 V (L_{max} ~45,530 cd m^{-2} at 12 V) and the highest η_L attainable is 34.8 cd A^{-1} at 1 mA cm^{-2} and 6 V. This corresponds to peak η_P of 18.2 lm W^{-1} and η_{ext} of 10.5%. The CIE coordinates of this **154**-doped OLED are (0.50, 0.49), with a color saturation of ~93%.

Efficient all-phosphor WOLEDs have also been fabricated which use dual component blue phosphor [FIr(Pic)] and an orange phosphor **154** doped into separate layers, and this device has the CIE color coordinates of (0.31, 0.41) with the highest efficiencies being 17.8 cd A^{-1} and 7.6 lm W^{-1}, respectively [143]. Experimentally, it is necessary to deposit the orange emission layer first, followed by the blue emission layer in the fabrication process in order to ensure a good CIE white color balance. In such device configuration, a voltage dependence of the EL spectrum was observed, with the blue emission becoming stronger relative to the orange color at increasing driving voltage, owing to the requirement for high-energy excitation of the blue phosphor. This can also be rationalized by the fact that the holes have higher mobilities under higher electrical field condition and they will drift to the blue recombination region without being completely recombined in the orange-emitting layer.

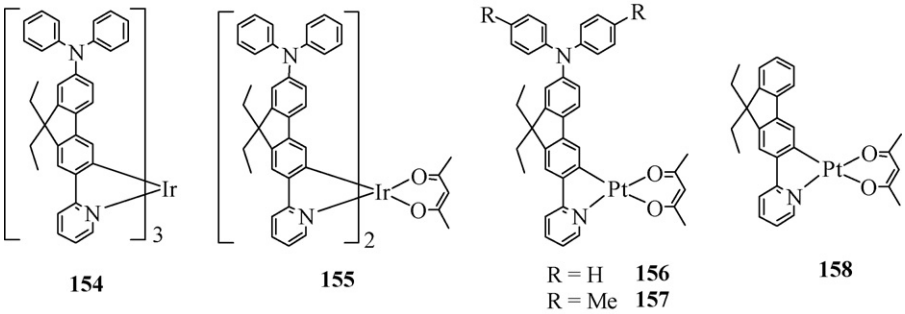

154 **155** **156** (R = H), **157** (R = Me) **158**

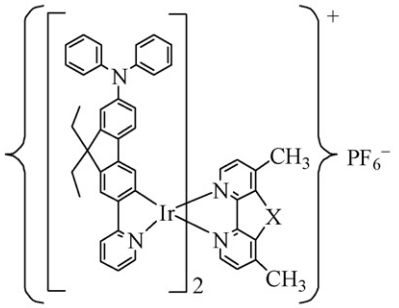

159 (X = none), **160** (R = CH=CH)

In subsequent work, the synthesis, redox, photophysical and EL properties of new multi-component orange phosphorescent cyclometalated platinum(II) complexes with diarylaminofluorene moiety **156** and **157** have been pursued in which hole-injection/hole-transporting and EL functional groups are combined into one molecular unit catering for more efficient charge transport in the EL process. Both platinum complexes together with the unsubstituted analogue **158** were characterized by spectroscopic and X-ray crystallographic methods [144]. All of the platinum complexes are thermostable up to ca. 300 °C. Complexes **156** and **157** show higher T_g (~175 °C) than that of **158** (136 °C). The 9-substituted fluorene moiety will be mainly responsible for conferring the amorphous properties to the complexes while the diarylamino unit plays a crucial role in improving T_g. Again, CV results revealed that each of **156** and **157** can show an elevated HOMO energy level (−5.12 eV for **156** and −5.06 eV for **157**) relative to **158** (−5.29 eV), indicating that they have a better hole-transporting ability in **156** and **157** than **158**. In other words, the diarylamino capping group has the function of facilitating the hole carrier injection and transport of both bifunctional triplet emitters. Efficient pure orange-emitting OLEDs based on **156** were fabricated. The merits of improved hole transportation and suppressed excimer formation render the fabricated PHOLEDs with the CBP host to show efficiencies up to 6.6% and 15.4 cd A^{-1} at 7.5 V. Unlike the PHOLEDs made from other cyclometalated Pt(β-diketonato) complexes in which the EL spectra generally displayed both the monomeric and excimeric emissions with different relative intensities upon variation of dopant concentration [145,146], these devices emitted a strong pure orange light with stable CIE color coordinates and no evidence of low-energy excimeric emission from the aggregate states was observed for a doping level up to 12 wt.%. The present work confers a good platform for providing robust platinum-based triplet emitters in the fabrication of highly efficient monochromatic OLEDs using multi-functional

chelating ligands. Additionally, these bifunctional platinum phosphors have the potential to excel in the development of WOLEDs through a wise combination with an appropriate blue host or emitter [144].

Work from our laboratory also showed that a novel class of multi-component sublimable charged iridium(III) phosphors are useful alternative for use in evaporated devices for the realization of highly efficient doped PHOLEDs. However, compared with neutral complexes, charged iridium(III) complexes were demonstrated to possess many merits that make them eminent candidates for solid-state lighting and display applications [147–149]. The power consumption of such OLED devices can be low even using inert metal electrodes and the excellent redox stability of charged iridium(III) complexes can remarkably improve the device stability. They also show good charge-transfer properties. The synthesis and characterization of two new phosphorescent cationic iridium(III) cyclometalated diimine complexes **159** and **160** are reported [150]. Both complexes are coordinated by cyclometalated ligands consisting of hole-transporting diphenylamino and fluorene-based ppy moieties. The X-ray crystal structure of **160** was determined. For the first time in the electrophosphorescent OLED area, these charged metal phosphors can be vacuum-evaporated without thermal decomposition. Presumably due to the intrinsically ionic nature of both complexes, devices doped with 5 wt.% **159** can produce efficient electrophosphorescence with a maximum brightness of up to 15,610 cd m^{-2} and a peak η_{ext} of ~6.5% that corresponds to a η_L of ~19.7 cd A^{-1} and a η_P of ~18.4 lm W^{-1}. Such strategy is very promising for the continual development of using vacuum-sublimable charged iridium(III) phosphors for high-efficiency devices. These results would be advantageous to the design of new LECs based on light energy harvesting from the triplet excitons.

The concept was then extended to the studies of highly amorphous cyclometalated iridium(III) and platinum(II) metallophosphors **161–164** functionalized with two sterically bulky electron-rich triphenylamino groups at the 9-position of fluorene ring [151]. All of them are thermally stable solids (T_d > 320 °C) and possess high T_g (183–250 °C), suggesting the pivotal role of triphenylamine moieties in improving the amorphous nature of the phosphor molecules (versus T_g of 118 °C for **53**). Complexes **161–163** can exhibit strong anti-triplet–triplet annihilation properties even at high operating current densities for PHOLEDs, which are in accordance with both the experimental and theoretical simulation results. By meticulous selection of the cyclometalating ligand, these complexes not only provide new outlets to dendronized triplet emitters (with no aggregate/excimer emission for **161–163**) for high-performance solution-processed PHOLEDs, but also present new examples of metallophosphors with negligible or reduced triplet–triplet annihilation even at high doping levels. Inclusion of the pendant hole-trapping triphenylamino moieties in these phosphors offer advantages in terms of improving the hole-injection as well as suppressing the crystallinity and aggregation of the materials as compared to the neat 2-pyridinylfluorene congener, which makes them good multi-component phosphorescent materials. This enables efficient stable PHOLEDs to be obtained without the need for an additional hole-transporting layer. The devices were fabricated in the configuration of ITO/PEDOT:PSS/*x*% Ir or Pt dopant:CBP/BCP/Alq_3/LiF/Al. Orange-emitting devices from **161** (or **162**) achieves the highest luminance of 25,660 (20,100) cd m^{-2} at 24 (25) V, maximum η_{ext} of 4.63 (6.43)%, η_L of 15.07 (20.42) cd A^{-1} and η_P of 2.36 (3.05) lm W^{-1}. The pure red-emitting device from **163** (3 wt.%) can attain a maximum luminance of 6,471 cd m^{-2} at 21 V, peak η_{ext} of 4.23%, η_L of 1.69 cd A^{-1} and η_P of 0.27 lm W^{-1}. Device prepared with **164** (10 wt.%) shows an encouraging performance with a peak brightness of 16,070 cd m^{-2} at 17 V, maximum η_{ext} of 3.36%, η_L of 9.55 cd A^{-1} and η_P of 2.31 lm W^{-1}. Excitingly, η_{ext} generally increases with increasing current density values within the usual operating range (≥100 mA cm^{-2}) in many cases, especially for the devices doped with the iridium emitters **161–163**, and this suggests that saturation of the phosphorescence sites is not severe. Even at the higher doping level, the roll-off of η_{ext} is only gentle with increasing current density for **161–163**. These interesting results are contrary to most of the literature data, in which the decrease in η_{ext} with increasing current density usually takes place rapidly due to the severe triplet–triplet annihilation caused by the strong bimolecular quenching effect. The molecular design strategy here opens a new avenue for designing organometallic triplet emitters with minimal T–T annihilation that usually depends strongly on the molecular size factor.

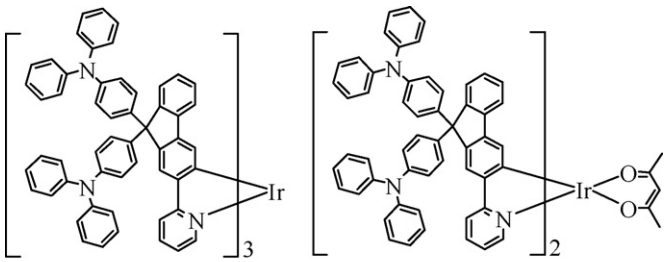

161 **162**

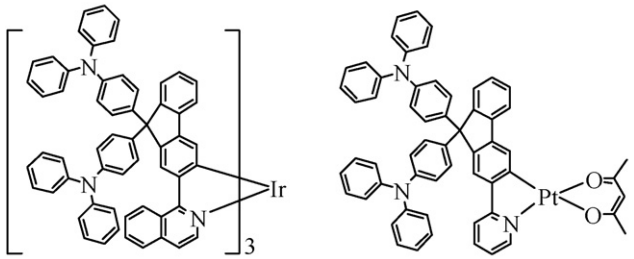

163 **164**

Chan et al. also reported the synthesis and light-emitting properties of two interesting trifunctional molecules **165** and **166** derived from the luminescent rhenium(I) and ruthenium(II) bipyridyl chromophore coupled with the hole-transporting triphenylamine as well as the electron-transporting oxadiazole units within a single species [152]. Both compounds exhibit high thermal stability (T_d: 378 °C for **165** and 368 °C for **166**). It is expected that the electronic and luminescent properties of these complexes can be manipulated easily by changing the metal and/or ligand component, both of which can influence the excited state properties. The MLCT [$d\pi(Re) \rightarrow \pi^*$(diimine)] transitions of **165** and **166** at 440 and 478 nm, respectively, are lowered in energy relative to that for other rhenium(I) diimine tricarbonyl complexes, owing to the effect of electron-withdrawing oxadiazole units that can lower the energy of the π^* orbitals. The PL spectra of both complexes are characterized by a red band due to the MLCT emissive states. EL devices of the ITO/**165**/poly(vinyl alcohol)/Al and ITO/**166**/polycarbonate/Al were fabricated which showed a low turn-on voltage of ~4–5 V and a rectification ratio >10^3 at 25 V. The η_{ext} values of these devices are about 0.1%, with peak luminance of 730 cd m^{-2} in each case. The hole and electron carrier mobilities of both complexes were determined by the time-of-flight (TOF) method to be of the order of 10^{-4} cm^2 V^{-1} s^{-1} at 12 kV cm^{-1}, which appear to be significantly higher than those of some triarylamine-doped polycarbonate films or oxadiazole derivatives. This is indicative of the separate functional roles of triphenylamine and oxadiazole ring in the hole and electron transport processes. The same research team further undertook an investigation into the role of ruthenium and rhenium diimine cores in the optoelectronic properties of some

conjugated poly(phenylenevinylene) polymers **167–169** (with different monomer feed ratios) [153]. Polymer **169** acts as the model compound to study the impact of 1,3,4-oxadiazole ring addition. These polymers can function as charge-transport species, photosensitizers and light emitters. The presence of metal complexes could facilitate the charge-transport process and, in general, the charge-carrier mobilities increase with the metal complex content in the polymers. The electron-carrier mobility of the polymers can be promoted in **167** and **168** since the polymers with oxadiazole and bipyridyl groups tend to be more electron-deficient and act as extra charge carriers in the charge-transport process. The hole- and electron-carrier mobilities of **167–169** were estimated by TOF experiments to be in the order of 10^{-4} to 10^{-5} $cm^2\,V^{-1}\,s^{-1}$. From the plot of temperature-dependent charge mobility, the activation energies of charge transport were found to be ~0.1–0.2 eV. The uniqueness of their redox and excited-state properties govern the resulting photosensitivity and light emission of these materials. A two-layered photovoltaic cell with the structure of ITO/**167** ($x = 1$, $y = 0$)/C_{60}/Al was made to result in a short-circuit current density of 0.05 mA cm^{-2}, an open-circuit voltage of 0.35 V and a power conversion efficiency of ~0.5%. While these polymers consist of two luminescent centers (i.e. the metal complex and the π-conjugated chain), they show a rather broad emission spectrum in each case in the yellow-red region that can extend to very long wavelengths (>750 nm), depending on the actual metal content. For polymer **167** with high metal content (e.g. $x = 1$, $y = 0$), its PL and EL spectra were dominated by an emission peaking at 690 nm due to the emission from the MLCT states of the ruthenium complex. The EL efficiencies of the PLEDs range from 0.05 to 0.2% using these metal-containing polymers.

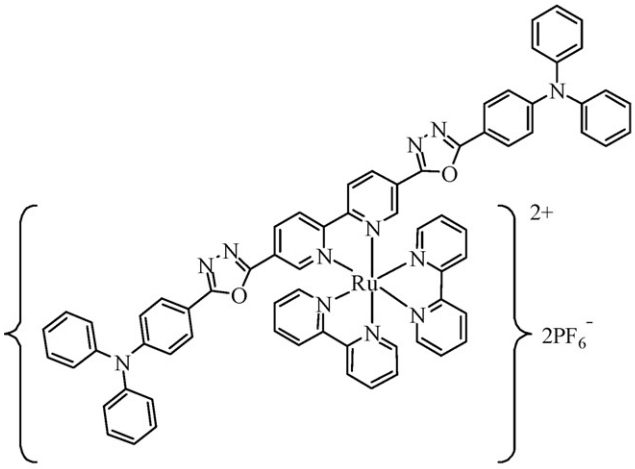

165

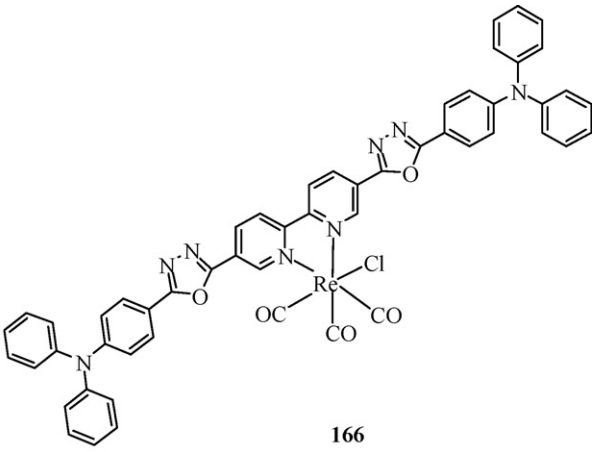

166

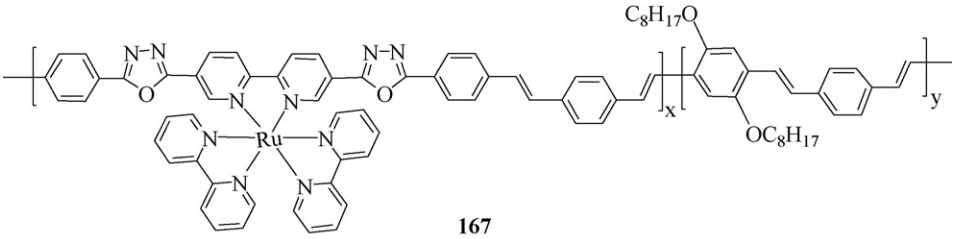

167

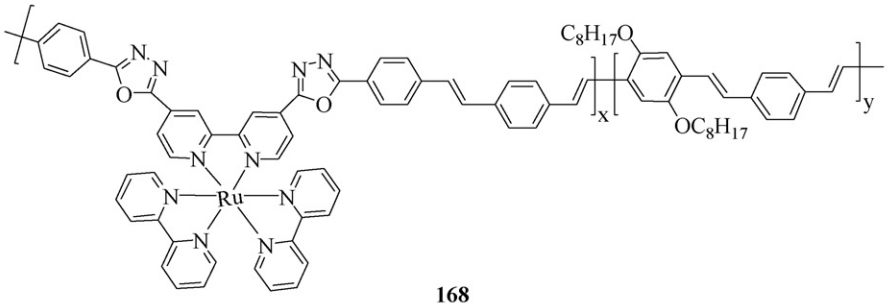

168

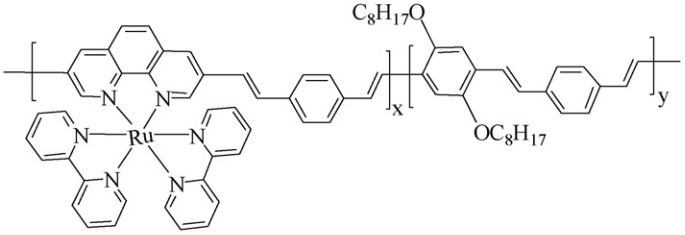

169

Our group also successfully developed synthetic routes to a novel class of trifunctional platinum(II) cyclometalated complexes **170–173** in which the hole-transporting triarylamine, electron-transporting 1,3,4-oxadiazole and EL metal components are integrated into a single molecule [154]. The photophysical, electrochemical and EL properties of these molecules were studied. These neutral platinum(II) chelates display good thermal stability (>250 °C under N_2) and morphological stability. All of them exhibit intense ligand-centered fluorescence and phosphorescence in fluid solutions at room temperature but the emission spectra become largely dominated by triplet emission bands in CH_2Cl_2 glass at 77 K. Substituents with different electronic properties were introduced into the bipolar cyclometalating ligands to fine-tune the absorption and emissive characteristics of the compounds and the results were correlated with theoretical calculations using the DFT method. Comparison of the photophysics and electrochemistry of our multi-functional systems to those only derived from each of the constituent components **174** and **175** was also made and discussed. The single-crystal structures of **170–175** were unambiguously established. For **170–173**, each of them shows dual emission peaks (viz. fluorescence and phosphorescence) at room temperature. Upon introduction of both triarylamino and oxadiazole functional groups into the ppy ligands, the platinum(II) center should show a reduced spin–orbit interaction. As a result, both ligand-centered fluorescence and phosphorescence can be observed. While the higher-lying fluorescent emission was found to show a red-shift in wavelength along the series **170** → **171** → **172** → **173**, attachment of different *R* groups does not seem to alter the phosphorescent emission energies of these complexes. Based on the DFT data, the diarylamino groups govern the feature of the HOMOs while the LUMO is derived from the π* orbitals of the oxadiazole ring and the ppy group. Compounds **170–173** reveal a gentle decrease in the oxidation potentials in the sequence *R* = F > H > Me > OMe, which is a manifestation of the inductive effect induced by the R substituents (viz. negative effect for F and positive effect for both Me and OMe substituents). The elevated HOMO energy levels for **170–173** (−5.05 to −5.50 eV) as compared to **174** (−5.69 eV) indicate that the former series has lower ionization potentials, and hence a better hole-transport character, than **174**. The LUMO levels of **170–173** (−2.48 to −2.77 eV) are lower than that of PBD (−2.4 eV), showing the good electron-transporting ability for **170–173**. Our data can be related to the poorer electron-transporting property for the prototypical [Pt(ppy)(acac)] with a higher LUMO level of −2.41 eV [102,145]. Complexes **170–173** are thus anticipated to display intriguing bipolar character. The LUMO levels are also compatible to that of TPBI (−2.70 eV) [155]. These trifunctional platinum complexes can be

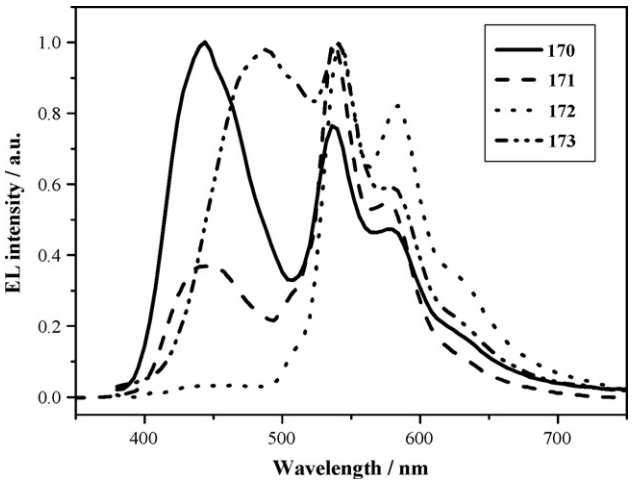

Fig. 4. EL spectra of **170–173** showing the co-existence of both fluorescence and phosphorescence peaks (see Ref. [154]).

vacuum-sublimed and applied as emissive dopants for the fabrication of vapor-deposited PHOLEDs. Like the PL spectra, the electrofluorescence energy depends on the nature of *R* groups, but the electrophosphorescence energy is rather invariant of *R* (Fig. 4). The best performance was realized in the green-yellow device from **172** where maximum efficiency values of 3.6%, 11.0 cd A^{-1} and 5.7 lm W^{-1} were obtained. The higher efficiency and superior performance of **172** than the others may be attributed to the better match of its HOMO level with NPB that leads to excellent balancing of holes and electrons.

The sublimability and multi-functional nature of **170** also render it a suitable candidate for a simple vacuum-deposited device. A device of ITO/CuPc/**170**/Ca:Al was fabricated where a single active layer of **170** as the neat emissive film was obtained by vacuum evaporation [156]. This device exhibited a strong orange-yellow EL at 538 and 578 nm (CIE coordinates: $x = 0.52$, $y = 0.47$ for forward bias) with a low turn-on voltage at around 6 V. The EL spectrum resembles its corresponding PL spectrum from thin film and shows a weak aggregate shoulder at 648 nm due to contribution from its excimer. The EL spectra for this PHOLED exhibited no significant change with variation of operating bias voltages. The device reached a maximum η_L of 1.2 cd A^{-1} and a luminance of 1065 cd m^{-2} was obtained at 14 V that appears to perform better than that for the ppy derivative in a multi-layer configuration [157]. It is worthwhile to compare the device performance with single-layer EL devices fabricated using **165** and **166** with similar ligands which showed the maximum brightness of 730 cd m^{-2} [152]. At the brightness of 100 cd m^{-2}, the device showed a η_L of 0.6 cd A^{-1} at 9.5 V.

Saliently, single-dopant white light EL, triggered by the simultaneous fluorescence/phosphorescence emission of the metal complexes and a variation of applied driving voltages, has also been realized based on multi-functional complexes **170** and **172** (Fig. 5). At 10 wt.% **170**, an almost white emission can be observed within the voltage range of 10–16 V and the EL spectrum at 12 V in Fig. 5 shows a good CIE of (0.31, 0.33). Additionally, WOLED devices comprising 10 and 12 wt.% of the dopant **172** were demonstrated and the former case gave peak η_{ext}, η_L and η_P of 2.6%, 6.8 cd A^{-1} and 4.1 lm W^{-1}, respectively. The highest achieved luminance is 3,270 cd m^{-2} at 11 V. The performance of these two WOLED devices are slightly better than the previously reported results for some platinum(II) Schiff base emitters (η_{ext} ~1.1% and η_P ~0.8 lm W^{-1}) [158]. The CIE coordinates of both **172**-doped white-light devices are (0.33, 0.39) and (0.30, 0.36), respectively, which closely approaches that of white light (defined as 0.33, 0.33). Here, the near-white emission is produced by the simultaneous EL of both singlet and triplet excitons of the trifunctional molecules in the EL device. Thus, the concentration-dependent color tuning can be accomplished by making use of the relationship between the singlet–triplet intensity ratio of the dual emission spectrum and the dopant concentration.

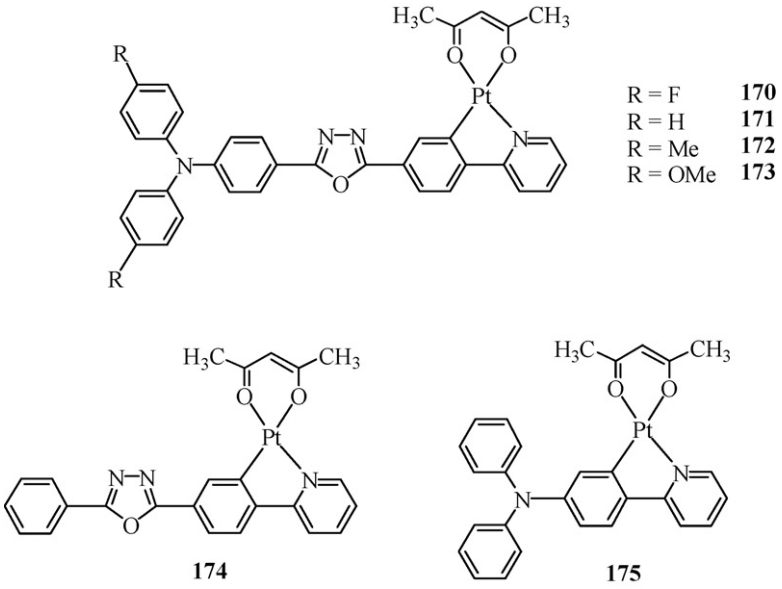

Multi-functional platinum-derivatized random terpolymers with different monomer content **176** were reported by Thompson et al. which are made of hole-transporting triphenylamine, electron-transporting 1,3,4-oxadiazole and emissive [Pt(C^N)$_2$(acac)] modules [159]. These air-stable metallopolymers are organic-soluble and emit simultaneously from the monomer and aggregate states in the blue and orange regions, respectively. These render the materials promising for use in solution-processible near-white PLEDs. Devices with the structure of ITO/PEDOT:PSS/**176**/BCP/Alq_3/LiF/Al achieved white light emission with efficiency up to 4.6% for **176a**. The best CIE coordinates at (0.30, 0.43) were obtained for **179d** with its large proportion of hole-transporting moieties where the higher ratio of non-polar triphenylamine to polar oxadiazole favors the monomeric form over the excimeric species. This approach was also adopted in the development of an ambipolar terpolymer **177** containing [Ir(ppy)$_2$(acac)], *N*,*N*′-diphenyl-*N*,*N*′-bis(3-methylphenyl)-[1,1′-biphenyl]-4,4′-diamine (TPD) and PBD functional side groups for phosphorescence, hole- and electron-transportation, respectively [160]. An optimized green phosphorescent PLED fabricated from **177c** affords the best efficiencies of 11.8% and 38.6 lm W^{-1} using cesium metal as the electron-injection layer. An increase in PBD loading improves the efficiency of PLEDs. The high efficiency is ascribed to the combination of good hole-transporting and electron-transporting abilities for balancing of holes and electrons, but the charge mobility data have not been reported.

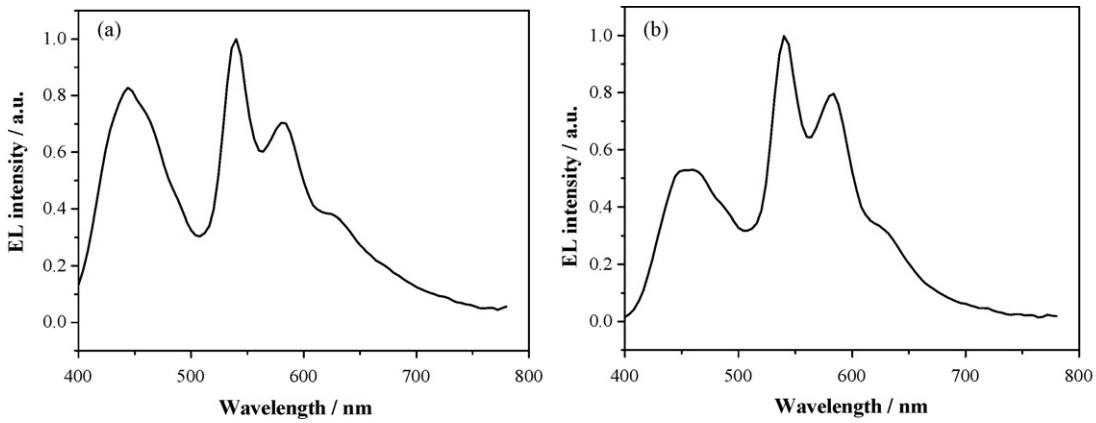

Fig. 5. EL spectra of (a) **170**-doped device (10 wt.%) at 12 V and (b) **172**-doped device (10 wt.%) at 8 V (see Ref. [154]).

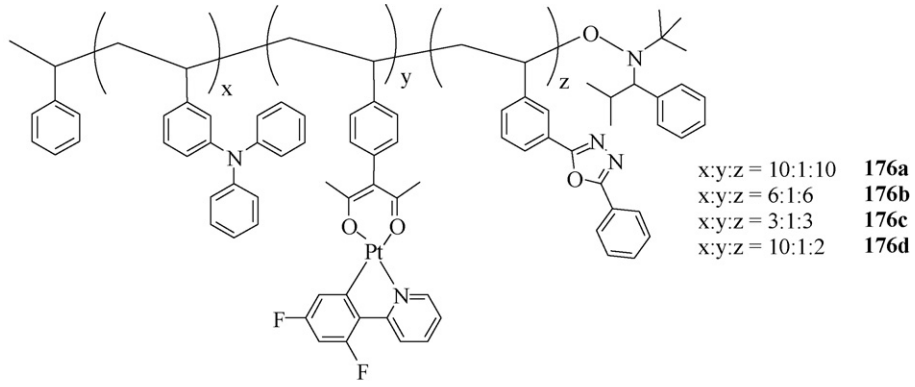

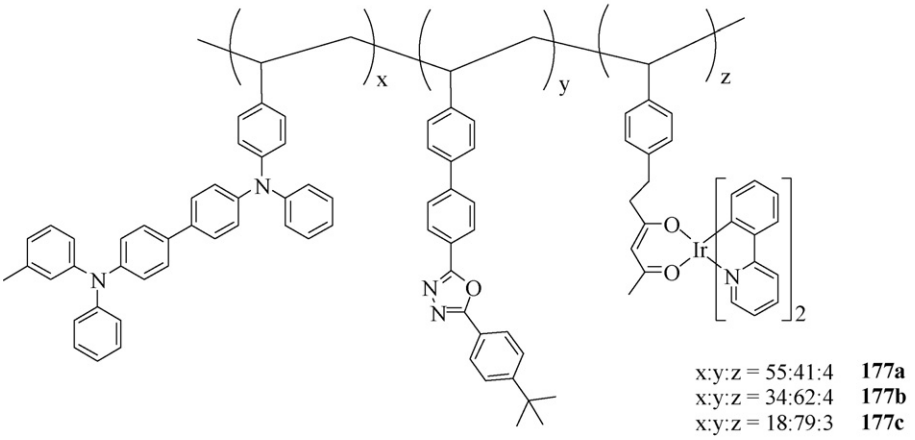

4. Conclusions and future prospects

As a common understanding, balanced charge transport is one of the important factors for achieving high device efficiency in OLEDs. This review provides a comprehensive and recent literature review of the advances in the synthesis, light-emitting properties and OLED/DLED/PLED applications of a vast range of interesting organometallic heavy metal chelates derived from different functional components. The various classes of these small-molecular, dendritic and polymeric materials are described according to the optoelectronic properties of their special functional cores. Encouragingly, impressive progress has been made over the past few years and these heavy metal organometallic materials possess phosphorescent chromophores coupled with hole-transporting and/or electron-transporting entities that can display tunable charge-transporting and triplet light-emitting properties. These multi-component molecules have potentials to excel in making highly efficient and charge-balanced devices with simplified device structures and possibly reduced fabrication cost. Work along this line is certainly worthy of serious investigations and should be of great commercial importance. Greater control of molecular properties and rational design of new materials through innovative chemical synthetic methodologies will ensure a bright and exciting future for these multi-purpose organometallic phosphors. In the short run, the valuable properties shown from this work will act as a spur to international researchers working on molecular

optoelectronics and such research can offer a good platform for the continual development of this area. Of more long-term impact will be that research knowledge can be expanded towards the future technology of organometallic optoelectronics and photonics based on molecular functional materials.

Acknowledgements

Financial support from a CERG grant from the Research Grants Council of the Hong Kong SAR, People's Republic of China (Project No. HKBU202106) and the Hong Kong Baptist University is gratefully acknowledged for this work. We also thank the Hong Kong Baptist University for a postdoctoral research fellowship to Dr. Cheuk-Lam Ho.

References

[1] A. Misra, P. Kumar, M.N. Kamalasanan, S. Chandra, Semicond. Sci. Technol. 21 (2006) R35.
[2] B.W. D'Andrade, S.R. Forrest, Adv. Mater. 16 (2004) 1585.
[3] A. Kraft, A.C. Grimsdale, A.B. Holmes, Angew. Chem. Int. Ed. 37 (1998) 402.
[4] R.H. Friend, R.W. Gymer, A.B. Holmes, J.H. Burroughes, R.N. Marks, C. Taliani, D.D.C. Bradley, D.A. Dos Santos, J.L. Brédas, M. Lögdlund, W.R. Salaneck, Nature 397 (1999) 121.
[5] J.L. Segura, Acta. Polym. 49 (1998) 319.
[6] C.H. Chen, J. Shi, Coord. Chem. Rev. 171 (1998) 161.
[7] J.K. Borchardt, Mater. Today 7 (2004) 42.
[8] M.A. Baldo, M.E. Thompson, S.R. Forrest, Nature 403 (2000) 750.
[9] A. Köhler, J.S. Wilson, R.H. Friend, Adv. Mater. 14 (2002) 701.
[10] M. Wohlgenannt, Z.V. Vardenty, J. Phys. Condens. Mater. 15 (2003) R83.
[11] A. Köhler, J. Wilson, Org. Electron. 4 (2003) 179.
[12] M.A. Baldo, D.F. O'Brien, M.E. Thompson, S.R. Forrest, Phys. Rev. B 60 (1999) 14422.
[13] J.S. Wilson, A.S. Dhoot, A.J.A.B. Seeley, M.S. Khan, A. Köhler, R.H. Friend, Nature 413 (2001) 828.
[14] M. Segal, M.A. Baldo, R.J. Holmes, S.R. Forrest, Z.G. Soos, Phys. Rev. B: Condens. Matter. 68 (2003) 075211.
[15] M. Reufer, M.J. Walter, P.G. Lagoudakis, B. Hummel, J.S. Kolb, H.G. Roskos, U. Scherf, J.M. Lupton, Nat. Mater. 4 (2005) 340.
[16] N.J. Turro, Modern Molecular Photochemistry, Benjamin/Cummings Publishing, Menlo Park, CA, USA, 1978.
[17] (a) M.A. Baldo, D.F. O'Brien, Y. You, A. Shoustikov, S. Sibley, M.E. Thompson, S.R. Forrest, Nature 395 (1998) 151;
(b) Y. Cao, I.D. Parker, G. Yu, C. Zhang, A.J. Heeger, Nature 397 (1999) 414.
[18] M.A. Baldo, S. Lamansky, P.E. Burrows, M.E. Thompson, S.R. Forrest, Appl. Phys. Lett. 75 (1999) 4.
[19] B. Carlson, G.D. Phelan, W. Kaminsky, L. Dalton, X. Jiang, M.S. Liu, A.K.Y. Jen, J. Am. Chem. Soc. 124 (2002) 14162.
[20] S. Bernhard, J.A. Barron, P.L. Houston, H.D. Abruna, J.L. Ruglovksy, X. Gao, G.G. Malliaras, J. Am. Chem. Soc. 124 (2002) 13624.
[21] P.-T. Chou, Y. Chi, Eur. J. Inorg. Chem. (2006) 3319.
[22] R.C. Evans, P. Douglas, C.J. Winscom, Coord. Chem. Rev. 250 (2006) 2093.
[23] E. Holder, B.M.W. Langeveld, U.S. Schubert, Adv. Mater. 17 (2005) 1109.
[24] P.-T. Chou, Y. Chi, Chem. Soc. Rev. 36 (2007) 1421.
[25] P.-T. Chou, Y. Chi, Chem. Eur. J. 13 (2007) 380.
[26] H. Yersin, Top. Curr. Chem. 241 (2004) 1.
[27] M.A. Baldo, M.E. Thompson, S.R. Forrest, Pure Appl. Chem. 71 (1999) 2095.
[28] P.L. Burn, S.-C. Lo, I.D.W. Samuel, Adv. Mater. 19 (2007) 1675.
[29] K.A. King, P.J. Spellane, R.J. Watts, J. Am. Chem. Soc. 107 (1985) 1431.
[30] C.W. Tang, S.A. VanSlyke, Appl. Phys. Lett. 51 (1987) 913.
[31] G. Hughes, M.R. Bryce, J. Mater. Chem. 15 (2005) 94.
[32] J. Kido, Y. Okamoto, Chem. Rev. 102 (2002) 2357.
[33] M.S. Lowry, S. Bernhard, Chem. Eur. J. 12 (2006) 7970.
[34] X. Yang, D. Neher, D. Hertel, T.K. Daubler, Adv. Mater. 16 (2004) 161.
[35] S. Tokito, M. Suzuki, F. Sato, M. Kamachi, K. Shirane, Org. Electron. 4 (2003) 105.
[36] F.-C. Chen, S.-C. Chang, G. He, S. Pyo, Y. Yang, M. Kurotaki, J. Kido, J. Polym. Sci.: Part B: Polym. Phys. 41 (2003) 2681.
[37] W.-Y. Wong, Coord. Chem. Rev. 249 (2005) 971.
[38] D.M. Pai, J.F. Yanus, M. Stolka, J. Phys. Chem. 88 (1984) 4714.
[39] H. Kanai, S. Ichinosawa, Y. Sato, Synth. Met. 91 (1997) 195.
[40] X.Z. Jiang, Y.Q. Liu, X.Q. Song, D.B. Zhu, Synth. Met. 91 (1997) 311.
[41] D.B. Romero, F. Nueesch, T. Bebazzi, D. Ades, A. Stove, L. Zuppiroli, Adv. Mater. 9 (1997) 1158.
[42] M. Bratcher, M. Declue, A. Grunnetjepsen, D. Wright, B. Smith, W. Moerner, J. Siegel, J. Am. Chem. Soc. 120 (1998) 9680.
[43] K. Meerholz, L.B. Volodin, B. Kippelen, N. Peyghambarian, Nature 71 (1994) 497.
[44] S.-J. Yeh, M.-F. Wu, C.-T. Chen, Y.-H. Song, Y. Chi, M.-H. Ho, S.-F. Hsu, C.-H. Chen, Adv. Mater. 17 (2005) 285.
[45] K. Brunner, A. van Dijken, H. Börner, J.J.A.M. Bastiaansen, N.M.M. Kiggen, B.M.W. Langeveld, J. Am. Chem. Soc. 126 (2004) 6035.
[46] M.-H. Tsai, H.-W. Lin, H.-C. Su, T.-H. Ke, C.-C. Wu, F.-C. Fang, Y.-L. Liao, K.-T. Wong, C.-I. Wu, Adv. Mater. 18 (2006) 1216.
[47] K.R. Justin Thomas, J.T. Lin, Y.-T. Tao, C.-W. Ko, J. Am. Chem. Soc. 123 (2001) 9404.
[48] P. Strohriegl, J.V. Grazulevicius, Adv. Mater. 13 (2003) 445.
[49] Y. Shirota, H. Kageyama, Chem. Rev. 107 (2007) 953.
[50] C.D. Entwistle, T.B. Marder, Angew. Chem. Int. Ed. 41 (2002) 2927.
[51] C. Yang, X. Zhang, H. You, L. Zhu, L. Chen, L. Zhu, Y. Tao, D. Ma, Z. Shuai, J. Qin, Adv. Funct. Mater. 17 (2007) 651.
[52] X. Zhang, Z. Chen, C. Yang, Z. Li, K. Zhang, H. Yao, J. Qin, J. Chen, Y. Cao, Chem. Phys. Lett. 422 (2006) 386.
[53] K. Zhang, Z. Chen, C. Yang, X. Zhang, Y. Tao, L. Duan, L. Chen, L. Zhu, J. Qin, Y. Cao, J. Mater. Chem. 17 (2007) 3451.
[54] S. Bettington, M. Tavasli, M.R. Bryce, A. Beeby, H. Al-Attar, A.P. Monkman, Chem. Eur. J. 13 (2006) 1423.
[55] R. Zhu, J. Lin, G.A. Wen, S.J. Liu, J.H. Wan, J.C. Feng, Q.L. Fan, G.Y. Zhong, W. Wei, W. Huang, Chem. Lett. 34 (2005) 1668.
[56] K. Ono, M. Joho, K. Saito, M. Tomura, Y. Matsushita, S. Naka, H. Okada, H. Onnagawa, Eur. J. Inorg. Chem. (2006) 3676.
[57] W.S. Huang, J.T. Lin, C.H. Chien, Y.T. Tao, S.S. Sun, Y.S. Wen, Chem. Mater. 16 (2004) 2480.
[58] W.-Y. Wong, C.-L. Ho, Z.-Q. Gao, B.-X. Mi, C.-H. Chen, K.-W. Cheah, Z. Lin, Angew. Chem. Int. Ed. 45 (2006) 7800.
[59] C.-L. Ho, Q. Wang, C.-S. Lam, W.-Y. Wong, D. Ma, L. Wang, Z.-Q. Gao, C.-H. Chen, K.-W. Cheah, Z. Lin, Chem. Asian J. 4 (2009) 89.
[60] C.-L. Ho, W.-Y. Wong, Q. Wang, D. Ma, L. Wang, Z. Lin, Adv. Funct. Mater. 18 (2008) 928.
[61] C.-L. Ho, M.-F. Lin, W.-Y. Wong, W.-K. Wong, C.-H. Chen, Appl. Phys. Lett. 92 (2008) 083301.
[62] C.-L. Ho, W.-Y. Wong, Z.-Q. Gao, C.-H. Chen, K.-W. Cheah, B. Yao, Z. Xie, Q. Wang, D. Ma, L. Wang, X.-M. Yu, H.-S. Kwok, Z. Lin, Adv. Funct. Mater. 18 (2008) 319.
[63] Y. Sun, N.C. Giebink, H. Kanno, B. Ma, M.E. Thompson, S.R. Forrest, Nature 440 (2006) 908.
[64] M.-F. Lin, L. Wang, W.-K. Wong, K.-W. Cheah, H.-L. Tam, M.-T. Lee, M.-H. Ho, C.-H. Chen, Appl. Phys. Lett. 91 (2007) 1.
[65] B. Ma, P.I. Djurovich, S. Garon, B. Alleyne, M.E. Thompson, Adv. Funct. Mater. 16 (2006) 2438.
[66] C.-T. Chen, Chem. Mater. 16 (2004) 4389.
[67] S.C. Lo, E.B. Namdas, C.P. Shipley, J.P.J. Markham, T.D. Anthopolous, P.L. Burn, I.D.W. Samuel, Org. Electron. 7 (2006) 85.
[68] E.B. Namdas, A. Ruseckas, I.D.W. Samuel, S.C. Lo, P.L. Burn, Appl. Phys. Lett. 86 (2005) 091104.
[69] T. Tsuzuki, N. Shirasawa, T. Suzuki, S. Tokito, Jpn. J. Appl. Phys. 44 (2005) 1451.
[70] J. Ding, J. Gao, Y. Cheng, Z. Xie, L. Wang, D. Ma, X. Jing, F. Wang, Adv. Funct. Mater. 16 (2006) 575.
[71] J. Ding, J. Lü, Y. Cheng, Z. Xie, L. Wang, X. Jing, F. Wang, Adv. Funct. Mater. 18 (2008) 2754.
[72] Z. Liu, M. Guan, Z. Bian, D. Nie, Z. Gong, Z. Li, C. Huang, Adv. Funct. Mater. 16 (2006) 1441.
[73] Q. Zhao, S. Liu, M. Shi, F. Li, H. Jing, H. Jing, T. Yi, C. Huang, Organometallics 26 (2007) 5922.
[74] Z. Liu, D. Nie, Z. Bian, F. Chen, B. Lou, J. Bian, C. Huang, Chem. Phys. Chem. 9 (2008) 634.
[75] A. Kimyonok, B. Domercq, A. Haldi, J.Y. Cho, J.R. Carlise, X.Y. Wang, L.E. Hayden, S.C. Jones, S. Barlow, S.R. Marder, B. Kippelen, M. Weck, Chem. Mater. 19 (2007) 5602.
[76] Q. Liu, J. Lu, J. Ding, Y. Tao, Macromol. Chem. Phys. 209 (2008) 1931.
[77] C.L. Lee, N.G. Kang, Y.S. Cho, J.S. Lee, J.J. Kim, Opt. Mater. 21 (2002) 119.
[78] X.Y. Wang, R.N. Prabhu, R.H. Schmshl, M. Weck, Macromolecules 19 (2006) 3140.
[79] W.-Y. Wong, C.-L. Ho, Coord. Chem. Rev. 250 (2006) 2627.
[80] D. Neher, Macromol. Rapid Commun. 22 (2001) 1365.
[81] A. Tsuboyama, H. Iwawaki, M. Furugori, T. Mukaide, J. Kamatani, S. Igawa, T. Moriyama, S. Miura, T. Takiguchi, S. Okada, M. Hoshino, K. Ueno, J. Am. Chem. Soc. 125 (2003) 12971.
[82] X.-M. Yu, G.-J. Zhou, C.-S. Lam, W.-Y. Wong, X.-L. Zhu, J.-X. Sun, M. Wong, H.-S. Kwok, J. Organomet. Chem. 693 (2008) 1518.
[83] X. Gong, M.R. Robinson, J.C. Ostrowski, D. Moses, G.C. Bazan, Adv. Mater. 14 (2002) 581.
[84] H. Kanno, R.J. Holmes, Y. Sun, S. Kena-Cohen, S.R. Forrest, Adv. Mater. 18 (2006) 339.
[85] B.W. D'Andrade, J.J. Brown, Appl. Phys. Lett. 88 (2006) 192908.
[86] X. Gong, J.C. Ostrowski, D. Moses, G.C. Bazan, A.J. Heeger, Adv. Funct. Mater. 13 (2003) 439.
[87] X. Gong, J.C. Ostrowski, G.C. Bazan, D. Moses, A.J. Heeger, M.S. Liu, Adv. Mater. 15 (2003) 45.
[88] X. Gong, W. Ma, J.C. Ostrowski, K. Bechgaard, G.C. Bazan, A.J. Heeger, S. Xiao, D. Moses, Adv. Funct. Mater. 14 (2004) 393.
[89] J.C. Ostrowski, M.R. Robinson, A.J. Heeger, G.C. Bazan, Chem. Commun. (2002) 784.
[90] X. Gong, H. Benmansour, G.C. Bazan, A.J. Heeger, J. Phys. Chem. B 110 (2006) 7344.
[91] M. Tavasli, S. Bettington, M.R. Bryce, H.A.Al. Attar, F.B. Dias, S. King, A.P. Monkman, J. Mater. Chem. 15 (2005) 4963.

[92] F.I. Wu, H.J. Su, C.F. Shu, L. Luo, W.G. Diau, C.H. Cheng, J.P. Duan, G.H. Lee, J. Mater. Chem. 15 (2005) 1035.
[93] L. Chen, H. You, C. Yang, X. Zhang, J. Qin, D. Ma, J. Mater. Chem. 16 (2006) 3332.
[94] R.N. Bera, N. Cumpstey, P.L. Burn, I.D.W. Samuel, Adv. Funct. Mater. 17 (2007) 1149.
[95] S.J. Liu, Q. Zhao, R.F. Chen, Y. Deng, Q.L. Fan, F.Y. Li, L.H. Wang, C.H. Huang, W. Huang, Chem. Eur. J. 12 (2006) 4351.
[96] X. Zeng, M. Tavasli, I.F. Perepichka, A.S. Batsanov, M.R. Bryce, C.J. Chiang, C. Rothe, A.P. Monkman, Chem. Eur. J. 14 (2008) 933.
[97] N.R. Evans, L.S. Devi, C.S.K. Mak, S.E. Watkins, S.I. Pascu, A. Köhler, R.H. Friend, C.K. Williams, A.B. Holmes, J. Am. Chem. Chem. 128 (2006) 6647.
[98] C. Mei, J. Ding, B. Yao, Y. Cheng, Z. Xie, Y. Geng, L. Wang, J. Poly. Sci: Part A: Poly. Chem. 45 (2007) 1746.
[99] T. Ito, S. Suzuki, J. Kido, Polym. Adv. Technol. 16 (2005) 480.
[100] B.L. Li, Z.T. Liu, Y.M. He, J. Pan, Q.H. Fan, Polymer 49 (2008) 1527.
[101] C.-L. Ho, W.-Y. Wong, G.-J. Zhou, B. Yao, Z. Xie, L. Wang, Adv. Funct. Mater. 17 (2007) 2925.
[102] I.R. Laskar, S.F. Hsu, T.M. Chen, Polyhedron 24 (2005) 881.
[103] Y.H. Sun, X.H. Zhu, Z. Chen, Y. Zhang, Y. Cao, J. Org. Chem. 71 (2006) 6281.
[104] K.A. Knights, S.G. Stevenson, C.P. Chipley, S.C. Lo, S. Olsen, R.E. Harding, S. Gambino, P.L. Burn, I.D.W. Samuel, J. Mater. Chem. 18 (2008) 2121.
[105] J. Jiang, C. Jiang, W. Yang, H. Zhan, F. Huang, Y. Cao, Macromolecules 38 (2005) 4072.
[106] Y. Xu, R. Guan, J. Jiang, W. Yang, H. Zhen, J. Peng, Y. Cao, J. Polym. Sci. Part A: Polym. Chem. 46 (2008) 453.
[107] K. Zhang, Z. Chen, Y. Zou, C. Yang, J. Qin, Y. Cao, Organometallics 26 (2007) 3699.
[108] H. Zhen, W. Xu, W. Yang, Q. Chen, Y. Xu, J. Jiang, J. Peng, Y. Cao, Macromol. Rapid Commun. 27 (2006) 2095.
[109] K. Zhang, Z. Chen, C. Yang, S. Gong, J. Qin, Y. Gao, Macromol. Rapid Commun. 27 (2006) 1926.
[110] H. Zhen, C. Jiang, W. Yang, J. Jiang, F. Huang, Y. Cao, Chem. Eur. J. 11 (2005) 5007.
[111] H. Zhen, J. Luo, W. Yang, Q. Chen, L. Ying, Z. Jianhua, H. Wu, Y. Cao, J. Mater. Chem. 17 (2007) 2824.
[112] S.J. Liu, Q. Zhao, Y. Deng, Y.J. Xia, J. Lin, Q.L. Fan, L.H. Wang, W. Huang, J. Phys. Chem. 111 (2007) 1166.
[113] X. Chen, J.L. Liao, M.O. Ahmed, H.E. Yseng, S.A. Chen, J. Am. Chem. Soc. 125 (2003) 636.
[114] J. Gao, H. You, Z.P. Qin, J. Fang, D. Ma, X. Zhu, W. Huang, Semicond. Sci. Technol. 20 (2005) 805.
[115] G.-J. Zhou, Q. Wang, C.-L. Ho, W.-Y. Wong, D. Ma, L. Wang, Z. Lin, Chem. Asian J. 3 (2008) 1830.
[116] G.-J. Zhou, C.-L. Ho, W.-Y. Wong, Q. Wang, D. Ma, L. Wang, Z. Lin, T.B. Marder, A. Beeby, Adv. Funct. Mater. 18 (2008) 499.
[117] F.-M. Hwang, H.-Y. Chen, P.-S. Chen, C.-S. Liu, Y. Chi, C.-F. Shu, F.-I. Wu, P.-T. Chou, S.-M. Peng, G.-H. Lee, Inorg. Chem. 44 (2005) 1344.
[118] C.S.K. Mak, A. Hayer, S.I. Pascu, S.E. Watkins, A.B. Holmes, A. Köhler, R.H. Friend, Chem. Commun. (2005) 4708.
[119] S.C. Lo, C.P. Shipley, R.N. Bera, R.E. Harding, A.R. Cowley, P.L. Burn, I.D.W. Samuel, Chem. Mater. 18 (2006) 5119.
[120] T. Sajoto, P.I. Djurovich, A. Tamayo, M. Yousufuddin, R. Bau, M.E. Thompson, R.J. Holmes, S.R. Forrest, Inorg. Chem. 44 (2005) 7992.
[121] P. Coppo, E.A. Plummer, L. De Cola, Chem. Commun. (2001) 1774.
[122] J. Nishida, H. Echizen, T. Iwata, Y. Yamashiya, Chem. Lett. 34 (2005) 1378.
[123] A.J. Sandee, C.K. Williams, N.R. Evans, J.E. Davies, C.E. Boothby, A. Köhler, R.H. Friend, A.B. Holmes, J. Am. Chem. Soc. 126 (2004) 7041.
[124] T.D. Anthopoulos, M.J. Frampton, E.B. Namdas, P.L. Burn, I.D.W. Samuel, Adv. Mater. 16 (2004) 557.
[125] G.-J. Zhou, W.-Y. Wong, B. Yao, Z. Xie, L. Wang, Angew. Chem. Int. Ed. 119 (2007) 1167.
[126] D.K. Rayabarapu, B.M.J.S. Paulose, J.-P. Duan, C.-H. Cheng, Adv. Mater. 17 (2005) 349.
[127] J. Gao, H. You, J. Fang, D. Ma, L. Wang, X. Jing, F. Wang, Synth. Met. 155 (2005) 168.
[128] K.R. Justin Thomas, M. Velusamy, J.T. Lin, C.-H. Chien, Y.-T. Tao, Y.S. Wen, Y.-H. Hu, P.-T. Chou, Inorg. Chem. 44 (2005) 5677.
[129] C. Jiang, W. Yang, J. Peng, S. Xiao, Y. Cao, Adv. Mater. 16 (2004) 537.
[130] L. Flamigni, E. Baranoff, J.P. Collin, J.P. Sauvage, Chem. Eur. J. 12 (2006) 6592.
[131] L. Flamigni, B. Ventura, E. Baranoff, J.P. Collin, J.P. Sauvage, Eur. J. Inorg. Chem. (2007) 5189.
[132] K.T. Kamtekar, C. Wang, S. Bettington, A.S. Batsanov, I.F. Perepichka, M.R. Bryce, J.H. Ahn, M. Rabinal, M.C. Petty, J. Mater. Chem. 39 (2006) 3823.
[133] P. Wang, C. Chai, Y. Chuai, F. Wang, X. Chen, X. Fan, Y. Xu, D. Zou, Q. Zhou, Polymer 48 (2007) 5889.
[134] C. Wang, M. Kilitziraki, L.O. Pälsson, M.R. Bryce, A.P. Monkman, I.D.W. Samuel, Adv. Funct. Mater. 11 (2001) 4.
[135] C. Adachi, T. Tsutsui, S. Saito, Appl. Phys. Lett. 56 (1990) 799.
[136] A.R. Brown, D.D.C. Bradley, J.H. Burroughs, R.H. Friend, N.C. Greenham, P.L. Burn, A. Kraft, Appl. Phys. Lett. 61 (1992) 2793.
[137] C. Zhang, S. Höger, K. Pakbaz, F. Wudl, A.J. Heeger, J. Electron. Mater. 23 (1994) 453.
[138] L. Chen, C. Yang, J. Qin, J. Gao, H. You, D. Ma, J. Organomet. Chem. 691 (2006) 3519.
[139] L. Chen, H. You, C. Yang, D. Ma, J. Qin, Chem. Commun. (2007) 1352.
[140] Z. Xu, Y. Li, X. Ma, X. Gao, H. Tian, Tetrahedron 64 (2008) 1860.
[141] N.J. Lundin, A.G. Blackman, K.C. Gordon, D.L. Officer, Angew. Chem. Int. Ed. 45 (2006) 2582.
[142] W.-Y. Wong, G.-J. Zhou, X.-M. Yu, H.-S. Kwok, B.-Z. Tang, Adv. Funct. Mater. 16 (2006) 838.
[143] X.-M. Yu, H.-S. Kwok, W.-Y. Wong, G.-J. Zhou, Chem. Mater. 18 (2006) 5097.
[144] G.-J. Zhou, X.-Z. Wang, W.-Y. Wong, X.-M. Yu, H.-S. Kwok, Z. Lin, J. Organomet. Chem. 692 (2007) 3461.
[145] J. Brooks, Y. Babayan, S. Lamansky, P.I. Djurovich, I. Tsyba, R. Bau, M.E. Thompson, Inorg. Chem 41 (2002) 3055.
[146] F. Barigelletti, D. Sandrini, M. Maestri, V. Balzani, A. von Zelewsky, L. Chassot, P. Jolliet, U. Maeder, Inorg. Chem. 27 (1988) 3644.
[147] M.K. Nazeeruddin, R. Humphry-Baker, D. Berner, S. Rivier, L. Zuppiroli, M. Graetzel, J. Am. Chem. Soc. 125 (2003) 8790.
[148] E.A. Phummer, A. Dijken, H.W. Hofstraat, L. De Cola, K. Brunner, Adv. Funct. Mater. 15 (2005) 281.
[149] J.D. Slinker, A.A. Gorodetsky, M.S. Lowry, J. Wang, S. Parker, R. Rohl, S. Bernhard, G.G. Malliaras, J. Am. Chem. Soc. 126 (2004) 2763.
[150] W.-Y. Wong, G.-J. Zhou, X.-M. Yu, H.-S. Kwok, Z. Lin, Adv. Funct. Mater. 17 (2007) 315.
[151] G.-J. Zhou, W.-Y. Wong, B. Yao, Z. Xie, L. Wang, J. Mater. Chem. 18 (2008) 1799.
[152] X. Gong, P.K. Ng, W.K. Chan, Adv. Mater. 10 (1998) 1337.
[153] P.K. Ng, X. Gong, S.H. Chan, L.S.M. Lam, W.K. Chan, Chem. Eur. J. 7 (2001) 4358.
[154] Z. He, W.-Y. Wong, X. Yu, H.-S. Kwok, Z. Lin, Inorg. Chem. 45 (2006) 10922.
[155] Y.T. Tao, C.H. Chuen, C.W. Ko, J.W. Peng, Chem. Mater. 14 (2002) 4256.
[156] W.-Y. Wong, Z. He, S.-K. So, Z. Lin, Organometallics 24 (2005) 4079.
[157] A.S. Ionkin, W.J. Marshall, Y. Wang, Organometallics 24 (2005) 619.
[158] C.-M. Che, S.-C. Chan, H.-F. Xiang, M.C.W. Chan, Y. Liu, Y. Wang, Chem. Commun. (2004) 1484.
[159] P.T. Furuta, L. Dan, S. Garon, M.E. Thompson, J.M.J. Fréchet, J. Am. Chem. Soc. 126 (2004) 15388.
[160] M. Suzuki, S. Tokito, F. Sato, T. Igarashi, K. Kondo, T. Koyama, T. Yamaguchi, Appl. Phys. Lett. 86 (2005) 103507.